Inaugural dissertation

for

obtaining the doctoral degree

of the

Combined Faculty of Mathematics, Engineering and Natural Sciences

of the

Ruprecht - Karls - University

Heidelberg

Presented by

Patricio Doldan, M.Sc.

Born in Formosa, Argentina

Oral examination: 7th of June 2022

Live-cell microscopy analysis of rotavirus-infection spread and its associated innate immune response in human intestinal epithelial cells

Referees:

Prof. Dr. Oliver Fackler

Prof. Dr. Steeve Boulant

Table of contents

Acknowledgements

I would like to thank my supervisors Prof. Dr. Steeve Boulant and Dr. Megan Stanifer for taking me into their group and allowing me to carry out my PhD under their guidance. Thank you for pushing me to give my all while always taking into consideration my personal matters and points of view. I could not have asked for better mentors. The last years have been nothing but positive for me, you helped me to become more confident and gain experience in many aspects. I felt inspired by your passion for science, which motivated me to keep working hard and not lose my curiosity about the project. I am very grateful for the possibility to test every hypothesis I came up with and every technique that I felt worth trying. I cannot thank you enough for your support.

I want to thank Prof. Dr. Oliver Fackler for being my first referee and always being willing to help me with documentation. Also, thank you for being part of my Thesis Advisory Committee together with Prof. Dr. Volker Lohmann and Prof. Dr. Mathias Heikenwälder. The comments I received during our meetings were very important to steer the project in the right direction. Your suggestions were very appreciated and helped me approach my aims from different perspectives.

I am very grateful to have met Carmon and Camila in the lab, which have made my PhD experience much more enjoyable. Thank you for tolerating my mood swings and listening to endless hours of ranting and nonsense. I am happy we could go through the same obstacles at the same time and help each other out. More importantly, thank you for the moments outside of the lab, all the dinners and parties we shared made me feel more at home. I am also thankful to the people that were in the lab before me, Marta and Popi, who made me feel comfortable when I first joined the group and helped me settle in Germany. Special thanks to the other members of the lab: Cuncai, Jose, Nick, Yagmur, Francesco and Lisa. The lab would not have been so fun without you there, and also thank you for all those days and nights we spent together.

El agradecimiento más importante es para mi mamá y amigos en Argentina. Creo que ninguna de las cosas que logré hubiera sido posible sin su apoyo. Gracias a mi mamá por siempre haberme mantenido en el camino correcto y no haberme dejado bajar los brazos en ningún momento. Incluso cuando en su momento no le veía sentido a muchos cosas, siempre me apoyó y recordó cuales son las cosas que realmente importan. Creo que tampoco hubiera logrado atravesar todo lo que conlleva hacer un PhD sin haber tenido a mis amigos presentes a su manera. Ya sea a través del celular o durante mis visitas a Buenos Aires, siempre estuvieron presentes para recordarme que todo esto valía la pena.

Abstract

Intestinal epithelial cells (IECs) line the surface of the intestinal epithelium and act as a barrier against commensal microbiota. When enteric viruses infect IECs, they induce the production of two types of cytokines, type-I and type-III interferons (IFNs), which can set an antiviral state in the tissue. One of the main pathogens of the intestines is rotavirus, which was shown to elicit the upregulation of both types of IFNs in mice models and commercial cell lines. Nevertheless, the role that each type of IFN plays during rotavirus spread has not been thoroughly evaluated.

Here, I generated a collection of fluorescent tools to evaluate rotavirus infection and spread in different contexts using live cell fluorescence microscopy. I could show that rotavirus efficiently blocks type-I IFN-mediated upregulation of interferon stimulated genes (ISGs) through its NSP1 protein, and only type-III IFNs can be upregulated. Moreover, even in the absence of NSP1, only type-III IFNs were able to rapidly establish an antiviral state in a large number of IECs and prevent the spread of rotavirus. On the contrary, type-I IFNs had a delayed antiviral effect, which allowed infection of IECs by newly produced viruses. Moreover, I could observe that rotavirus infection is strongly dependent on ADP-mediated calcium waves. Live microscopy experiments showed that second rounds of infection seem to take place in areas defined by calcium waves elicited by the first round of infection. Importantly, blocking of ADP signaling through the P2Y1 purinergic receptor prevented new infections from taking place, highlighting the importance of calcium waves during rotavirus infection.

In conclusion, my results suggest that only type-III IFNs are able to control rotavirus infection and spread in IECs, and that type-I IFNs do not seem to play a role at least in the antiviral state of the intestinal epithelium. Furthermore, calcium waves generated by the first round of infection likely alter the integrity of IECs to allow viruses to more easily infect the culture. I propose that IECs can efficiently control the spread of enteric viruses due low amounts of type-III IFNs being needed to set an antiviral response in a notably high number of cells, and that rotavirus-induced calcium waves alters the polarized nature of IECs to facilitate infection.

Zusammenfassung

Darmepithelzellen kleiden die Oberfläche des Darmepithels aus und wirken als Barriere gegen kommensale Mikrobiota. Wenn enterische Viren IECs infizieren, induzieren sie die Produktion von zwei Arten von Zytokinen, Typ-I- und Typ-III-Interferonen, die einen antiviralen Zustand im Gewebe einstellen können. Einer der Hauptpathogene des Darms ist das Rotavirus, von dem gezeigt wurde, dass es die Hochregulierung beider Typen von IFNs in Mausmodellen und kommerziellen Zelllinien hervorruft. Dennoch wurde die Rolle, die jeder IFN-Typ bei der Rotavirus-Ausbreitung spielt, nicht gründlich untersucht.

Hier habe ich eine Sammlung von fluoreszierenden Werkzeugen erstellt, um Rotavirus-Infektionen und die Ausbreitung in verschiedenen Kontexten mithilfe der Fluoreszenzmikroskopie lebender Zellen zu bewerten. Ich konnte zeigen, dass Rotavirus die Typ-I-IFN-vermittelte Hochregulierung von Interferon-stimulierten Genen durch sein NSP1-Protein effizient blockiert und nur Typ-III-IFNs hochreguliert werden können. Darüber hinaus waren selbst in Abwesenheit von NSP1 nur Typ-III-IFNs in der Lage, in einer großen Anzahl von Darmepithelzellen schnell einen antiviralen Zustand herzustellen und die Ausbreitung des Rotavirus zu verhindern. Im Gegensatz dazu hatten Typ-I-IFNs eine verzögerte antivirale Wirkung, was eine Infektion von IECs durch neu produzierte Viren ermöglichte. Außerdem konnte ich beobachten, dass eine Rotavirus-Infektion stark von ADP-vermittelten Kalziumwellen abhängt. Live Mikroskopie Experimente zeigten, dass zweite Infektionsrunden in Bereichen stattzufinden scheinen, die durch Kalziumwellen definiert sind, die durch die erste Infektionsrunde ausgelöst wurden. Wichtig ist, dass die Blockierung der ADP-Signalübertragung durch den purinergen P2Y1-Rezeptor neue Infektionen verhinderte, was die Bedeutung von Kalziumwellen während einer Rotavirus-Infektion unterstreicht.

Zusammenfassend legen meine Ergebnisse nahe, dass nur Typ-III-IFNs in der Lage sind, die Rotavirusinfektion und -ausbreitung in Darmepithelzellen zu kontrollieren, und dass Typ-I-IFNs zumindest im antiviralen Zustand des Darmepithels keine Rolle zu spielen scheinen. Darüber hinaus verändern Kalziumwellen, die durch die erste Infektionsrunde erzeugt werden, wahrscheinlich die Integrität von Darmepithelzellen, damit Viren die Kultur leichter infizieren können. Ich schlage vor, dass Darmepithelzellen die Ausbreitung enterischer Viren effizient kontrollieren können, da

geringe Mengen an Typ-III-IFNs benötigt werden, um eine antivirale Reaktion in einer bemerkenswert hohen Anzahl von Zellen auszulösen, und dass Rotavirus-induzierte Kalziumwellen die polarisierte Natur von Darmepithelzellen verändern, um dies zu erleichtern Infektion.

1 Introduction

1.1 The intestinal epithelium

1.1.1 Structure of the epithelium and cell types

The intestinal epithelium is the largest mucosal tissue in our body, constituting a barrier between ourselves and external environments. One of the main functions of this organ is the absorption of nutrients, and thus, it has undergone morphological adaptations to improve its functions, for example the development of the crypt-villi axis. This structure forms by the invagination of the epithelial monolayer, forming the crypts, and protrusions into the lumen that form the villi. This arrangement not only guarantees an increased surface area, and thus a bigger intake of nutrients, but also the localization of different cell types in specific areas (Figure 1). Intestinal stem cells are localized at the bottom of the crypts, in what is known as the stem cell niche, and give rise to all other cell types in the epithelium [1]. Intertwined between the stem cells are the Paneth cells, which not only secrete antimicrobial molecules but also maintain the identity of stem cells through the secretion of specific growth factors [2]. As stem cells divide, they push cells outside of the stem cell niche, inducing their differentiation into other lineages, for example enterocytes. Enterocytes are highly polarized columnar cells, are the most abundant ones in the intestinal epithelium, and are in charge of absorption, protection against pathogens and the production of digestive enzymes [3]. Goblet cells are located among enterocytes and are more common in the large intestine. Their main function is the secretion of mucus, which prevents microorganisms from being in close contact with epithelial cells and also lubricates the tissue to allow easier movement of food through the intestinal tract [4,5]. Another cell type is the enteroendocrine cell, which secrete hormones into the blood upon different stimuli, regulating digestion and the state of the intestinal barrier [6]. A less common cell type is the Tuft cell, which serve as a source of interleukin-25 in the intestines, which help fight against parasites [7]. Microfold cells (M cells) are the antigen-presenting cells of the intestinal epithelium,

transferring antigens from their apical side to immune cells located at their basolateral side, and thus initiating an immune response against pathogens [8].

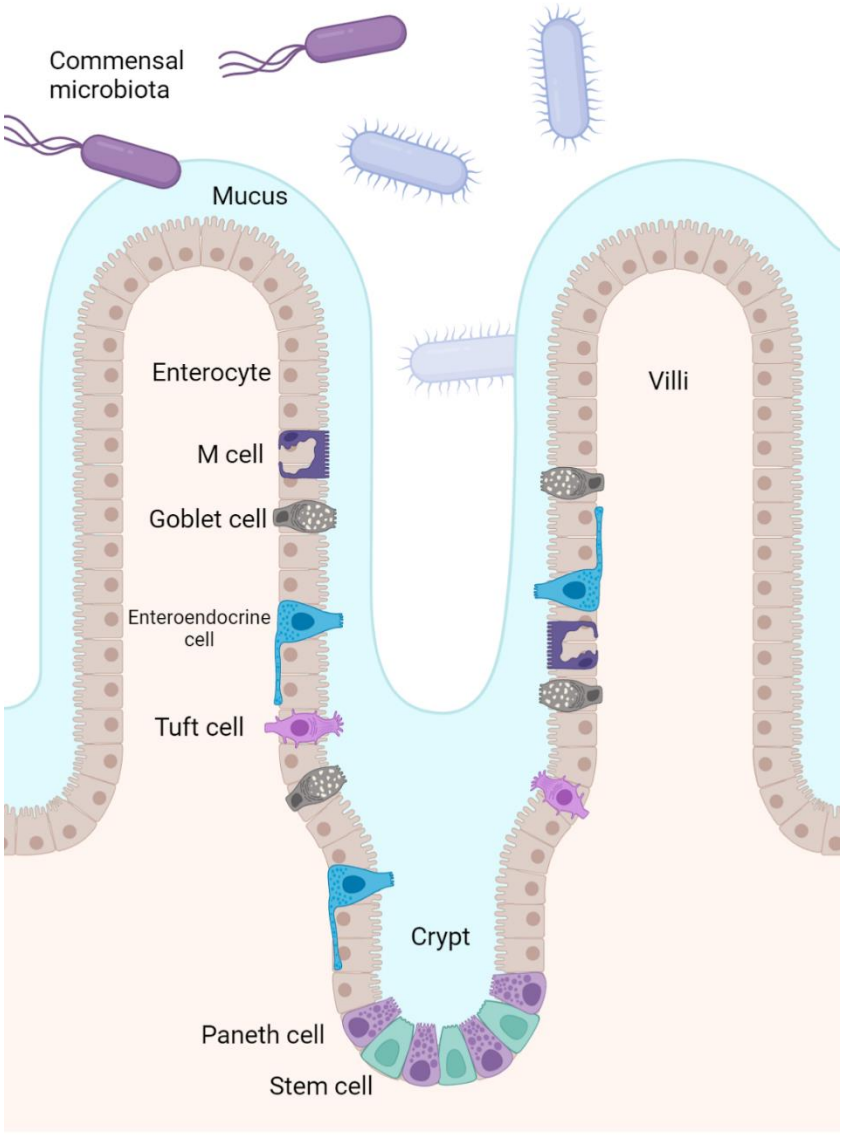

Figure 1. Structure of the intestinal epithelium and different cell types along the crypt-villus axis. The commensal microbiota is found at the lumen of the tissue. Stem cells are located at the bottom of the crypt, surrounded by Paneth cells, which help maintain their identity. As stem cells divide, they push cells outside of the niche and induce their differentiation into the secretory lineages (enteroendocrine, tuft or goblet cells), the absorptive lineage (enterocytes) or M cells. Image created with Biorender.com.

1.1.2 Tight junctions and cell polarization

Intestinal epithelial cells form a tight barrier that protects the underlying tissue from invasion by pathogens. These cells are kept together through the expression of apical

bridging proteins that form adherens junctions (AJs) and tight junctions (TJs) (Figure 2). These structures maintain cell-cell adhesion and associate with the actin cytoskeleton, forming a scaffold that maintains the barrier function of the intestinal epithelium and allows paracellular passage of ions and solutes [9]. The first contacts between neighboring cells are carried out by the extracellular domains of E-cadherin, forming adherens junctions (Figure 2). The intracellular domain of these proteins can bind to catenins, which then allows the complex to interact with the cytoskeleton of the cell [10]. After these connections have been made, tight junctions can be established at the apical side of IECs, preventing microorganisms and toxins from reaching the basal side of the tissue. TJs are composed of three proteins: occludins, claudins, and junctional adhesion molecules (JAMs) (Figure 2) [11]. The extracellular domains of these proteins interact with those of an adjacent cell, and the intracellular ones bind to adapter proteins that allow association with the cytoskeleton. In the case of occludins, two extracellular loops form connections with neighbor cells, while their intracellular domain binds to the zonula occludens 1 and 2 proteins (ZO-1/2), which are key proteins involved in bridging the TJs with the cytoskeleton of the cell. Although the function of occludins is not entirely understood, they have been associated with paracellular permeability and stability of the tight junction belt [12]. Similar to occludins, claudins also possess two extracellular domains that interact with the extracellular domains exposed on neighboring IECs, and also interact with the cytoskeleton through binding to ZO-1/2. These proteins have been involved in a wide variety of functions, for example the formation of ion-selective channels, cell motility, and most importantly, preventing leakage and water loss [13–15]. The third component of TJs are JAMs, composed of two immunoglobulin folds at their extracellular chains, and binding motifs for ZO-1/2 at the intracellular side. Like claudins and occludins, JAMs have been shown to support paracellular permeability and the formation of functional TJs [16]. The establishment of AJs and TJs regulates important processes in intestinal cells, including vesicle trafficking and apical-basal cell polarity. During the early steps of AJ assembly, tight junction components like ZO-1 start to be recruited to the site, and the adhesion protein JAMA recruits the PAR3-PAR6-aPKC complex, a key determinant of apical polarity [11,17]. Through increased recruitment of signaling and tight junction components, for example guanine nucleotide exchange factors for signaling through the GTPases CDC42 and RHOA, actomyosin becomes activated and the formation of tight junctions is initiated. Enrichment of actomyosin is important for determining the shape of

epithelial cells and its interaction with TJs is a key stage during cell polarization. Activated CDC42 GTPase can now interact with the recruited PAR3-PAR6-aPKC complex to develop microvilli, typical of the apical side of polarized epithelial cells, as well as the recruitment of other apical-specific proteins [18,19].

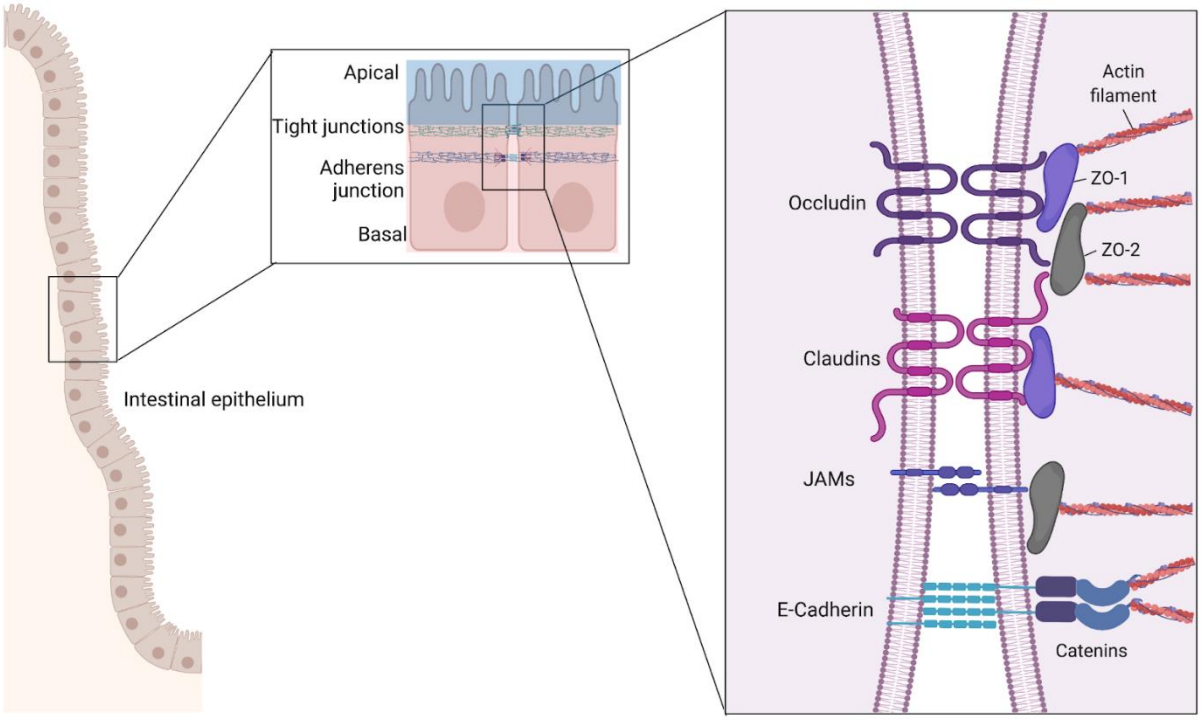

Figure 2. Adherens Junctions (AJs) and Tight Junctions (TJs) are established between intestinal epithelial cells to maintain their barrier properties. The main component of AJs is E-Cadherin, which interacts with the actin cytoskeleton through catenins. TJs are composed of occludins, claudins and JAMs, interacting with the cytoskeleton through ZO-1/2.

1.1.3 Common pathogens and the innate immune response

Besides the digestive and barrier functions of the intestinal epithelium, another important role is combating enteric pathogens while remaining tolerant to the commensal microbiota. This group of microorganisms is composed of viruses, fungi, protozoa and about 100 trillion bacteria by adulthood. These commensal microorganisms help in the digestion process and the development of intestinal immunity [20]. It is known that germ-free mice possess an underdeveloped immunity, lacking key cellular and structural components of their immune system [21]. Unlike the commensal microbiota, enteric viruses can cause serious gastroenteritis, with

approximately 700 million cases per year in children below the age of 5 [22]. The development of electron microscopy allowed the discovery of a great variety of intestinal viruses, which are classified in four families: Reoviridae (reovirus and rotavirus), Caliciviridae (norovirus), Astroviridae (Astrovirus) and Adenoviridae [23]. A summary of different characteristics of the viruses relevant for this work can be found in Table 1 [22].

Pathogen	Capsid organization	Genome	Genomic organization
Astrovirus	Precursor split into smaller fragments	Positive single-stranded RNA	Two ORFs (1a, 1b and 2)
Norovirus	Two structural proteins	Positive single-stranded RNA	Three ORFs (1,2 and 3)
Rotavirus	Four structural proteins	Double stranded RNA	11 individual segments

Table 1. Characteristics of the capsid and genome of viruses relevant for this work. These enteric pathogens are the main cause of gastroenteritis worldwide. Adapted from [22].

In the case of a viral infection in the intestines, intestinal epithelial cells (IECs) can recognize conserved structures that are not present in the host, known as pathogen associated molecular patterns (PAMPs). These motifs can be detected by IECs through pattern-recognition receptors (PRRs), which differ in their localization inside the cell and also the type of molecule they recognize (Figure 3). When viral RNA is released into the cytosol, it is detected by the retinoic acid-inducible gene 1-(RIG-I)-like family of receptors (RLRs): the Retinoic acid-inducible gene I (RIG-I) which detects short uncapped RNA, Melanoma differentiation-associated protein 5 (MDA-5) for longer RNA molecules, and the Laboratory of Genetics and Physiology 2 (LGP2) (Figure 3) [24–26]. Furthermore, the viral DNA present in the cytoplasm can be detected by the cyclic GMP-AMP (cGAMP) synthase (cGAS) receptor [27]. When viral infections take place through the endosomal machinery, the viral genome is recognized by another type of PRR located inside the endosomes, the Toll-like receptors (TLRs).

TLR3, 7 and 8 can detect dsRNA and ssRNA and TLR9 recognize dsDNA (Figure 3) [28].

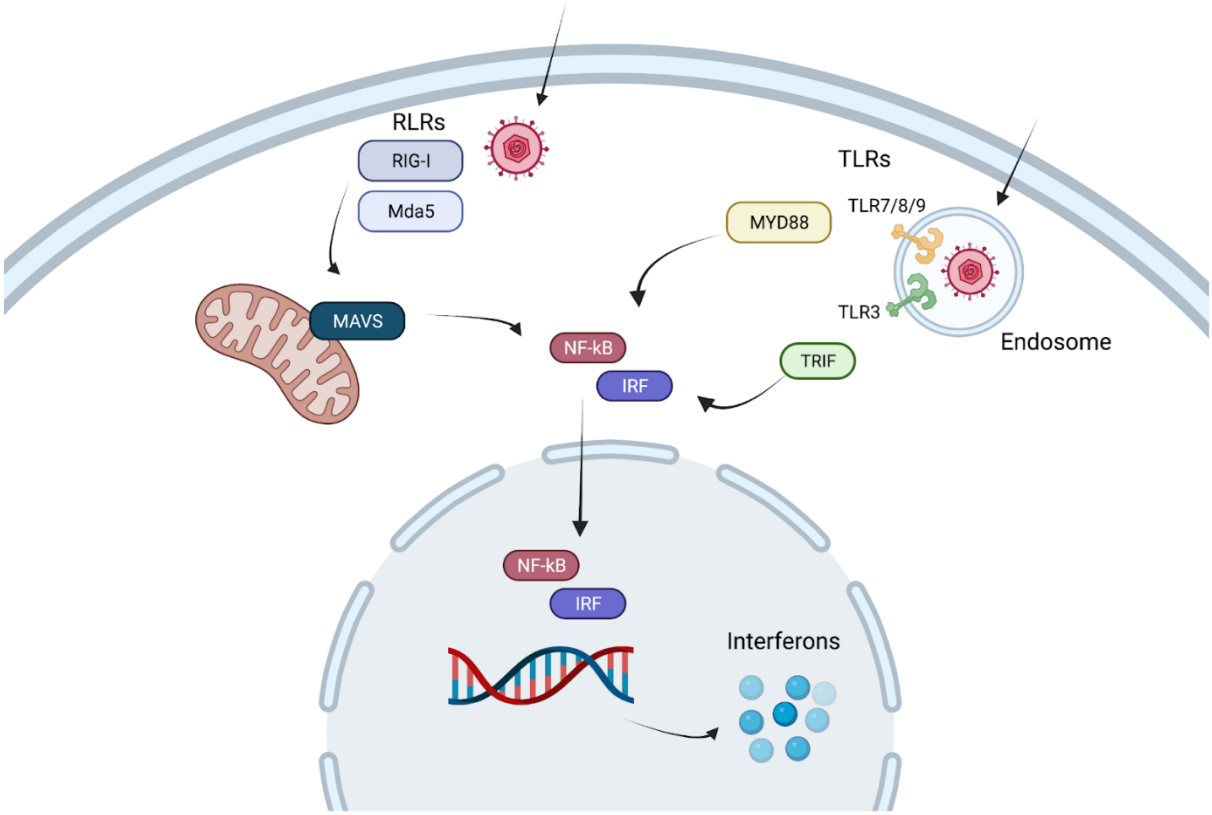

Figure 3. Viral sensing is carried out by several pathogen recognition receptors. The two most common TLRs and RLRs, are depicted here. TLRs detect viral nucleic acids inside endosomes, and induce the nuclear translocation of the transcription factors NF-kB and members of the IRF family through adapter proteins like MYD88 and TRIF. RLRs detect viral genome in the cytoplasm, inducing the nuclear translocation of NF-kB and IRFs through a different pathway involving the mitochondrial protein MAVS. Once in the nucleus, NF-kB and the IRFs induce the production of interferons. Created with Biorender.com.

Upon detection of viral genome by the different cellular sensors, complex pathways are activated to alert neighboring cells of the infection and prevent viral spread. In the case of TLRs, binding to viral genome induces homo-dimerization and recruitment of adaptor proteins like MyD88 and TRIF [29,30]. These adaptors can then interact with signaling molecules belonging to different pathways, converging in the phosphorylation and nuclear translocation of either nuclear factor kB (NF-kB) [29,31] or the interferon regulatory factor (IRF) transcription factors [32]. On the other hand, when RLRs bind to

viral genome, a conformational change exposes their N-terminal CARD domain [33]. RLRs can then use this domain to interact with the mitochondrial protein MAVS, generating aggregates that recruit kinases to the site and activate NF-kB or IRFs [34]. Once in the nucleus, these transcription factors can activate the production of interferons, the most important antiviral cytokines, which alarm cells in the vicinity to promote an antiviral state.

1.2 Interferons

1.2.1 Types of interferons

Upon detection of pathogens through PRRs, a complex cascade leads to the nuclear translocation of the cytoplasmic transcription factors NF-kB and IRFs to induce the transcription of IFNs. These cytokines are key mediators to fight viral infections, acting in an autocrine and paracrine manner to establish an antiviral state. IFNs are classified into three types depending on the set of receptors they use, type-I, type-II and type-III IFNs. The first IFNs to be discovered were type-I IFNs, consisting of the best described IFNs: α, β, ε, κ and ω [35]. The genes encoding for these cytokines are found in chromosome 9 and share great similarity in their sequences, highlighting the possibility of a common origin through gene duplication [36]. All cells are able to produce type-I IFNs, but the different subtypes show specificity for different cell types [37]. The two most important IFNs in this group are IFNα, which is mainly secreted by leukocytes, and IFNβ, mostly produced by fibroblasts [37,38]. All members of this family signal through the same two receptors, IFN-α receptor 1 (IFNAR1) and IFN-α receptor 2 (IFNAR2), which are expressed by all cells in our body (Figure 4) [39]. The only member of the type-II IFNs family is IFNγ, produced mainly by immune cells like activated T cells, natural killer cells and macrophages. This cytokine is an immunomodulator that can act against intracellular bacteria and parasites [40]. The receptor complex through which this type of IFN acts is a tetramer composed of two subunits of IFN-γ receptor 1 (IFNGR1) and two of IFN-γ receptor 2 (IFNGR2) [41]. Two decades ago, two research groups discovered a new family of IFNs, type-III IFNs, which exhibited great similarities with type-I IFNs in terms of antiviral response. These cytokines are also known as IFNλ, and so far four different type III IFNs have been described: IFNλ1 (also known as interleukin-29), IFNλ2 (also known as interleukin-28a), IFNλ3 (also known as interleukin-28b) and IFNλ4 [42]. The genes coding for these IFNs are clustered in chromosome 9, exhibiting

a great degree of similarity in their sequences, except for the recently discovered IFNλ4 [43]. Type-III IFNs show similarity in their sequences with the IL-10 superfamily of cytokines, explaining why one of the two receptors they signal through is the IL-10R2 (Fig 1.4) [44]. The other subunit of the heterodimeric receptor is the IFNLR1, the expression of which is restricted to epithelial cells of the lung, skin, intestines, and also some immune cells [45,46]. This restriction of type-III IFNs to specific tissues highlights the possibility that they exhibit beneficial properties at mucosal surfaces. In fact, studies have shown that epithelial cells can produce especially large amounts of these cytokines upon viral infections [47–49].

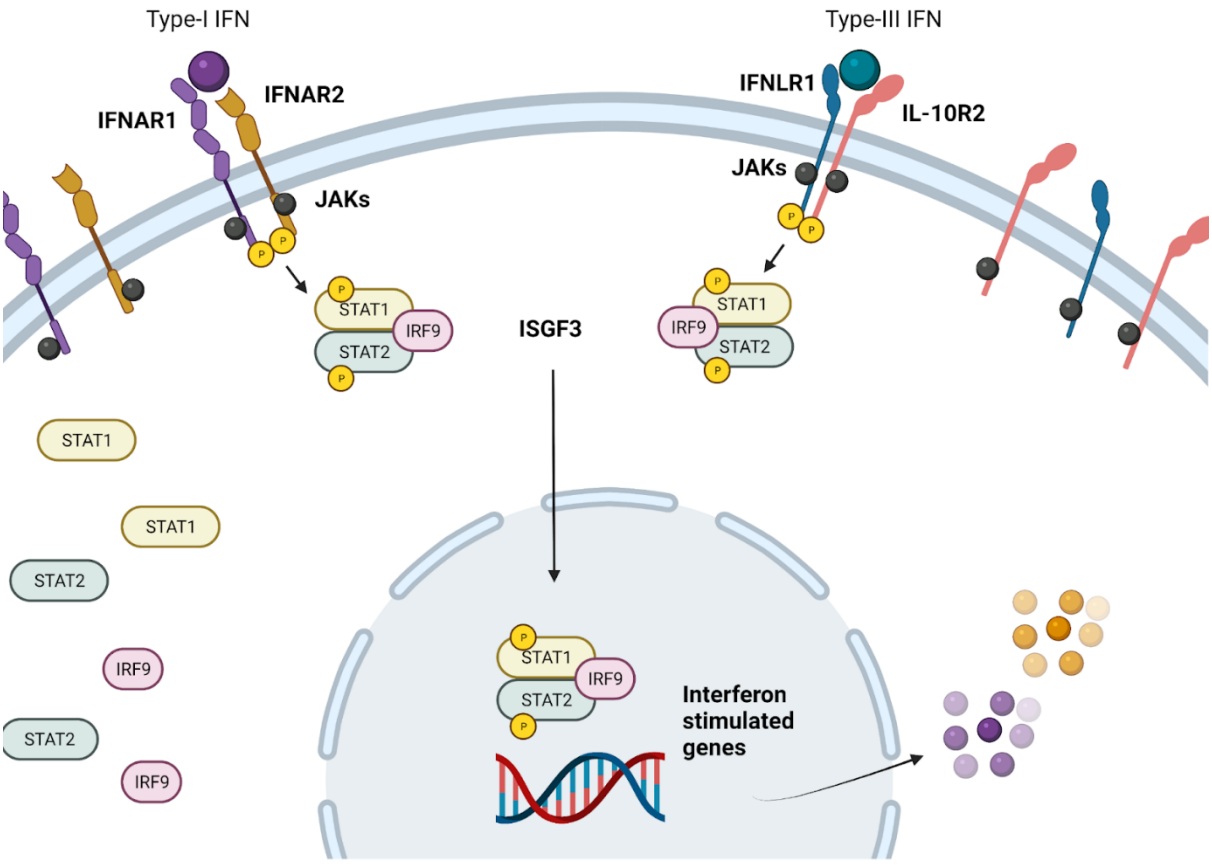

Figure 4. Infected intestinal epithelial cells secrete IFNs, which bind to a specific set of receptors: IFNAR1 and IFNAR2 for type-I IFNs, and IFNLR1 and IL-10R2 for type-III IFNs. Binding to their receptors brings janus kinases (JAKs) closer, allowing the phosphorylation of specific tyrosine residues in the inner domain of the receptors. This induces the recruitment of signal transducer and activator of transcription proteins (STATs) to the site, allowing their phosphorylation and dimerization. STATs interact with IRF9 to form the ISGF3 complex, which translocates to the nucleus to activate the expression of interferon stimulated genes and fight viral infections.

1.2.2 JAK-STAT signalling

Upon secretion of IFNs by the infected cells, these cytokines can act in an autocrine or paracrine manner, binding to a specific set of receptors and starting a signaling cascade to establish an antiviral response (Figure 4). Since all components of the pathway are already present in the cell at a basal level, this signaling happens at a rapid rate. As mentioned above, type-I IFNs bind to the IFNAR1 and IFNAR2 receptors, whereas type-III IFNs bind to the IFNLR1 and IL-10R2 receptors. Binding of IFNs to these sets of receptors induces a conformational change in their intracellular region, bringing them closer to each other. Constitutively-bound members of the janus kinases (JAK) family (JAK1, JAK2 and TYK2) can now trans-phosphorylate tyrosine residues on the opposite receptor (Figure 4) [50]. Once these residues are phosphorylated, signal transducer and activator of transcription (STAT) proteins are recruited to the site and also become phosphorylated by the JAKs. In the case of stimulation by type-I and type-III IFNs, only STAT1 and STAT2 proteins are recruited and phosphorylated. Activated STATs can now form homo or heterodimers, and also interact with IRF9, forming the IFN-stimulated gene factor 3 (ISGF3) complex (Figure 4) [51]. ISGF3 can then translocate to the nucleus and activate the transcription of hundreds of interferon stimulated genes (ISGs) through a conserved upstream region, the IFN-stimulated regulatory elements (ISREs) [52].

1.2.3 Interferon-stimulated genes

ISGs play the most important role in controlling viral infection and spread, targeting key steps of their replication cycle to shut them down. Although most ISGs are activated through the IFN-dependent JAK-STAT pathway, some can be induced directly by the IRFs, possibly to avoid pathogen strategies blocking IFN sensing or negatively regulating JAK-STAT signaling [53]. Some of the best described ISGs target viral entry, for example the myxovirus resistance Mx1 and Mx2 genes, which encode for guanosine triphosphatases (GTPases). Studies have shown that Mx1 forms a ring-like structure through self-oligomerization, which helps capture viruses at early entry steps [54]. Aggregation of these ring-like structures around viral components activates Mx1 GTPase activity to induce its degradation. Mx2 has also been shown to interact with the capsid of some viruses and prevent the viral genome from reaching the nucleus and integrating into the genome [55]. Other ISGs target viral translation and replication, for example ISG15, an ubiquitin-like protein that targets viral proteins through

ISGylation, a process similar to ubiquitylation [56]. Through this process, ISG15 can prevent nuclear import of viruses, nucleoprotein oligomerization to reduce viral protein synthesis or the release of new particles, among other targets [57]. Moreover, ISGs can also prevent viral release from the cell, but this group of antiviral genes are not very well understood. An example of them is Viperin, which prevents HIV-1 and Influenza A virus budding from the membrane by targeting enzymes involved in altering membrane fluidity [58,59].

1.2.4 Type-I versus type-III IFN signaling

Since both type-I and type-III IFNs are secreted by intestinal epithelial cells upon viral infections and share the same signaling pathway, their antiviral functions were believed to be redundant [24]. As mentioned above, type-I IFNs establish an antiviral state in most tissues of the body, whereas type-III IFNs protect specifically mucosal surfaces, highlighting a preference of these epithelia for the latter [38,46]. Intestinal epithelial cells express especially high levels of IFNLR1 and type-III IFNs, and thus, only these cells are sensitive to the antiviral actions of this type IFNs [60,61]. On the contrary, secreted type-I IFNs have been shown to be important to protect viral dissemination to the underlying tissues, having little antiviral impact on the intestinal epithelium itself. This is the case during reovirus infection in mice, in which large amounts of type-III IFNs are produced by ICEs compared to those of type-I, and their actions are restricted to specific tissues [62]. These differences have also been described thoroughly in the case of murine norovirus, with type-III IFNs hindering viral replication at the epithelium and reducing viral load, and type-I IFNs preventing systemic spread [63,64]. Interestingly, it has been shown that the ability of mice to sense each type of IFN is age-dependent, with the intestines of suckling mice being able to respond to both type I and III IFNs, whereas adult mice only respond to type-III [65]. Besides the tissue specificity, several studies have shown that the magnitude and kinetics of the antiviral state elicited by these two types of IFN are different. During infection with Hepatitis C virus of the human hepatoma cell line Huh7.5, both types of IFN upregulated almost the same group of ISGs, but type-I IFNs did it more rapidly, whereas type-III IFNs had a more delayed and sustained action [66]. Similarly, in lung carcinoma epithelial cells A549 infected with vesicular stomatitis virus (VSV), both IFNs upregulated similar genes but a delayed type-III IFN-mediated antiviral state was observed [67]. Similar results have been

observed at the intestinal epithelium, in which treatment of IECs with both type-I and type-III IFNs showed an upregulation of ISGs but with opposite kinetics [68]. On one hand, type-I IFNs induced a strong and short lasting antiviral state, whereas type-III IFNs established a weak but long lasting immune profile. Furthermore, these differences were shown to be unrelated to the expression levels of each receptor, but the kinetics were intrinsic to the signaling pathway downstream of each receptor complex [68]. Unlike type-I IFNs, type-III IFNs rely exclusively on the mitogen-activated protein kinases signaling pathway, highlighting non-redundant functions of this type of IFN in the intestines [69]. Since intestinal epithelial cells are in constant contact with microbiota, it is likely that type-III IFNs establish a weak and long-lasting immune state, avoiding constant and acute inflammation of the tissue. Interestingly, the polarized nature of IECs also impacts their ability to respond to different types of IFNs. Studies have shown that non-polarized murine intestinal cells respond weakly to type-III IFNs, but when cells are cultured for long periods and reach polarity the induction of ISGs is strongly enhanced [70]. This is not observed in type-I IFNs, in which the induction of ISGs is not affected by cell polarity in murine intestinal cells. Since intestinal epithelial cells exhibit a polarized status in healthy epithelia, it is expected then that they respond better to secreted type-III IFNs upon a viral challenge.

1.3 Rotavirus

Rotavirus is the main cause of gastroenteritis worldwide, accounting for approximately 40% of gastroenteritis hospitalizations in children below the age of 5 [71]. More than 200,000 children die of rotavirus gastroenteritis and associated diarrhea per year [72]. The first vaccines against rotavirus, Rotarix and RotaTeq, were commercialized by GSK and Merck respectively. These vaccines have shown to be efficient in preventing approximately 85% of rotavirus gastroenteritis cases in low mortality regions, and about 50% in high mortality regions [73]. Similar vaccines were later developed in Asia, showing comparable efficacy. Due to these low protection rates in high mortality regions, understanding how rotavirus replicates and spreads in human intestinal epithelial cells and how it can be controlled is critical as it could offer novel therapeutic solutions to control rotavirus infection.

1.3.1 Structure

Rotaviruses' shape resembles a wheel under electron microscopy, taking their name from the Latin word for wheel "rota", since they are visualized as a ring-like structure with small spikes [74]. The genome is segmented and consists of 11 genes, each coding for one protein, except NSP5 and NSP6 which are coded by segment 11. Six of these segments code for structural proteins (VP1, VP2, VP3, VP4, VP6 and VP7), and five for non-structural proteins (NSP1, NSP2, NSP3, NSP4 and NSP5/6) [74]. Viral particles are composed of three structures, an outer capsid, an intermediate capsid and the inner core, where the viral double-stranded RNA genome is located. The infectious particles possess these three layers, and thus are referred to as triple-layered particles (TLPs). These virions are made of an outer layer of VP7 proteins forming a shell, and VP4 proteins creating spikes all around it (Figure 5). Underneath, VP6 proteins form the middle layer that covers an inner layer of VP2 proteins, which surround the viral genome as well as VP1 and VP3 proteins (the replication complex). The VP4 protein needs to be cleaved by intestinal proteases to undergo conformational changes that allow cell entry [75].

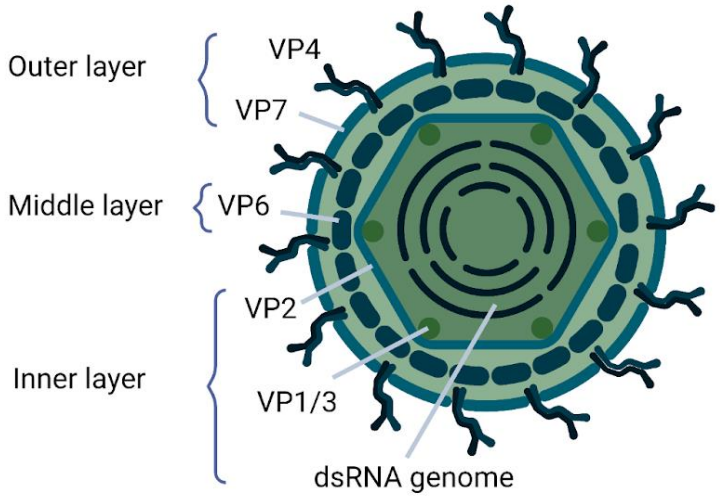

Figure 5. Rotavirus is composed of three protein layers. The outer layer is formed by the spike protein VP4 and the shell protein VP6. Underneath, VP6 proteins constitute the middle layer and surround the inner layer protein VP2. The double-stranded RNA genome is localized at the core, as well as the replication complexes formed by VP1 and VP3.

1.3.2 Replication cycle

Once activated by trypsin-like proteases, the VP4 protein can interact with sialic acid present in membrane receptors [76]. The process of virus entry is not well understood, but it is believed to take place through receptor-mediated endocytosis or direct membrane penetration (Figure 5). Interestingly, some components of the endosomal machinery are required for entry, for example Rab7 has been shown to play a role [77,78]. Due to low amounts of Ca2+ in endosomes, the outer layer of TLP dissolves, giving rise to double-layered particles (DLPs) (Figure 5) [79]. Outer layer proteins are believed to help lyse the endosomal membrane and release DLPs into the cytoplasm [80]. As mentioned above, below the VP2 protein layer, transcription complexes formed by VP1 (a RNA-dependent RNA polymerase) and VP3 (a capping enzyme) are in charge of genome replication [81]. Once DLPs reach the cytoplasm, the negative strand of the genome is used as a template to synthesize new positive single-stranded RNA molecules, which can leave the DLP through specific channels. These molecules can be used to generate double-stranded RNA genomes, or for translation of viral proteins [82].

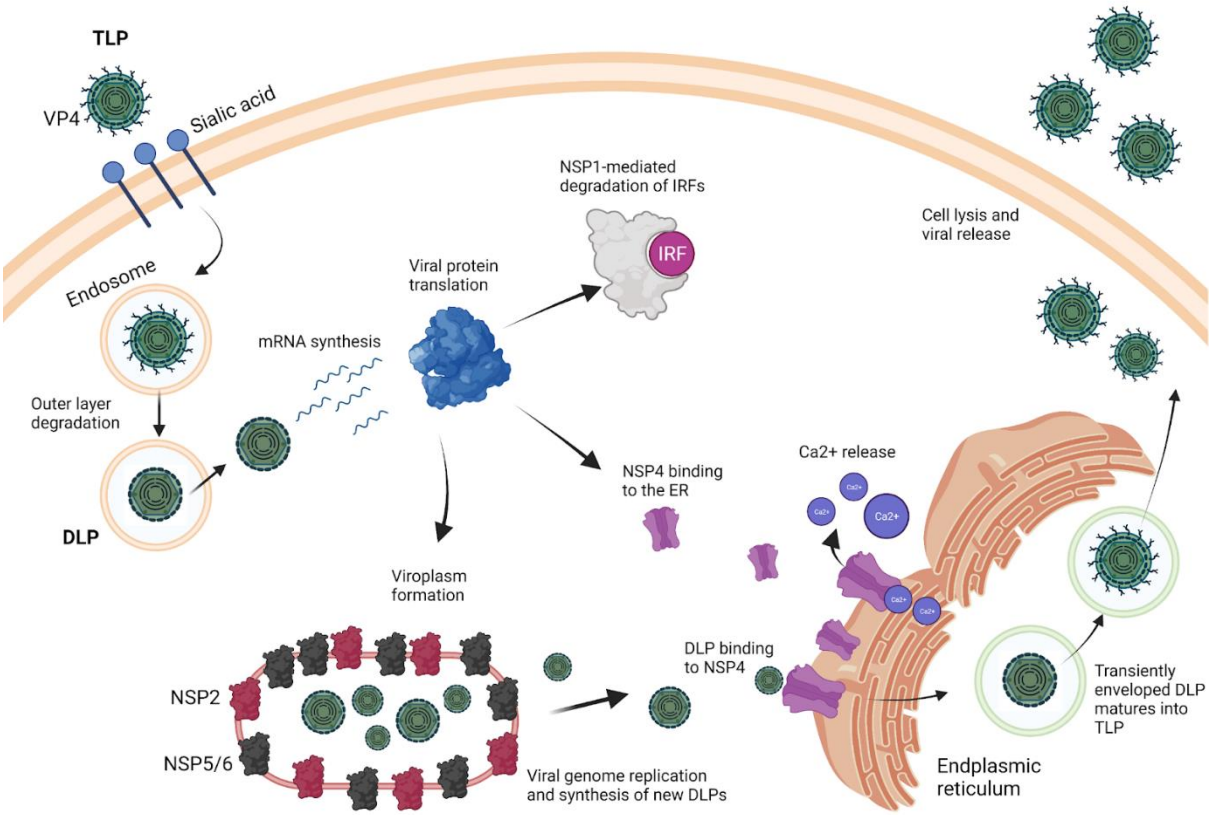

Figure 5. The rotavirus replication cycle. Triple-layered particles (TLPs) can bind to sialic acid found on the cell membrane following trypsin-induced maturation of VP4. TLPs then get endocytosed and low levels of Ca2+ in endosomes induce the degradation of the outer layer, forming double-layered particles (DLPs). Lysis of the endosome by outer layer proteins releases DLPs into the cytoplasm. DLPs are transcriptionally active, releasing large amounts of mRNA, which get translated into the different viral proteins. NSP1 antagonizes the immune system by inducing the degradation of the interferon regulatory factors (IRFs). NSP4 binds to the ER, inducing the release of Ca2+ for stabilization of TLPs and cytoskeleton damage. NSP2 and NSP5/6 help form the viroplasm, where double-stranded RNA genome is synthesized and new DLPs assemble. New DLPs bind to NSP4 at the ER and are transiently enveloped, where proteins of the outer layer assemble to form new TLPs. Newly produced viral particles are released upon cell death.

Once the NSP2 and NSP5 proteins are translated, they induce the formation of the viroplasm, inclusion bodies where replication takes place [83]. The NSP4 proteins associates itself with the endoplasmic reticulum (ER), where it acts as a receptor for DLPs [84] and also induces the cytoplasmic release of Ca2+ from ER storages [85]. The viroporin function of NSP4 has been shown to be due to its interaction with Ca2+ sensor STIM1, and it helps stabilize the outer layer of newly formed TLPs [86]. The NSP3 protein prevents translation of cellular mRNA by hindering the ability of the polyA binding protein (PABP) to bind to mRNA. NSP3 hijacks the function of PABP, but only binds to newly synthesized viral ssRNA at one of its ends, and to the translation factor eIFG4 at the other end, circularizing the RNA and helping its translation [87,88]. NSP1 is the main antagonist of the innate immune response, it has been shown to induce the degradation of many components of the cascade, for example IRF3 [89] and MAVS [90], preventing IFN production. For packaging of new viral particles, the different ssRNA interact with the core proteins (VP1 and VP3) and also VP2 [91] to form the core of TLPs, but it remains unclear how the 11 different segments are correctly arranged. This core is encapsulated by VP6 proteins to form DLPs and leave the viroplasm by budding through the ER, acquiring a temporary envelope that is later replaced by VP4, VP6 and VP7 proteins [92,93]. Interestingly, rotavirus TLPs are released from the cells through different mechanisms, in the case of non-polarized cells they do so by cell lysis, but in polarized cells they bud out and lose their envelope in the process [94,95]. See Figure 5 for an illustration of the rotavirus replication cycle and Table 2 for a summary of the functions of each viral protein.

Viral protein	Function
VP4	Spike protein for binding to cell receptors
VP7	Main component of the outer layer
VP6	Main component of the middle layer
VP2	Main component of the inner layer
VP1	RNA-dependent RNA polymerase
VP3	Viral capping enzyme
NSP1	Interferon antagonist
NSP2	Formation of the viroplasm
NSP3	Inhibition of translation of cellular proteins
NSP4	Viroporin for Ca2+ release. Intracellular receptor of DLPs. Enterotoxin.
NSP5/6	Formation of the viroplasm

Table 2. Main functions of the 11 viral proteins encoded in the rotavirus genome.

1.3.3 Rotavirus infection-induced innate immune response

1.3.1.1 Type-I and type-III IFN-mediated control of rotavirus

The ability of type I and III IFNs to control rotavirus infection has been evaluated in mice, commercial cell lines and also in primary cells. These studies have shown that rotavirus infection induces the production of IFNs, however, each model induced a unique set of IFNs (IFNλ1, IFNλ2,3 or IFNβ1) to combat rotavirus infection [96–98]. IECs of suckling mice have been shown to upregulate the production of IFNβ and IFNλ2,3 upon infection, and the replication of the virus was significantly enhanced in mice lacking a functional IFNLR1, whereas those lacking IFNAR1 receptors behaved like WT mice [99]. This study showed that IFNλ2,3 acted specifically on IECs, preventing viral replication, whereas IFNβ acted on lamina propria cells, allowing higher viral loads at the villi. Nevertheless, a second study has shown that rotavirus replicates efficiently both in WT mice and in mice insensitive to IFNs, but this depended on whether the virus was of murine or primate origin [65]. Only homologous murine rotavirus was able to avoid the innate immune system and spread, whereas heterologous simian rotavirus replicated poorly in IFNLR1-/- and IFNAR1-/- mice. In this case, both types of IFN were able to block viral replication at the intestinal epithelium, highlighting the evolutionary adaptations of rotavirus to antagonize its host species.

In the case of commercial cell lines the difference in antiviral properties of type-I and type-III IFNs are less clear. The colorectal cancer cells Caco2 exhibited an upregulation of IFNα, IFNβ and IFNλ1 upon rotavirus infection, but not of IFNλ2,3 [96]. Nevertheless, no IFNs were detected in the supernatant of infected cells and there was no upregulation of ISGs, indicating a viral shutdown after the transcript level. Furthermore, pretreating cells with any type of IFN before infection showed significant reduction in viral genome, indicating that they exhibit similar antiviral properties. Similarly, the colorectal cancer cell line HT-29 showed an upregulation of type-I IFNs upon infection with rotavirus, showing that these IFNs could play an important role during viral replication at the intestinal epithelium [100]. Moreover, the HT-29 and HCA-7 colorectal cancer cells showed an upregulation of IFNβ upon infection both at the transcript level and also in the supernatant [101]. This is also the case for children infected with rotavirus, in which there is an increased level of IFNα/β in their blood [102]. On the contrary, the MA104 monkey kidney cell line showed that type-I IFNs have little impact

on rotavirus replication [103]. The development of stem cell derived intestinal organoids has shed light on the importance of type-I and type-III IFNs in a model that better resembles the human in vivo-like situation. Human intestinal enteroids have shown a strong upregulation of IFNλ1 and IFNλ2 upon infection, and of IFNβ1 to a lesser extent [98]. Blocking either type-I or type-III IFN receptors through neutralizing antibodies showed that the upregulation of ISGs was stimulated exclusively by type-III IFNs, but this did not restrict viral replication. On the contrary, exogenous treatment of organoids with IFNs showed a significant decrease in viral genome, with type-I IFNs having a stronger effect. These results were obtained in another study, in which all types of IFNs had antiviral effects when added exogenously, showing that extra-epithelial sources of IFN could be key in stopping viral replication and spread [96].

1.3.1.2 NSP1, the IFN antagonist

More than two decades ago, a study showed that rotaviruses that have acquired random rearrangements in their segment 5 (coding for NSP1) formed significantly smaller plaques than WT viruses [104]. These rearrangements generated premature stop codons and truncated proteins, which were unable to interfere with the immune system and failed to help rotavirus spread. Later studies showed that the main targets of NSP1 were the interferon regulatory elements (IRFs) 3, 5, 7 and 9, which were degraded upon overexpression of the viral protein [105,106]. NSP1 was shown to target the dimerization domain shared by all IRFs, and thus block their nuclear translocation and induction of IFNs [107]. Besides the IRFs, NSP1 is also able to interfere with type-I IFN signaling through blocking the activation of NF-κB and inducing the degradation of IFNAR1 [108,109]. It has been suggested that NSP1 acts as an E3 ubiquitin ligase through a RING domain at its N terminus, although evidence to prove this is lacking. Only IRF3 was shown to interact directly with NSP1, but other targets may do so through other intermediary proteins [110].

1.3.4 NSP4 and ADP-mediated calcium waves

When trying to understand rotavirus pathogenesis, a group showed that administration of purified NSP4 to mice readily induced diarrhea, becoming the first viral enterotoxin

described [111]. Moreover, mice treated with purified NSP4 exhibited an increase in intracellular levels of Ca2+ at their intestinal epitheliums [112]. This is achieved through viroporin domains present in NSP4, which allow the formation of an ion channel at the ER that specifically allows the passage of Ca2+ [85,113]. Increased levels of cytoplasmic Ca2+ induce autophagy and also damage of the cytoskeleton and tight junctions [114,115]. Rotavirus infection has been shown to cause alterations in microfilaments and generation of stress fibers [114]. Moreover, this study showed that the distribution of microtubules was altered upon infection, with tubulin observed towards the periphery of cells. One of the main components of tight junctions in epithelial cells, occludin, has shown to get degraded in Caco2 cells upon infection with rotavirus, whereas the scaffolding proteins ZO-1 and ZO-3 remained intact [115]. On the contrary, another study carried out on Caco2 cells showed that all three components of tight junctions (ZO-1, Occludin and Claudin) exhibited significant alterations upon infection, which was reflected in the decrease of transepithelial resistance [116]. Similarly, NSP4 treatment of sparse MDCK-II canine cells showed blockage of tight junction formation, observed by the lack of ZO-1 overtime. Interestingly, this process was reversible, as normal tight junction formation was recovered upon removing NSP4 [117]. For a long time, it was believed that infected cells release NSP4, which acts on neighboring cells to induce dysregulation through the activation of Ca2+-activated chloride channels, consequently causing diarrhea [118,119]. Furthermore, dysregulation of enteroendocrine cells present in the epithelium induce the release of serotonin, activating vomiting centers in the central nervous system [120]. Nevertheless, a recent study has challenged this hypothesis and showed that in fact the signaling molecule secreted by infected cells to dysregulate the epithelium is ADP [121]. Cytoskeleton damage and mechanical stress could induce the release of ADP from infected cells, which acts on the purinergic receptor P2Y1 of neighboring cells. This activates a signaling cascade that causes an increase in the levels of cytoplasmic Ca2+ of uninfected cells and subsequent diarrhea, generating an ADP-dependent intercellular calcium wave (Figure 6). Calcium waves and their effects on the cytoskeleton are described in more detail in section 1.4.

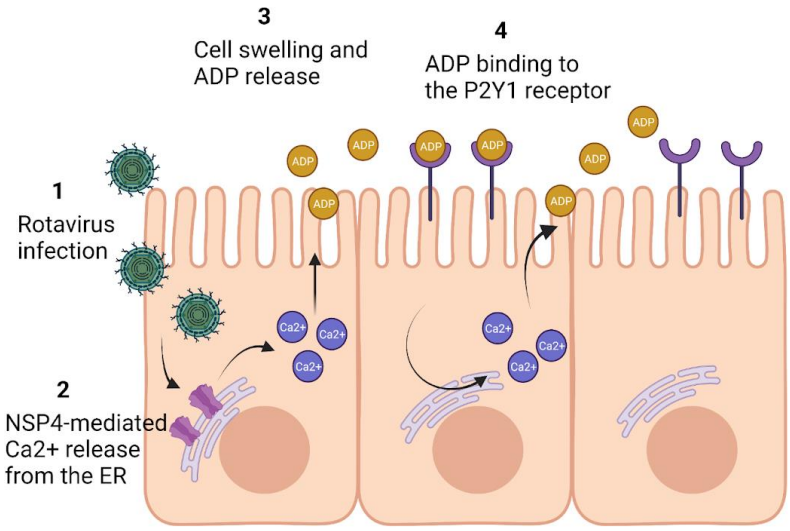

Figure 6. ADP-mediated intercellular calcium waves. The rotavirus NSP4 protein acts as a viroporin, binding to the ER and inducing the release of Ca2+ into the cytoplasm. Ca2+ increase induces damage of the cytoskeleton, cell swelling and the consequent release of ADP. ADP can bind to the purinergic receptor P2Y1 of neighboring cells, activating a signaling cascade that induces the release of Ca2+ from the ER, echoing the process along the epithelium.

1.4 Calcium waves

1.4.1 Intracellular calcium oscillations

Increases in the cytoplasmic levels of Ca2+ is part of many different pathways and takes place during muscle contraction, communication between neurons, apoptosis and regulation of the cell cycle, among other functions [122–125]. Interestingly, some transcription factors are activated at specific Ca2+ concentrations, for example NF-AT, which is only activated at low concentrations, or NF-κB at high transient ones [126]. Elevated levels of cytoplasmic Ca2+ are also associated with cell death, where it can either induce “death signals” and activate endonucleases or proteases, or it can be the consequence of other cell damage events [127]. The cytoplasmic level of Ca2+ is approximately 10,000 times lower than the extracellular concentration of Ca2+, which creates a gradient across the plasma membrane. To prevent toxic levels of Ca2+ in the cytosol, high amounts of it are stored in the ER and only released upon specific signals [128]. Ca2+ homeostasis is mainly maintained by the plasma membrane calcium pump (PMCA) and the sarco/endoplasmic reticulum calcium pump (SERCA), which use ATP to pump Ca2+ across membranes [129,130]. In most cases, calcium signaling is

mediated by the production of inositol-1,4,5-trisphosplate (IP3), which binds to the IP3 receptor at the ER and causes the release of calcium into the cytoplasm from cellular stores [131]. IP3 and Ca2+-mediated positive and negative feedback signaling can generate oscillations inside the cell by amplifying and weakening the signal, and thus helping regulate different cellular processes [132]. This concerted regulation of Ca2+ levels in the cytoplasm is known as Ca2+-induced Ca2+ release. Once activated by a weak stimulus, IP3 can rapidly diffuse across the cytoplasm, inducing the release of Ca2+ in a uniform manner and generating an intracellular calcium wave. On the contrary, a strong stimulus generates high levels of IP3 and a Ca2+ spike, with no calcium wave, likely having opposite effects on the cell [127].

1.4.2 Intercellular calcium waves

After the generation of an intracellular stimulus, Ca2+ can act on neighboring cells as a messenger that helps synchronize oscillatory signals among a [133]. This mechanism was discovered more than two decades ago in ciliated epithelial cells of the lung, in which mechanical stimulation increases the beat frequency of a cell, and this stimulus travels to adjacent cells in a Ca2+-dependent manner [134]. This process was later shown to take place in other tissues, including liver epithelial cells, endothelial cells and B cells of the pancreas [135–137]. Besides mechanical stimuli, glutamate and electrical stimulation can also be the starting point of intercellular calcium waves [138,139]. Importantly, intercellular signaling has been shown to be dependent on gap junctions for passage of diffusible molecules among cells. For example, gap junction blockers have been shown to stop calcium waves, and cells lacking gap junctions that were transfected with connexins could suddenly generate calcium waves [133,140]. It is then believed that an initial stimulus activates the generation of IP3, which travels to adjacent cells via junctions and induces the cytoplasmic release of Ca2+ from the ER. Importantly, since IP3 is only produced in the initial cell and diffuses as it moves to neighboring cells, intercellular calcium waves can only progress along the tissue until no more IP3 is left [141]. In the case of cells lacking junctions, ATP is believed to be fundamental in the establishment of intercellular calcium waves. This was first described in mast cells, where stimulated cells used ATP as a signaling molecule to initiate waves through an extracellular route [142]. Importantly, purinergic receptor blockers were demonstrated to partially stop calcium waves in epithelial cells, which

possess gap junctions, showing the implication of both pathways in wave propagation [135]. This was also shown to be the case for pancreatic B cells, which progress calcium waves through ADP acting on the P2U purinergic receptors [137].

1.4.3 Impact of calcium on the cytoskeleton and tight junctions

The involvement of calcium during tight junction formation has been proposed during the early 90s, after observations showing an increase in the levels of cytoplasmic Ca2+ during polarization [143]. Furthermore, it was shown that chelation of intracellular Ca2+ with permeable chelators retards the formation of tight junctions, visualized for example by a delay in the translocation of ZO-1 to the cell membrane [144]. It is likely that the importance of Ca2+ during these processes is due to kinases like protein kinase C requiring Ca2+ to function properly during tight junction assembly [145,146]. Importantly, depletion of Ca2+ from ER reservoirs by stimulation with thapsigargin, which inhibits calcium-ATPases, prevents the establishment of tight junctions in epithelial cells [145]. Cells pretreated with this drug did not show an increase in transepithelial electrical resistance over time and failed to properly stabilize and assemble tight junction proteins into the cytoskeleton [145]. Although this is not completely understood, this study highlighted that ER reservoirs of Ca2+ must be intact during the establishment of cell to cell contacts, and that their depletion due to stress or infections prevent the formation of a polarized monolayer. Interestingly, the inability of ZO-1 to associate itself with the cytoskeleton occurred in the absence of a significant change in the levels of intracellular Ca2+, but it rather relied on the presence of the Ca2+ stores themselves [145]. Similar results were recently observed in keratinocytes treated with high doses of thapsigargin or UVB, in which the formation of tight junctions was disrupted [147].

1.5 Objectives

Intestinal epithelial cells are the first line of defense against enteric viruses. Upon viral infection, a complex signaling cascade is activated and interferons are produced to alert the system and prevent viral spread. Both type-I and type-III IFNs are produced and sensed by intestinal cells, signaling through the same pathway and activating the production of hundreds of interferon stimulated genes. One of the main enteric pathogens is rotavirus, which has been shown to induce the production of type-I and type-III IFNs *in vivo* and *in vitro.* Additionally, rotavirus has been shown to shutdown the immune response to increase its spread efficiency. Nevertheless, the differences between these different types of IFNs in preventing rotavirus replication and spread are not well understood and seem to depend on the model used. Studies focusing on murine models have shown contradictory results, with some showing that only type-III IFNs can prevent viral spread, and others that neither type of IFN can impact virus replication and spread. Studies on human cell lines and organoids are limited and only focused on the amount of each IFN type produced upon infection, or on IFN pretreatments before infection. The main limiting factors in these studies are the lack of cell lines insensitive to a specific type of IFN, and the possibility of tracking infection and IFN response with live cell fluorescence microscopy. In this study, I generated a large set of fluorescent tools to track viral infection and IFN sensing in long live microscopy experiments, which allowed me to elucidate the differences between type-I and type-III IFNs in preventing viral spread. Furthermore, rotavirus has been recently shown to use ADP as an extracellular messenger to increase its pathogenicity, although not much is known about the impact of ADP on viral replication and spread. I have thus also focused on the impact that this signaling pathway may have on infected and neighboring cells and how it helps rotavirus spread more efficiently.

This thesis addresses three different objectives:

1. Generate fluorescent tools that allow the visualization and tracking of viral infection and sensing of interferons.

2. Elucidate the differences in the innate response established by type-I and type-III IFNs upon rotavirus infection

3. Determine the importance of calcium-induced ADP signaling during rotavirus replication and spread.

Altogether, this thesis focused on the generation of a large set of fluorescently tagged proteins and knock-out vectors to better understand how the innate immune cascade takes place during rotavirus infection. To this end, a collection of generated cell lines was imaged with long live cell fluorescence microscopy, aiming to expand the current knowledge of type-I and type-III IFN-mediated immune response. This methodology allowed me to determine single cell phenotypes and discover a new way of establishing a second round of infection. All together these studies help to broaden our understanding of how mucosal surfaces fight pathogens and how pathogens use several techniques to subvert these attacks.

2 Results

2.1 Generation of fluorescent reporters for visualization of viral infection-induced innate immune response

2.1.1 Reporters of onset of innate immune response

In order to efficiently track the innate immune response taking place in the intestinal epithelium upon viral infection, it is essential to first detect which cells have been infected. To this end, I have generated a series of fluorescent reporters based on the early steps of the innate immune cascade, which lead to the production of type-I and type-III IFNs. A summarized version of the generated reporters can be found in Table 3.

2.1.1.1 IRFs nuclear translocation and IFN promoters

As mentioned before, upon detection of viral genome by intestinal epithelial cells, transcription factors like IRF3 and IRF7 can undergo conformational changes and translocate to the nucleus. Once in the nucleus they can induce the upregulation of type-I and type-III IFNs to stop the virus from replicating. My first approach was then to use the nuclear translocation of these transcription factors as a read out for what cells have been infected. The eGFP-IRF3 fusion protein has been shown to efficiently translocate to the nucleus [148] upon stimulation, and a pWPI eGFP-IRF3 vector was received from Marco Binder (DKFZ, Heidelberg) as a gift. Nevertheless, when evaluating the ability of eGFP-IRF3 to translocate upon transfection with the double-stranded RNA mimic Poly I:C, the Boulant lab has previously observed that in confluent cultures of colorectal carcinoma T84 cells a considerable low number of cells exhibited nuclear translocation (Figure 7).

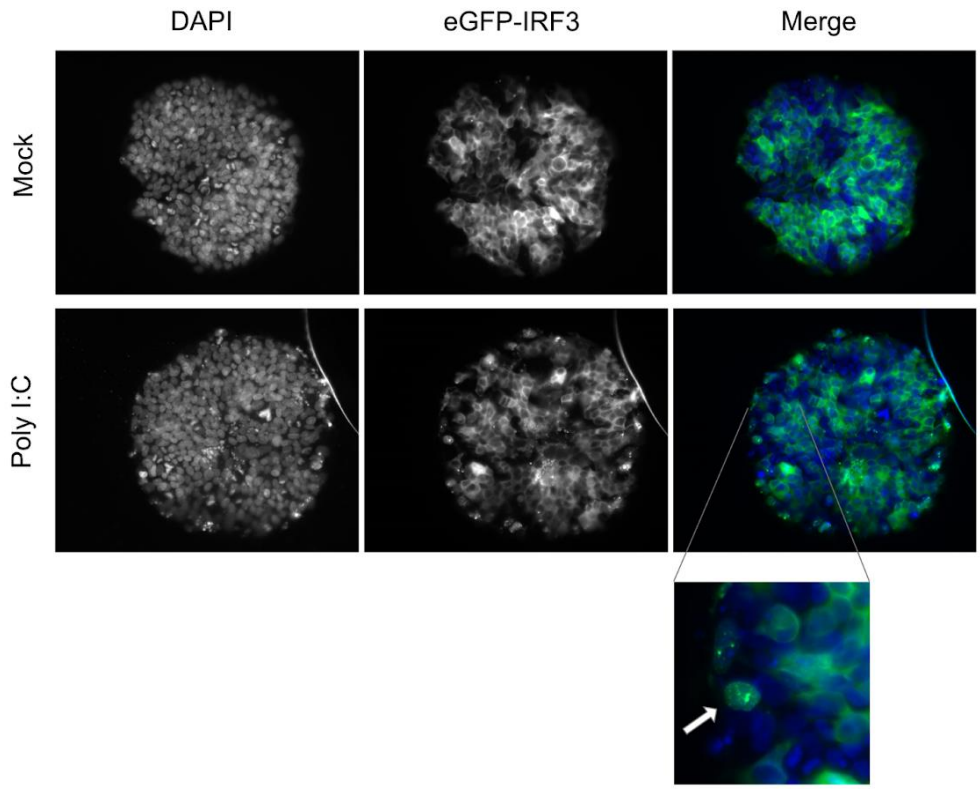

Figure 7. T84 cells carrying the eGFP-IRF3 fusion protein were mock treated or transfected with Poly I:C, fixed 4 hours post treatment and imaged using a PerkinElmer spinning disc microscope. Nuclear translocation of eGFP-IRF3 can be observed in a low number of Poly I:C treated cells (white arrow).

Since it is possible that these cells use a different IRF to activate IFN pathways, I generated IRF7-eGFP and eGFP-IRF7 fusion proteins through HiFi DNA Assembly. A pDONR-IRF7 (a kind gift from Marco Binder, DKFZ, Heidelberg) was used as template to amplify IRF7 and insert it before or after eGFP in a PENTR221 vector using primers 1-8 (Table 9). I used this entry vector to generate a pWPI lentiviral vector and later T84 cell lines overexpressing the fusion proteins. Both cell lines exhibited cytoplasmic localization of IRF7 when non-stimulated, but only the IRF7-eGFP fusion protein showed nuclear translocation 4 hours post-transfection with the double stranded RNA mimic poly I:C (Figure 8A). To study whether there is a difference in the nuclear translocation efficiency of IRF7-eGFP between sparse and confluent cells, cells were seeded at a 10% or 50% confluency respectively. Cells were transfected with poly I:C for 4 hours, fixed and translocation of the fusion protein was evaluated by microscopy. As observed before with the eGFP-IRF3 construct, upon reaching confluency, the IRF7-eGFP protein stopped translocating efficiently to the nucleus upon treatment with

poly I:C (Figure 8B). This represented a major drawback, since intestinal epithelial cells are normally cultured at high confluency to mimic the natural state of the epithelium.

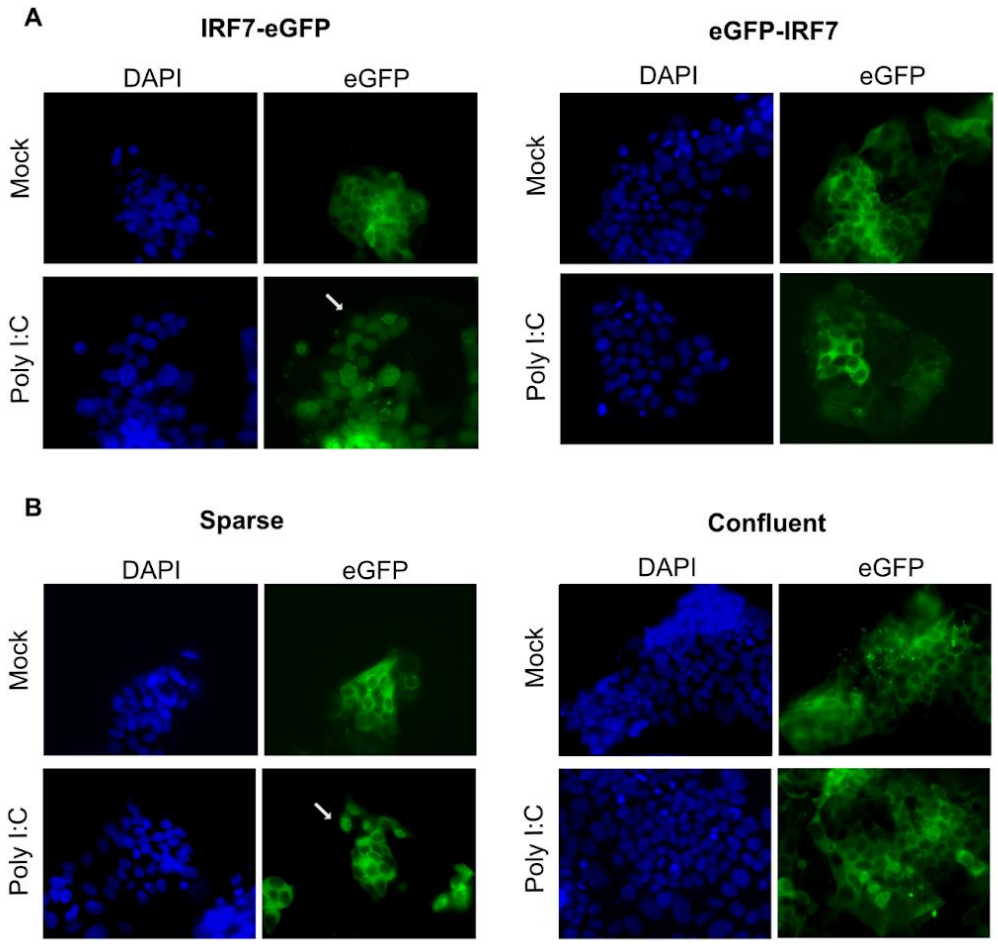

Figure 8. T84 cells were transduced with lentiviruses carrying either the IRF7-eGFP or eGFP-IRF7 constructs and selected using puromycin to achieve a population where 95% of cells were expressing the construct. (A) IRF7 expressing cells were mock transfected or transfected with poly I:C for 4 hours, fixed and nuclear translocation was examined. Only the IRF7-eGFP fusion protein showed translocation upon treatment (white arrow). (B) Nuclear translocation of IRF7-eGFP was compared between sparse and confluent cells. Poly I:C only induced translocation in sparse cells and not in confluent ones (white arrow).

Since fluorescent reporters based on the nuclear translocation of IRFs did not show promising results, I continued by focusing on tagging fluorescent proteins to the promoter region of type-I and type-III IFN genes. I have previously obtained a lentiviral vector carrying the fluorescent protein mCherry under the control of the promoter region of the IFNβ1 gene (Figure 9A) (a kind gift from Ronald Dijkman, University of Bern), which was used to generate a T84 cell stably carrying the reporter. Interestingly,

I could observe a high basal expression of mCherry, likely due to constitutive production of IFNβ1 in the cell line (Figure 9B, upper panel). To test the efficacy of the reporter during viral infection, T84 cells were seeded in 8-well glass bottom ibidi chambers 24 hours before the experiment, transfected with Poly I:C and the intensity of mCherry tracked over time using a PerkinElmer spinning disc microscope. Cells treated with Poly I:C did not show a considerable increase in mCherry levels, with only some cells exhibiting a notable change (Figure 9B).

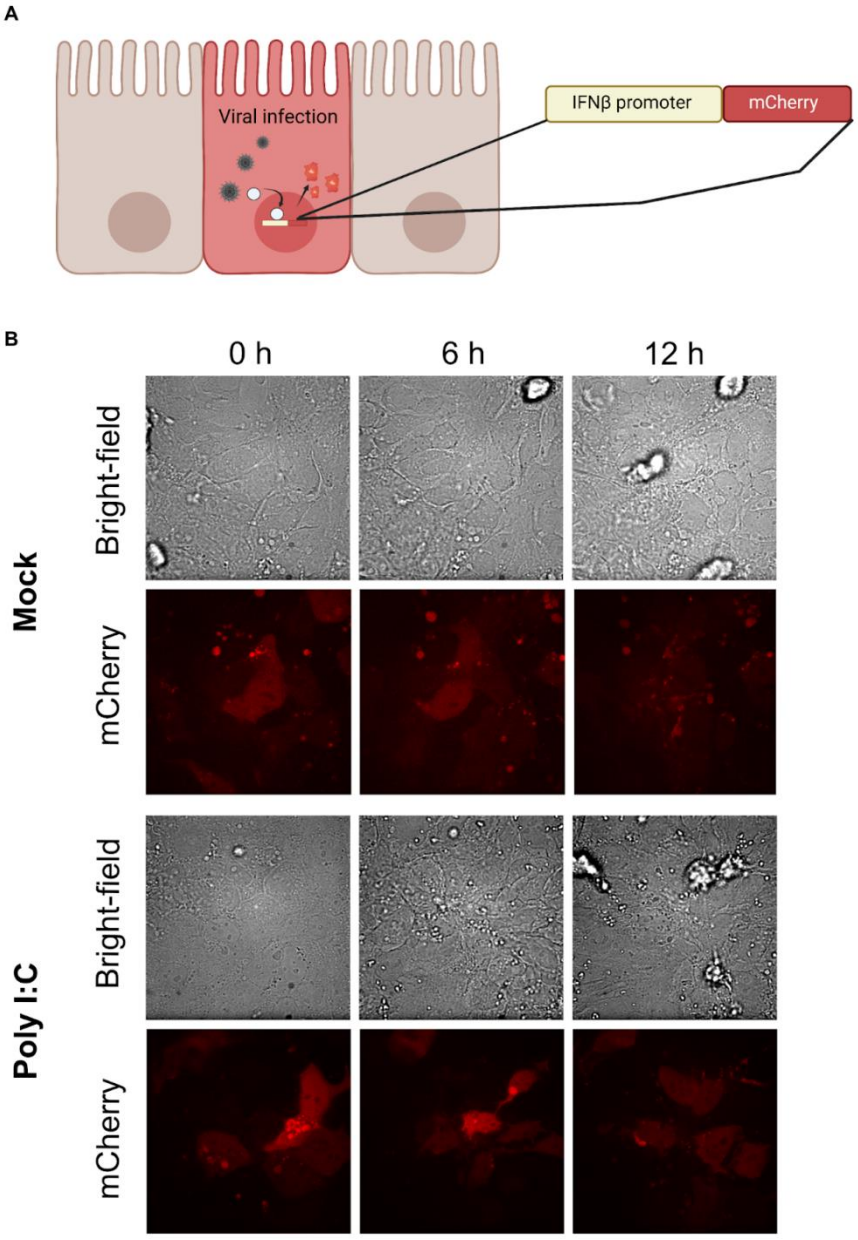

Figure 9. (A) Schematic showing IECs transduced with the pIFNβ-mCherry reporter. Upon sensing of viral infection, IRFs translocate to the nucleus and activate the production of mCherry. Generated with Biorender.com (B) T84 cells carrying the pIFNβ-mCherry were mock treated or treated with poly I:C and

imaged every 30 minutes with a PerkinElmer spinning disc microscope. Representative images at 0, 6 and 12 hours post treatment are shown.

To generate a similar reporter for type-III IFNs, I used the genome of T84 cells as a template to amplify the promoter region of the IFNλ2 and IFNλ3 genes using primers 9 and 10. These primers were designed based on [149], and amplify a ~1,000 bp fragment of the promoters and also contain overhangs that allow its annealing to a pENTR221 backbone containing mCherry at the C' terminus. This backbone was amplified from a pENTR221-pMx1-mCherry vector using primers 4 and 11, and the two fragments were fused to generate a pENTR221-pIFNλ2,3-mCherry. As described before, this entry vector was used to generate the promoterless lentiviral vector pLentiX1-pIFNλ2,3-mCherry and a T84 cell line carrying the reporter (Figure 10A). Unlike the pIFNβ1-mCherry reporter, this cell line exhibited no basal activation of the reporter (Figure 10B, upper panel). To test the induction of the promoter and increase of mCherry intensity, T84 cells carrying the reporter were seeded in 24-well plates, infected with reovirus and imaged over time using a CellDiscoverer 7 microscope. Interestingly, infected cells showed a significant increase in mCherry intensity starting at 12 hpi, which continued increasing during the full live experiment (Figure 10B). Fluorescent reporters based on tagging IFN promoters showed promising results, since unlike the nuclear translocation of STAT2, the intensity of mCherry was readily visualized. Nevertheless, the activation of each promoter is limited to the type of IFN produced by the cell line of interest and the type of stimulus.

2.1.1.2 Astrovirus and Norovirus infection

Another approach to detect infected cells that I have considered was adapting a reporter previously generated to detect infection by hepatitis C virus (HCV) [150] to detect infection by Astrovirus and Norovirus. This reporter was generated by fusing eGFP to an SV40 nuclear localization sequence (NLS) and the mitochondrial protein MAVS (eGFP-NLS-MAVS). In a basal state eGFP is located at the mitochondria, but upon infection by HCV, the viral protease cleaves MAVS and releases eGFP, which translocates to the nucleus due to the NLS. I have received a lentiviral vector containing this reporter (pWPI eGFP-NLS-MAVS, a kind gift from Volker Lohman,

Universitätsklinikum Heidelberg), and introduced the restriction site *CATATG* for the enzyme NdeI in between NLS and MAVS by site-directed mutagenesis (pWPI eGFP-NLS-NdeI-MAVS) (see section 4.2.6).

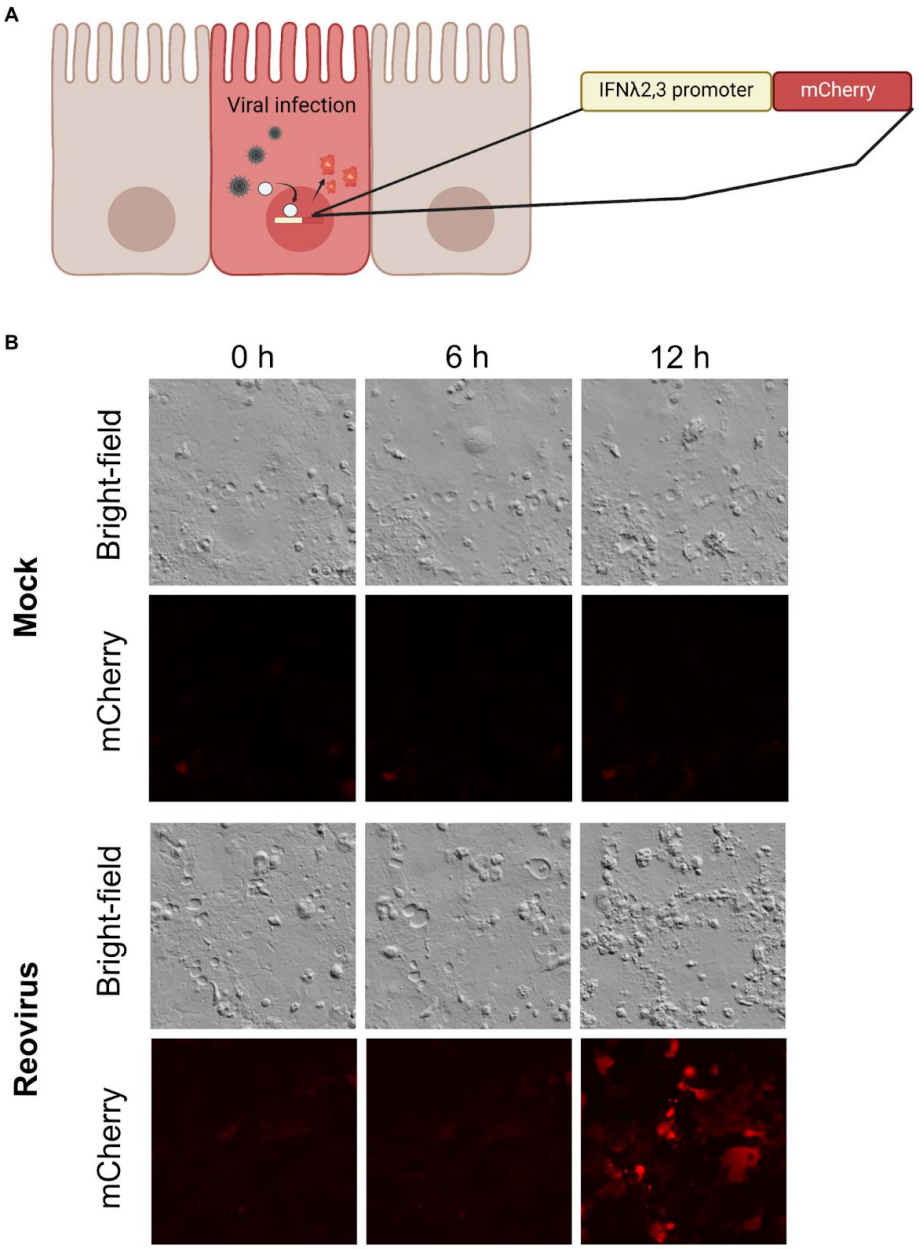

Figure 10. (A) Schematic showing IECs transduced with the pIFNλ2,3-mCherry reporter. Upon sensing of viral infection, IRFs translocate to the nucleus and activate the production of mCherry. Generated with Biorender.com (B) T84 cells carrying the pIFNλ2,3-mCherry were mock infected or infected with reovirus and imaged every 30 minutes with a CellDiscoverer7 microscope. Representative images at 0, 6 and 12 hours post infection are shown.

This site was used for insertion of oligonucleotides containing restriction sites found in the polyproteins produced by Astrovirus and Norovirus, and thus, allow cleavage of the reporter upon infection (Figure 11A). In the case of Astrovirus, the restriction sites Gln567-Thr568 [151] and Glu654-Ile655 [152] were used as targets. 66-bp oligonucleotides based on the viral genome were designed to contain 30 bp of linker to the left and right of the restriction site: (oligos number 12 and 13 for cleavage site Gln567-Thr568 and oligos number 14 and 15 for Glu654-Ile655). Furthermore, to allow ligation into the vector, NdeI sites were added to each end of the oligos: TATG at the 5' end and CA at the 3' end (see Table 9 and section 4.2.3.1). Ligation of the restricted vector with these oligonucleotides was carried out using a T4 ligase (see section section 4.2.3.1), generating the lentiviral vectors pWPI eGFP-NLS-Astro Cleavage 1-MAVS and pWPI eGFP-NLS-Astro Cleavage 2-MAVS. CaCo2 cells were transduced with lentiviruses carrying the reporters, and immunofluorescence showing confirm their correct localization at the mitochondria in a basal state (Figure 11B, upper panel). To test for their efficiency, 100,000 CaCo2 cells expressing the reporter were seeded in 24-well plates, infected with Human Astrovirus for 16 hours, fixed and stained. Neither of the reporters showed nuclear translocation upon viral infection, and all cells that were positive for astrovirus infection still maintained the tag at the mitochondria indicating that cleavage did not occur (Figure 11B, lower panel).

In the case of Norovirus, the cleavage sites found in the polyprotein between NS1.2 and NS3, and the one between NS3 and NS4 were cloned into the reporter [153]. As described above for the Astrovirus reporters, the 6 bases corresponding to the cleavage site, in addition to 18 bases the left and right of the cleavage site and the overhangs for annealing into the empty vectors were synthesized as oligonucleotides. Oligos 16 and 17 were used for cleavage 1 (NS1.2-NS3) and oligos 18 and 19 for cleavage 2 (NS3-NS4), generating the lentiviral vectors pWPI eGFP-NLS-Noro Cleavage 1-MAVS and pWPI eGFP-NLS-Noro Cleavage 2-MAVS respectively. These vectors were used for generation of lentiviruses and stably transduced hepatocellular carcinoma Lunet cells (a kind gift from Dr. Lohmann, Universitätsklinikum Heidelberg), in which eGFP could be visualized attached to the mitochondria (Figure 11C, upper panel). Due to difficulties in amplification of human norovirus in commercial cell lines, I tested the efficacy of the reporters by transfecting Lunet cells with a plasmid carrying the norovirus protease under the control of a T7 promoter (pTM_HA_Age_NS6, Dr. Lohmann, Universitätsklinikum Heidelberg). These Lunet cells were previously

transduced with a construct that allows the production of a T7 polymerase (Dr. Lohmann's group), and thus allow transcription of the transfected pTM_HA_Age_NS6. 100,000 cells were seeded in 24-well plates and transfected with 800 ng of pTM_HA_Age_NS6 using Lipofectamine 2000 (ThermoFisher Scientific), the media was changed after 8 hours, and cells were fixed 24 hours post transfection. Cells transfected with the norovirus protease showed nuclear localization of eGFP, whereas those mock transfected showed localization at the mitochondria (Figure 11C, lower panel). These results highlighted the efficiency of the system in allowing the visualization of cells infected with human norovirus.

Since it is known that Astroviruses and Noroviruses normally attach to the endoplasmic reticulum (ER) during viral replication, I considered generating a variation in the reporter and replacing MAVS for the ER protein SEC61B (Figure 12A). To achieve this more easily, I first moved the eGFP-NLS-Cleavage-MAVS constructs to a smaller vector, a pENTR221. Primers 20 and 21 were used on all viral cleavage reporters to add AttB cloning sites at each side, allowing Gateway cloning for generation of the entry vectors. Once the pENTR221-eGFP-NLS-Cleavage-MAVS vectors were obtained, I amplified the entire backbones but left the MAVS sequence out using primers 2 and 22. These were joined through HiFi assembly with the fragment coding for SEC61B, amplified from pUC_CMV-mEmerald-Sec61 (Prof. Dr. Oliver Fackler, Universitätsklinikum Heidelberg) using primers 23 and 24. The two fragments were ligated, obtaining the entry vectors pENTR221-eGFP-NLS-Cleavage-SEC61B that were used as described before to generate lentiviral vectors and transduced cell lines. CaCo2 cell lines transduced with the ER versions of the Astrovirus reporter efficiently displayed eGFP at the ER by microscopy (Figure 12B, upper panel). Nevertheless, infection with astrovirus did not seem to induce cleavage and nuclear translocation of eGFP, possibly due to a more complex structure of the cleavage site needed for the protease to recognize it (Figure 12B, lower panel). On the contrary, Lunet cells transduced with this alternative version of the norovirus reporters again showed efficient nuclear translocation of eGFP upon transfection with the norovirus protease (Figure 12C).

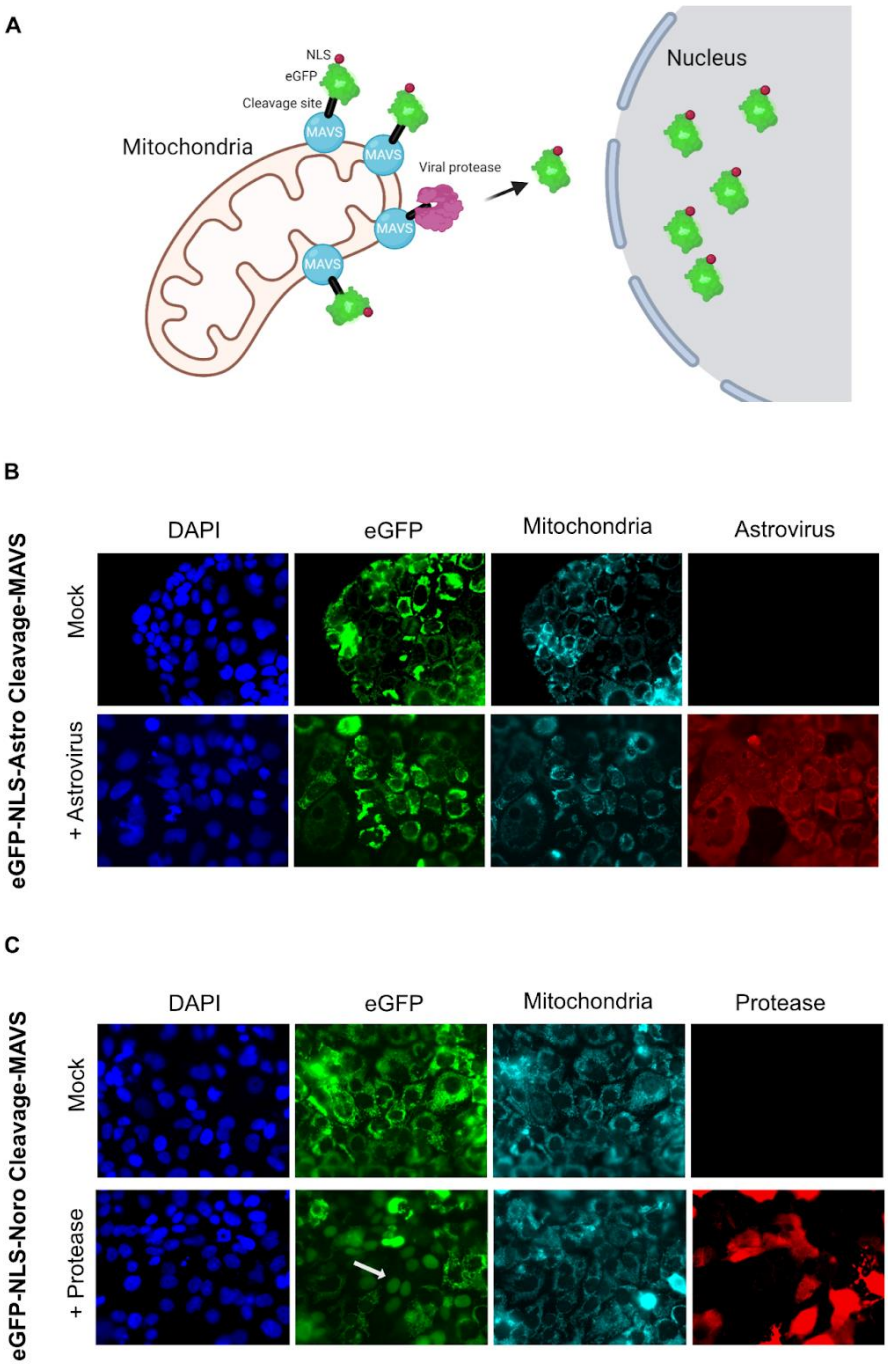

Figure 11. Cells were transduced with lentiviruses carrying either the Astrovirus or the Norovirus MAVS reporters. (A) Schematic of the eGFP-NLS-MAVS viral cleavage reporters. Generated with Biorender.com (B) CaCo2 cells carrying the eGFP-NLS-Astro Cleavage-MAVS reporters were infected with Astrovirus, showing no nuclear translocation of eGFP. (C) Lunet cells carrying the eGFP-NLS-Noro Cleavage-MAVS reporters transfected with a plasmid encoding the norovirus protease, showing efficient nuclear translocation of eGFP (white arrow). Mitochondria staining is done by targeting Cytochrome C.

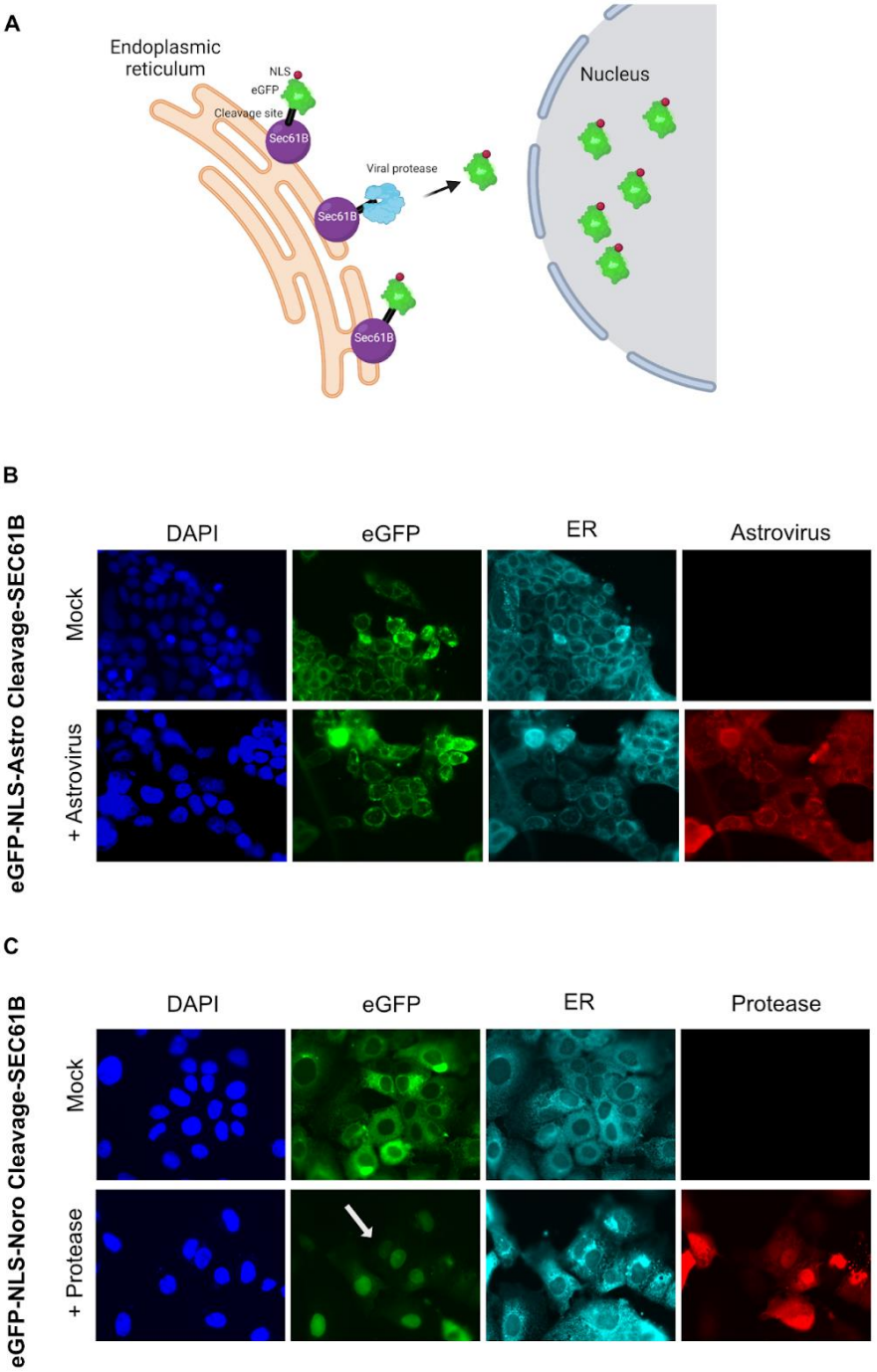

Figure 12. Cells were transduced with lentiviruses carrying either the Astrovirus or the Norovirus SEC61B reporters. (A) Schematic of the eGFP-NLS-Sec61B viral cleavage reporters. Generated with Biorender.com (B) CaCo2 cells carrying the eGFP-NLS-Astro Cleavage-SEC61B reporters were infected with Astrovirus, showing no nuclear translocation of eGFP. (C) Lunet cells carrying the eGFP-NLS-Noro Cleavage-SEC61B reporters transfected with a plasmid encoding the norovirus protease, showing efficient nuclear translocation of eGFP (white arrow). ER staining is done targeting protein disulfide isomerase (PDI).

2.1.1.3 Fluorescent rotaviruses

Rotaviruses carrying different fluorescent proteins as an extra gene in their genome were received from collaborators (Dr. John Patton, Indiana University). These viruses carry either the gene for the green protein UnaG or the red protein mKate fused to their NSP3 gene, and thus the fluorescent protein is only visualized after viral replication and translation of viral proteins [154]. Besides the WT version of the viruses, NSP1-deficient versions were received, which contain a deletion of 17 amino acids at the C' terminus of NSP1, hindering their ability to block the induction of interferons (Figure 13A) [155]. To validate that the fluorescent proteins can be used as a robust reporter of rotavirus infection, I infected the T84 colorectal carcinoma cells with UnaG or mKate rotavirus at an MOI of 1, and 24 hpi I fixed the cells for RNA-FISH targeting the rotavirus genome. Cells were imaged using a PerkinElmer spinning disc microscope. Results showed that all cells that were positive for the RNA-FISH fluorescent probes were also positive for UnaG or mKate, confirming that this system can act as a robust reporter for rotavirus infection (Figure 13B).

2.1.2 Reporters of interferon sensing

Once infected cells are identified, it is of interest to detect which cells in the culture are sensing the secreted IFNs and going into an antiviral state. The first steps after type-I and type-III IFN sensing are the phosphorylation of STAT1 and STAT2, the assembly of the ISGF3 complex with IRF9, and its nuclear translocation for activation of interferon stimulated genes. A Summarized version of the generated reporters can be found in Table 3.

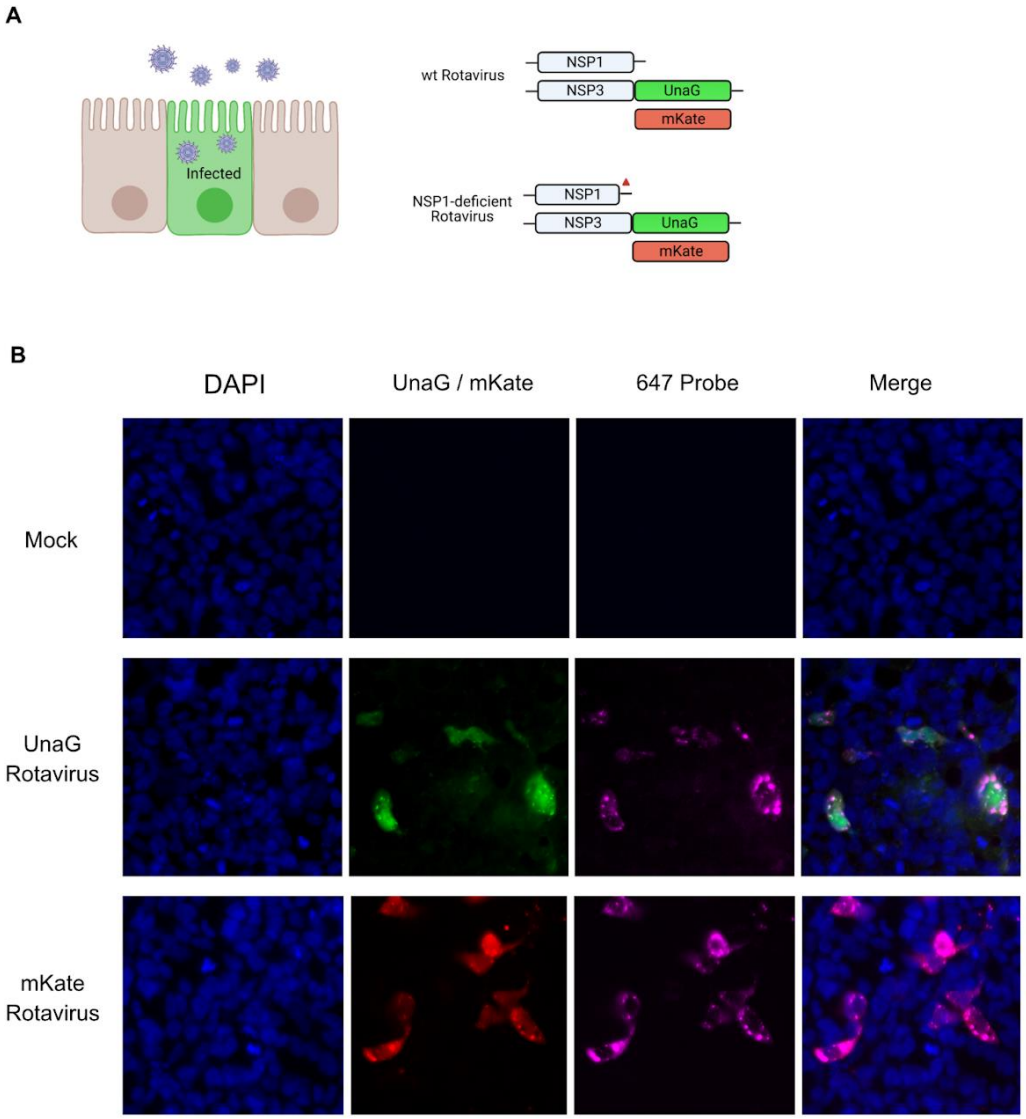

Figure 13. (A) Schematic showing epithelial cells fluorescing upon rotavirus replication and translation of viral proteins (left), and genome of the WT and NSP1-deficient rotavirus (right). (B) T84 cells were infected with WT UnaG or mKate rotavirus and RNA-FISH was carried out targeting the viral genome (647 fluorescent probe, magenta).

2.1.2.1 STAT1, STAT2 and IRF9

My first approach to be able to visualize cells in an antiviral state was to tag the three components of the ISGF3 complex and use their nuclear translocation as a readout. Plasmids carrying the human version of these proteins were obtained from Addgene (see table 8), and eGFP was tagged at the N' terminus of each to compare their translocation efficiency. First, primers 2 and 3, and primers 25 and 26 were used on the previously generated pENTR221-IRF7-eGFP vector to amplify an empty backbone

and eGFP respectively. Then, STAT1 was amplified from pLV-WT-STAT1 using primers 27 and 28, and the 3 fragments were assembled with HiFi Assembly, generating the entry vector pENTR221-eGFP-STAT1. From this plasmid, STAT1 was swapped for STAT2 and IRF9, generating the vectors pENTR221-eGFP-STAT2 and pENTR221-eGFP-IRF9. First, the backbone was amplified with primers containing overhangs for annealing to either protein, using primers 29 and 30 for STAT2 and 31 and 32 for IRF9. Then, STAT2 was amplified from pLV-STAT2 with primers 33 and 34, and IRF9 from pLV-IRF9 using primers 35 and 36, continuing with the annealing to the corresponding backbones. These entry vectors were used to generate pWPI lentiviral vectors carrying the reporters, and stably transduced T84 cells. Interestingly, I could not observe cells expressing the eGFP-STAT1 fusion protein, likely due to its overexpression being lethal for the cells. On the contrary, the eGFP-STAT2 construct exhibited a cytoplasmic location at its basal state, and the eGFP-IRF9 fusion protein an exclusively nuclear one (Figure 14A). To evaluate whether fusing eGFP to the N terminus of these proteins interferes with their localization or ability to translocate, I generated an alternative version with eGFP at the C terminus. First, the pENTR221-IRF7-eGFPa was used as a template to amplify a backbone with eGFP at the C terminus and a linker between the fused proteins using primers 3 and 37. STAT1, STAT2 and IRF9 were amplified from the vectors generated before with the corresponding overhangs for annealing to the C terminus versions of the pENTR221 backbones (primers 38-43). These vectors were used to generate lentiviral vectors and overexpressing T84 cell lines. Nevertheless, the results obtained matched what was observed with the N terminus versions of the reporters (Figure 14A). Because of this, only eGFP-STAT2 was considered as a good candidate, and thus, T84 eGFP-STAT2 cells were seeded on 8-well glass bottom chambers, prepared for imaging on a PerkinElmer spinning disc and treated with 2,000 IU/mL of IFNβ or 300 ng/mL of IFNλ1,2,3 right before imaging. Cells were imaged every 5 minutes for 1 hour using a 40X oil objective, showing that upon treatment with IFNλ there was a fast and short lasting nuclear translocation of eGFP-STAT2 (Figure 14B). This process seemed to start rapidly after treatment, visualized as “sparkles” in the nucleus and lasting for about 30 minutes. The short lasting characteristics of the nuclear translocation of eGFP-STAT2 complicates the visualization of cells in an antiviral state in long live experiments, and thus a longer lasting reporter is more suitable for this.

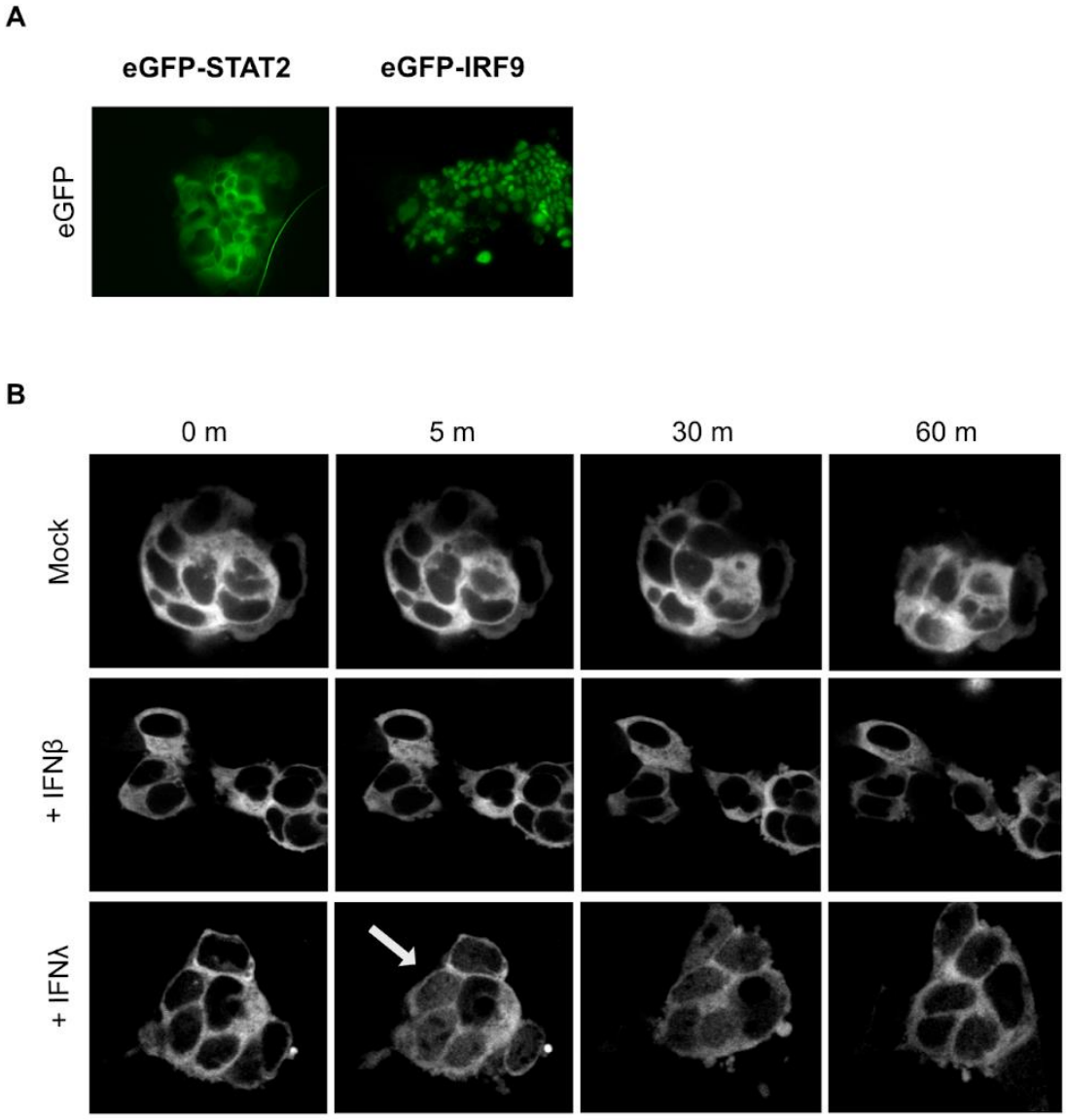

Figure 14. (A) T84 cells transduced with the eGFP-STAT2 or eGFP-IRF9 exhibit cytoplasmic localization in the case of STAT9 and nuclear localization of IRF9. (B) eGFP-STAT2 T84 cells were imaged every 5 minutes for 60 minutes upon treatment with IFNs. After 5 minutes of treatment with IFNλ, nuclear translocation of eGFP-STAT2 was observed (white arrow). Export into the cytoplasm started 30 minutes after nuclear translocation, and most of the fusion proteins were visualized in the cytoplasm 60 minutes post treatment.

2.1.2.2 Interferon Stimulated Genes

Upon IFN sensing, the ISGF3 complex translocates to the nucleus and activates the expression of hundreds of interferon stimulated genes (ISGs). I have received from collaborators (Dr. Ronald Dijkman, University of Bern) plasmids carrying the promoter region of three different ISGs (MX1, ISG54 and ISG56) tagged with the red fluorescent

protein mCherry: pLV pMX1-mCherry, pLV pISG54-mCherry, pLV pISG56-mCherry. Upon IFN sensing and nuclear translocation of the ISGF3 complex, the expression of mCherry can be visualized (Figure 15A). These lentiviral vectors were used to generate modified T84 cell lines and to test the expression of mCherry overtime after IFN treatment. When aiming at visualizing the basal intensity of mCherry, it was possible to observe different degrees of basal activation between the three different constructs. T84 cells carrying the pMX1-mCherry reporter showed low basal activity of the promoter, pISG54-mCherry exhibited a considerably higher activation than MX1, and pISG56-mCherry displayed the highest basal intensity of mCherry levels (Figure 15B). Because of this, I focused on using the pMX1-mCherry construct.

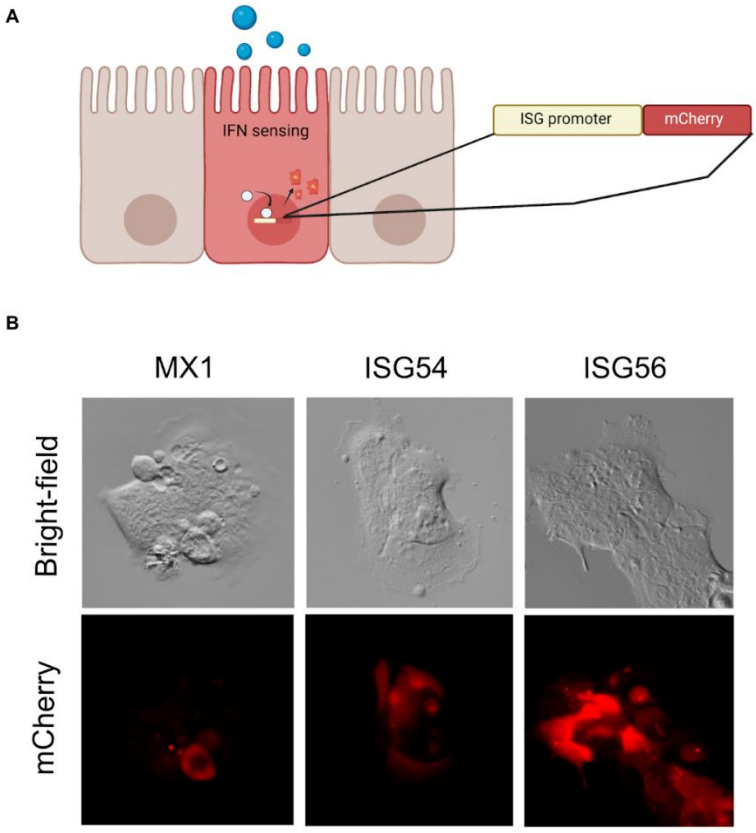

Figure 15. (A) Schematic showing IECs transduced with the ISG promoter-mCherry reporters. Upon sensing of IFNs, the ISGF3 complex translocates to the nucleus and activates the production of mCherry. Generated with Biorender.com. (B) T84 cells transduced with the pMX1-mCherry, pISG54-mCherry or pISG56-mCherry reporters were seeded on 8-well glass bottom chambers and imaged with a PerkinElmer spinning disc microscope. Cells are imaged 24 hours post seeding in the absence of treatment.

To evaluate the activation of the reporter over time, T84 pMX1-mCherry cells were seeded on 8-well glass bottom chambers at half confluency, treated with either 2,000

IU/mL of IFNβ or 300 ng/mL of IFNλ1,2,3 and imaged every 1 hour for 36 hours using a PerkinElmer spinning disc. Cells are kept at 37°C and 5% CO_2 during the live experiment. Time-lapse movies generated showed that upon treatment with either IFNs the intensity of mCherry increased significantly over time, whereas no change was observed in mock treated cells (Figure 16). Furthermore, an increase in intensity was observed throughout the entire experiment, with no loss of mCherry at any point. These results were promising, since it was of great importance to generate a cell line that could readily report for IFN sensing in long live cell fluorescence microscopy experiments.

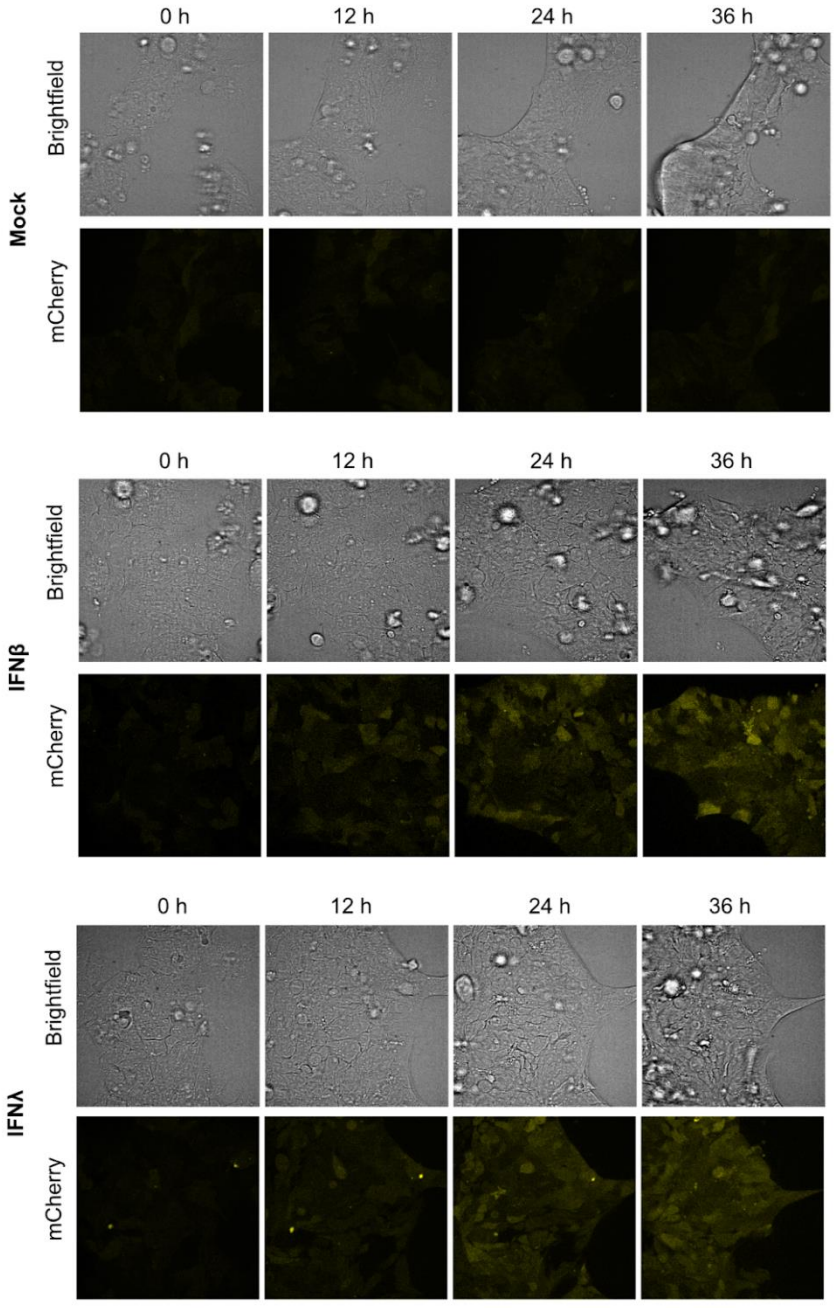

Figure 16. T84 cells carrying the pMx1-mCherry reporter were mock treated (upper panel), treated with IFNβ (middle panel) or IFNλ (lower panel) and imaged every 1 hour for 36 hours. Representative images for brightfield and a 561 laser (mCherry) are shown. An increase in fluorescence is observed at 12 hours post treatment and lasts for the entire experiment.

Fluorescent reporter	Characterization
IRF7-eGFP	Cytoplasmic localization when not stimulated. Nuclear translocation when stimulated, but mostly in sparse cultures
eGFP-IRF7	Cytoplasmic localization when not stimulated. Does not translocate upon stimulation
pIFNβ-mCherry	High basal fluorescence. Weak increase in fluorescence upon stimulation
pIFNλ2,3-mCherry	No basal fluorescence. Efficient increase in fluorescence upon stimulation
MAVS Astrovirus cleavage reporters	eGFP localizes in the mitochondria. No cleavage upon infection with astrovirus
Sec61B Astrovirus cleavage reporters	eGFP localizes in the ER. No cleavage upon infection with astrovirus
MAVS Norovirus cleavage reporters	eGFP localizes in the mitochondria. Efficient nuclear translocation upon transfection of protease
Sec61B Norovirus cleavage reporters	eGFP localizes in the ER. Efficient nuclear translocation upon transfection of protease
UnaG and mKate Rotaviruses	Visualization of fluorescent proteins after 4-6 hours of infection
N' and C' eGFP STAT1	Cell death occurs upon overexpression
N' and C' eGFP STAT2	Cytoplasmic localization at basal states. Fast and short lasting nuclear translocation upon IFN treatment
N' and C' eGFP IRF9	Nuclear translocation at basal states
pMX1-mCherry	Low basal levels of fluorescence. Increase of fluorescence upon viral infection or IFN treatment.
pISG54-mCherry	Medium basal levels of fluorescence
pISG56-mCherry	High basal levels of fluorescence

Table 3. Summary of fluorescent reporters generated in this thesis and provided by collaborators.

2.2 Tracking of the rotavirus-induced innate immune response in intestinal epithelial cells

2.2.1 NSP1 is key to control interferon induction in human intestinal epithelial cells

The ability of rotaviruses to induce IFNs upon infection and be controlled by IFNs has been a highly debated topic [96–98]. To determine how human intestinal epithelial cells respond to rotaviruses, WT and NSP1-deficient SA11 rotaviruses encoding the green fluorescent protein UnaG were used (Figure 13). To evaluate the innate immune response elicited by WT and NSP1-deficient rotaviruses, I infected T84 cells with either the WT or NSP1- deficient virus at an MOI of 1 and 24 hours post-infection (hpi), and I evaluated the upregulation of type I (IFNβ1) or type III IFNs (IFNλ1-3) by q-RT-PCR. Results show that WT rotaviruses did not induce IFNβ1 nor IFNλ1, as shown by the relative expression of IFNs compared to the housekeeping gene TATA box-binding protein (TBP) (Figure 17A, top panel) or the fold change of IFN transcript expression compared to mock infected cells (Figure 17A, bottom panel). Interestingly, expression of IFNλ2-3 was upregulated in cells infected with WT rotavirus (Figure 17A). Infection with the NSP1-deficient rotavirus resulted in a moderate induction of IFNβ1 and IFNλ1 and a strong upregulation of IFNλ2/3 expression (Figure 17A). These findings confirmed that NSP1 can efficiently interfere with IFN production in rotavirus infected T84 cells.

To detect the presence of IFNs in the supernatant of rotavirus-infected cells, I infected cells at an MOI of 1 with either WT or NSP1-deficient rotavirus and collected the supernatants 24 hpi. I added these supernatants to HEK-Blue reporter cells genetically modified to express a phosphatase alkaline under the control of the ISG54 promoter region (InvivoGen). 24 hours post-treatment, I carried out a colorimetric assay to quantify the amount of IFNs released by rotavirus infected cells. In accordance with the q-RT-PCR results, type-I IFNs were not produced by cells infected with WT rotavirus, whereas I was able to measure type I IFNs in the supernatant of cells infected with the NSP1-deficient rotavirus (Figure 17B, left panel). On the contrary, IFNλ was detectable in the supernatants of both WT and NSP1-deficient rotavirus infected cells though to a much larger extent upon NSP1-deficient rotavirus infection (Figure 17B, right panel). Together these results show that NSP1 is key to control interferon

production but while it is able to completely block the production of type-I IFNs, it appears to only partially impact the production of type-III IFNs.

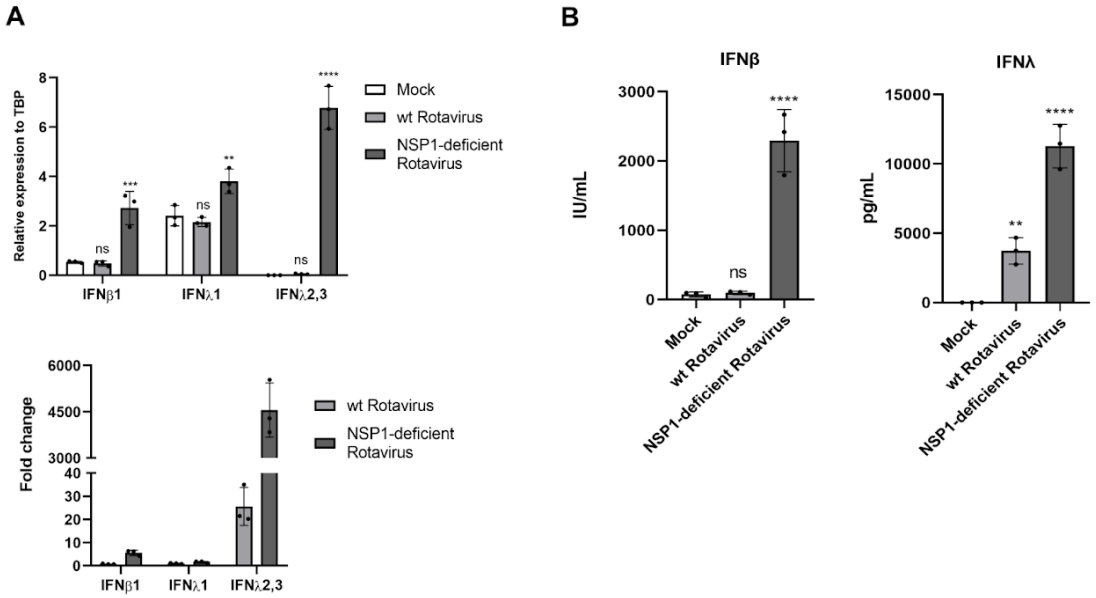

Figure 17. (A) T84 cells were infected with WT and NSP1-deficient rotaviruses. 24 hpi RNA was extracted and the upregulation of IFNβ1, IFNλ1, and IFNλ2/3 were analyzed by q-RT-PCR. (B) T84 cells were infected at an MOI of 1 with either WT or NSP1-deficient rotavirus, and the levels of IFNs produced were measured by adding the supernatants to HEK-Blue reporter cells 24 hpi. Error bars indicate standard deviation. n = 3 biological replicates. N.S.=not significant;. P<0.05 *, P<0.01 **, P<0.001 ***, P <0.0001 **** (Ordinary one-way ANOVA with Dunnett's multiple comparison test using non-infected infected cells as reference).

2.2.2 Exogenous treatment of interferons blocks rotavirus infection

In order to test the efficiency of type I (IFNβ1) or type III (IFNλ2/3) IFNs in preventing rotavirus infection, I pre-treated T84 cells with increasing concentrations of either IFN for 16 hours prior to infection. Following IFN treatment, I infected the cells with either WT or NSP1-deficient rotaviruses in the presence of IFNs for 24 hours and assayed infection 24 hpi by fluorescence microscopy (Figure 18A and C). Results showed that both type I and III IFNs were able to control WT rotavirus infection in a dose dependent manner (Figure 18A-B). Similarly, NSP1-deficient rotavirus displayed a sensitivity to type I and III IFNs comparable to that of WT viruses (Figure 18C-D). These results suggested that T84 cells are able to use both type I and type III IFNs to control rotavirus infection. Additionally, both WT and NSP1-deficient viruses were sensitive to

interferons, suggesting that they are not able to control antiviral signaling after the IFN sensing program has been established.

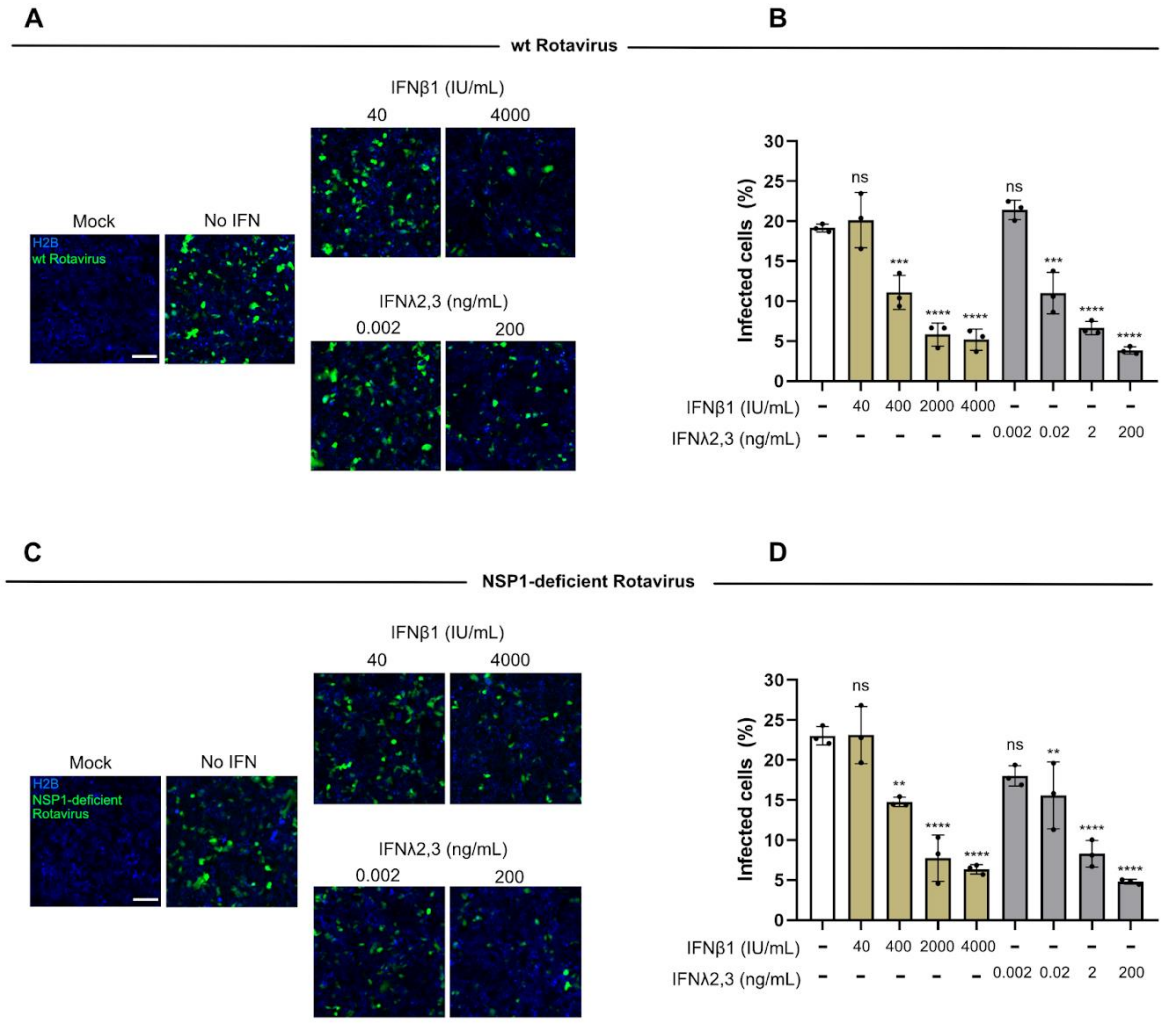

Figure 18. (A) H2B-mCherry T84 cells were pretreated with indicated concentrations of IFNβ1 and IFNλ2,3 for 16 hours and were subsequently infected with rotavirus-UnaG. 16hpi infection was analyzed by fluorescence microscopy. (A) Representative images of WT rotavirus infection by fluorescence microscopy. Scale bar, 100 μm. (B) Quantification of the fluorescence of WT rotavirus infection. Data are represented as the percentage of infected cells. (C) Same as A except for NSP-1 deficient virus. Scale bar, 100 μm. (D) Same as B except for NSP1-deficient virus. Error bars indicate standard deviation. n = 3 biological replicates. n.s.=not significant; P<0.05 *, P<0.01 **, P<0.001 ***, P <0.0001 **** (Ordinary one-way ANOVA with Dunnett's multiple comparison test using non-treated infected cells as reference).

2.2.3 IFNλ is essential to control the spread of rotavirus in human intestinal epithelial cells

While both type I and III IFNs seem to be able to block rotavirus infection when added exogenously (Figure 18), q-RT-PCR data showed that NSP1 is only able to completely block type I IFN production (Figure 17). This suggests that in human intestinal epithelial cells, type III IFN plays a central role in controlling rotavirus infection. To determine if the endogenously produced type I and type III IFNs are also capable of controlling rotavirus infection, I employed T84 cells previously generated in the group [156]. These cells had been depleted of either the type I IFN receptor (IFNAR-/-), the type III IFN receptor (IFNLR-/-) or both receptors (dKO).

To track rotavirus infection and spread, I first transduced WT and IFN receptor KO T84 cells with the fluorescent nuclear tag H2B-mCherry. Then, I infected cells at an MOI of 0.1 with either the WT or the NSP1-deficient rotavirus and monitored infection in 1 hour intervals for 36 hours by live cell fluorescent microscopy. Results showed that loss of the type I IFN receptor (IFNAR-/-) did not impact WT rotavirus infection and spread in human intestinal epithelial cells (Figure 19A-B). Importantly, cells lacking the type III IFN receptor (IFNLR-/-) or both receptors (dKO) supported a greater infection and spread of WT rotavirus, indicating that endogenous type III IFNs are key antiviral cytokines to combat rotavirus infection (Figure 19A-B). These results are in line with the previous observation that WT rotavirus only induces the production of IFNλ2/3 and not IFNβ1 (Figure 17). Similar results were observed when tracking the infection spread of the NSP1-deficient rotavirus. NSP1-deficient rotavirus could spread more efficiently in cells lacking type-III IFN receptors or cells lacking both IFN receptors (Figure 19C-D). Importantly, due to the higher levels of IFNs being produced following infection with the NSP1-deficient rotavirus (Figure 17), lower levels of infected WT and IFNAR1-/- cells were observed throughout the whole time course compared to infections with WT Rotavirus (Figure 19B vs. 19D).

Interestingly, although the NSP1-deficient rotavirus infection leads to the production of IFNβ1 (around 2000 IU/mL, Figure 17B), wild-type levels of infection were still observed in the IFNLR1-/- cell line (Figure 19D). As similar amounts of IFNβ1 provided *in trans* lead to a reduction of rotavirus infection (Figure 18C-D), this data suggests that IFNβ1 does not play a key role in controlling rotavirus infection. Altogether, these

results show that endogenously produced type III IFNs following rotavirus infection are key to control viral spread in human intestinal epithelial cells.

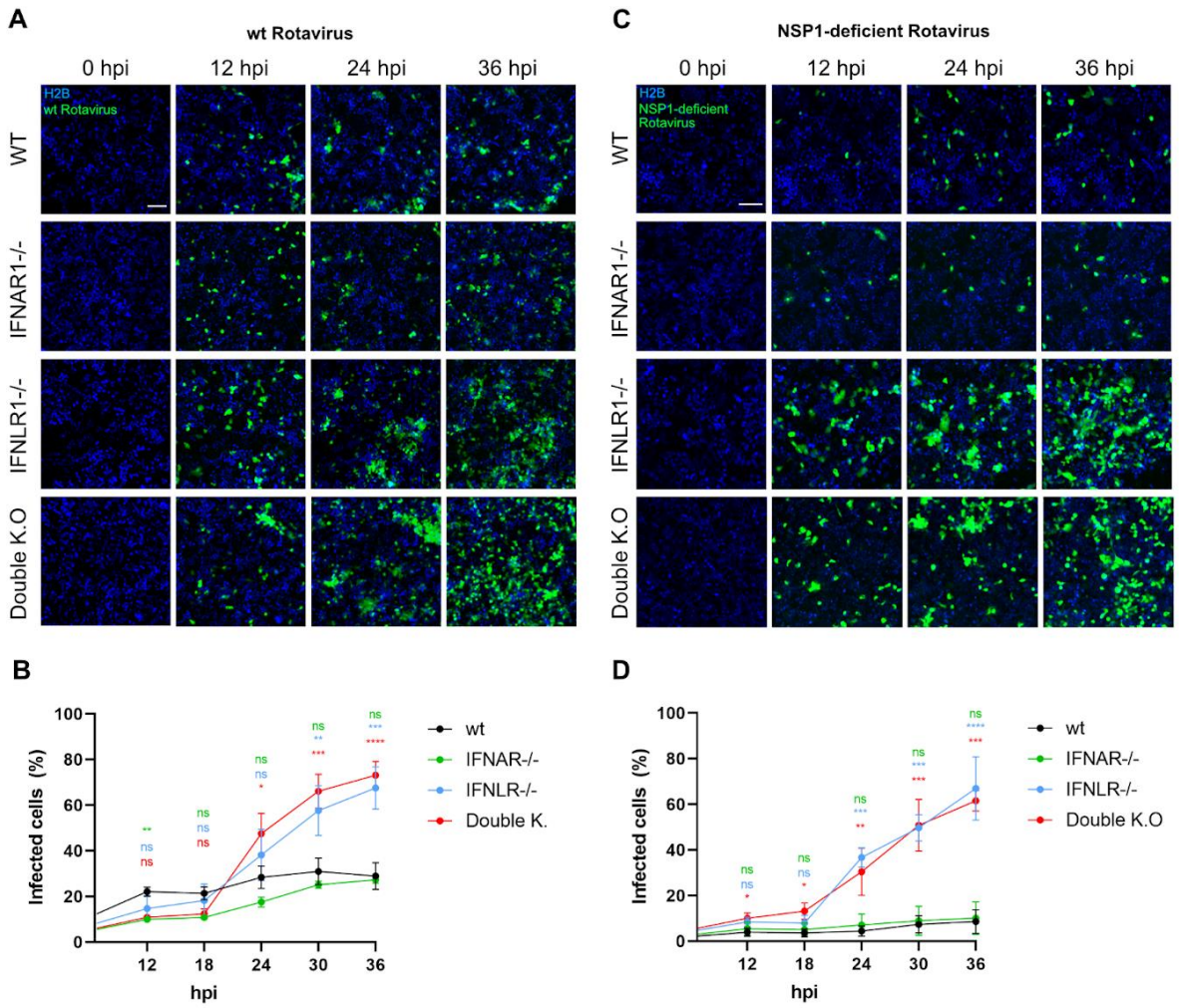

Figure 19. WT, IFNAR1-/-, IFNLR1-/- and IFNR double K.O T84 cells transduced with an H2B-mCherry nuclear tag (blue) were infected at an MOI of 0.1 (as determined in MA104 cells). Infection was followed by live fluorescence microscopy for 36hpi and images were acquired every 1 hour. (A) Fluorescent images of WT rotavirus infection and spread at indicated time points. Scale bar, 100 µm. (B) Quantification of infected cells in A over time. (C) Same as A except for the NSP1-deficient virus. Scale bar, 100 µm. (D) Same as B except for the NSP1-deficient virus. Error bars indicate standard deviation. n = 3 biological replicates. n.s=not significant;. P<0.05 *, P<0.01 **, P<0.001 ***, P <0.0001 **** (Multiple t-tests with multiple comparisons correction using the Holm-Sidak method. WT T84 cells are used as reference).

2.2.4 Human intestinal epithelial cells use type III IFNs to induce an antiviral state

To visualize the magnitude and timing of the antiviral response elicited by type I and type III IFNs, I took advantage of WT and IFNLR1-/- T84 cells carrying the pMx1-mCherry reporter (Figure 15). WT pMX1-mCherry cells are used to determine the antiviral state induced by the presence of either type I or type III IFNs, while the IFNLR1-/- pMx1-mCherry cell line can only report an antiviral state induced by type I IFNs. To track infection in these cell lines during live experiments, I transduced WT and IFNLR1-/- pMx1-mCherry cells with the fluorescent nuclear tag H2B-mTurquoise2. To test the efficacy of the reporter cell lines at sensing and responding to IFNs, I treated WT and IFNLR1-/- pMx1-mCherry cells with three different concentrations of either IFNβ1 or IFNλ2/3. 24 hours post-stimulation, I evaluated the number of Mx1-mCherry positive cells using fluorescence microscopy (Figure 20A and 20C). The quantification of Mx1-mCherry positive cells confirmed that the WT pMx1-mCherry cell line was activated by both type I and III IFNs (Figure 20A-B. Furthermore, increasing concentrations of either type I or type III IFN led to an increased number of Mx1-mCherry positive cells (Figure 20A-B). The quantification showed that high concentrations of IFNβ1 induced the activation of the MX1-cherry reporter in approximately 90% of the WT cells (Figure 20B). Interestingly, concentrations of IFNλ2/3 above 2 ng/ml were enough to activate the reporter in most WT cells (approximately 90%). Importantly, only IFNβ1 activated the IFNLR-/- pMx1-mCherry reporter cell line, further confirming its specificity for type I IFNs (Figure 20C-D). Quantifications showed that the IFNLR-/- pMx1-cherry cell line induced a smaller number of mCherry positive cells upon treatment with IFNβ1 compared to the WT pMx1-mCherry cell line (Figure 20D). To confirm that the fluorescent signal generated by the reporter was in line with ISG transcript levels, I treated WT and IFNLR-/- pMX1-cherry cells with IFNβ1 or IFNλ2/3 and harvested RNA 24 hours post-stimulation. q-RT-PCR revealed a similar upregulation of the endogenous Mx1 transcript, validating the accuracy of the fluorescently tagged promoter (Figure 20E).

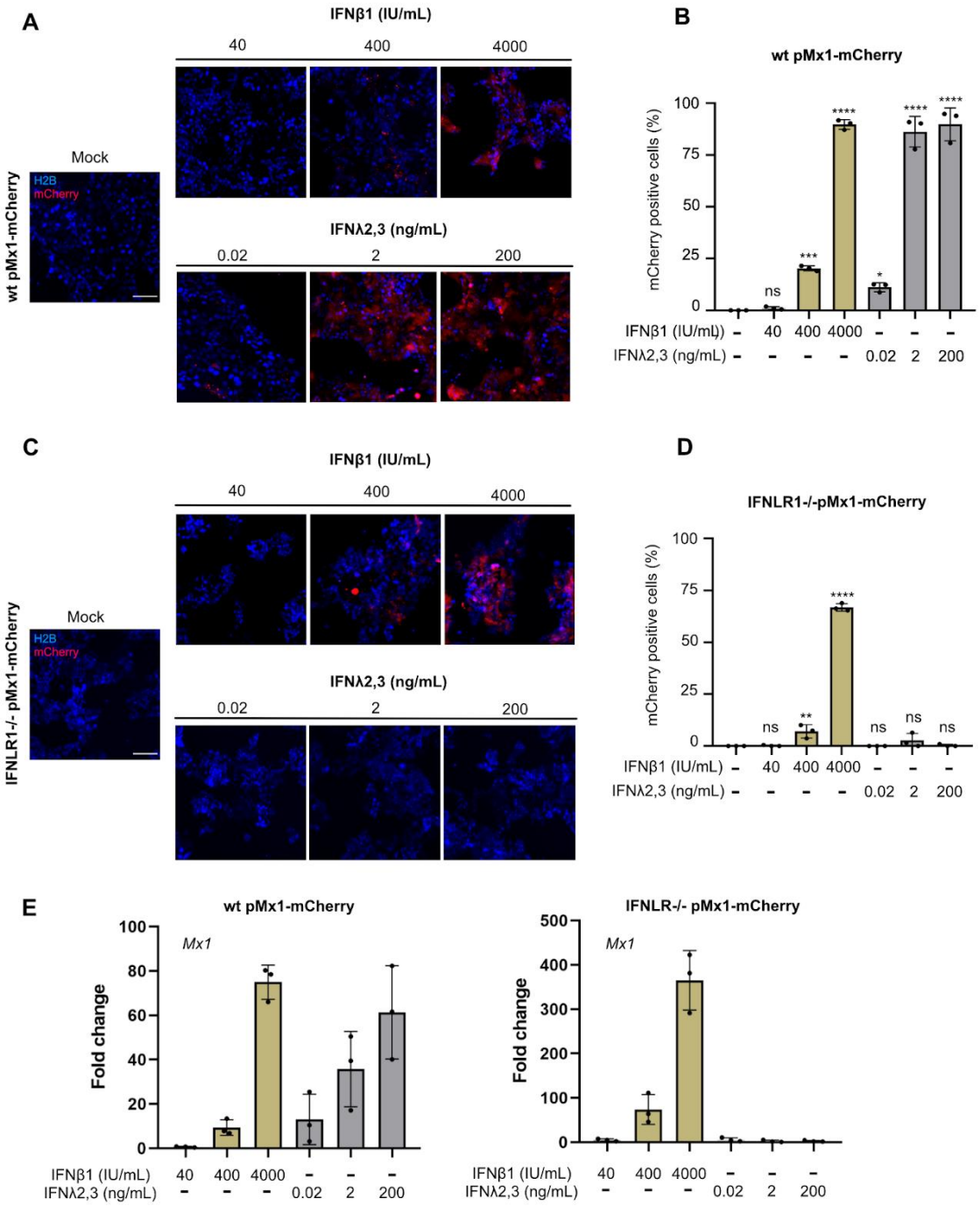

Figure 20. (A) WT pMx1-mCherry T84 cells were treated with increasing concentrations of either IFNβ1 and IFNλ2,3 for 24 hours. Representative fluorescent images are shown. Scale bar, 100 μm. (B) Quantification of the percentage of MX1-cherry cells from B. (C) IFNLR-/- pMx1-mCherry T84 cells T84 cells were treated with increasing concentrations of either IFNβ1 and IFNλ2,3 for 24 hours. Representative fluorescent images are shown. Scale bar, 100 μm. (D) Quantification of the percentage of MX1-cherry cells from D. (E) WT pMx1-mCherry (left panel) and IFNLR-/- pMx1-mCherry (right panel) T84 cells were treated with different concentrations of IFNβ1 and IFNλ2,3. 24 h after treatment, RNA was harvested and q-RT-PCR was carried out targeting Mx1. Error bars indicate standard deviation. n = 3 biological replicates. n.s.=not significant; P<0.05 *, P<0.01 **, P<0.001 ***, P <0.0001 **** (Ordinary one-way ANOVA with Dunnett's multiple comparison test using non-treated infected cells as reference).

To investigate whether infection with WT or NSP1-deficient rotavirus induces a type I or type III mediated antiviral response, I infected WT pMx1-mCherry and IFNLR1-/- pMx1-mCherry cells at an MOI of 0.1 and UnaG (rotavirus) and mCherry (ISG) positive cells were quantified over time. Results showed that WT rotavirus induced the production of Mx1-mCherry in WT cells only (Figure 21A). No activation was observed following WT rotavirus infection of IFNLR1-/- pMx1-mCherry (Figure 21A). These results are in line with previous observations that only IFNλ2,3 was produced following WT rotavirus infection and suggest that the Mx1-mCherry positive cells are due to type III IFN alone (Figure 17 and 21B). Quantifications showed that 40% of WT pMx1-mCherry cells were in an antiviral state at 24 hpi, which is when a second round of infection would take place, explaining the inability of the virus to continue spreading (Figure 21B, upper panel). After 36 hpi, approximately 80% of the cells were in an antiviral state, showing the impressive magnitude of IFNλ2,3 in establishing an antiviral response in intestinal epithelial cells. Conversely, there were almost no IFNLR1-/- pMx1-mCherry positive cells throughout the time course, showing that type I IFNs do not mediate the antiviral response observed upon rotavirus infection. This lack of an antiviral response led to a sharp increase in WT rotavirus infection and spread in IFNLR1-/- pMx1-mCherry cells (Figure 21B, lower panel).

Similar to WT rotavirus, the NSP1-deficient rotavirus infection of WT pMx1-mCherry cell line showed an induction of Mx1-mCherry signal and a subsequent low level of virus spread. The NSP1-deficient virus led to an induction of 40% mCherry positive cells at 24 hpi, which further increased to 85% at 36 hpi (Figure 21C-D, upper panel). Interestingly, unlike the WT rotavirus, the NSP1-deficient rotavirus led to an induction of Mx1-mCherry in the IFNLR1-/- pMx1-mCherry at late time points, indicating that type I IFNs were secreted following infection (Figure 21C-D, lower panel). This induction of type I IFNs is in line with previous q-RT-PCR and secreted IFN data (Figure 17). The percentage of Mx1-mCherry positive cells was reduced in IFNLR-/- cells as compared to WT cells, and this led to a higher amount of rotavirus infected cells. These results suggest that the magnitude and faster-paced paracrine action of type III IFNs are able to induce an antiviral state in non-infected cells before a second round of infection can take place. On the contrary, when produced in the context of an infection with the NSP1-deficient rotavirus, type I IFNs do not seem to induce a sufficient antiviral response required to control rotavirus spread. Altogether, these results show that upon rotavirus infection, human intestinal epithelial cells

produce type III IFNs and rely exclusively on this cytokine to control rotavirus spread within the epithelium.

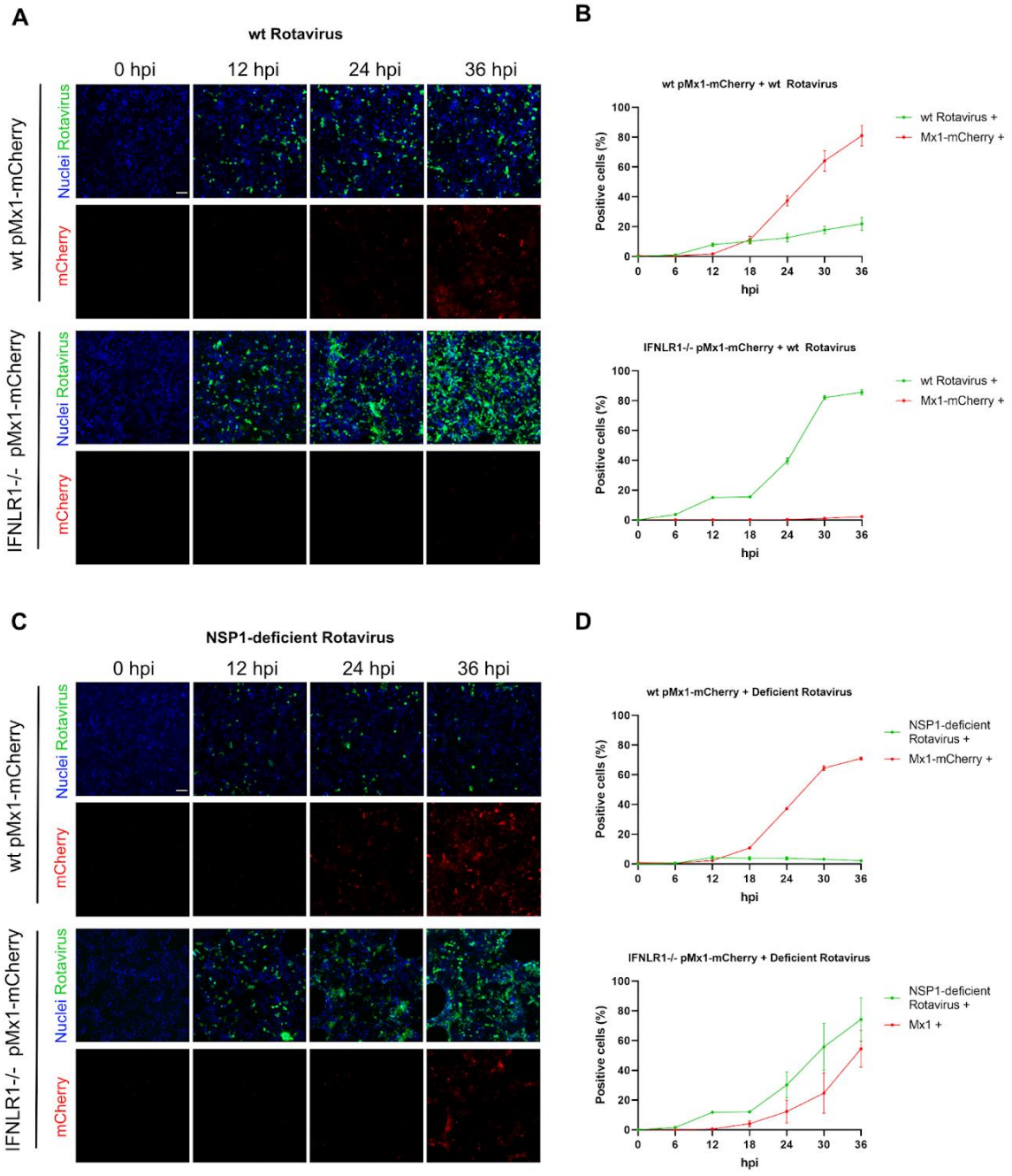

Figure 21. WT pMx1-mCherry cells and IFNLR-/- pMx1-mCherry cells were infected with either WT rotavirus (A-B) or NSP1-deficient rotavirus (C-D) at an MOI of 0.1 (calculated in MA104 cells). (A) Representative fluorescent images of WT rotavirus infection of WT pMx1-mCherry cells and IFNLR-/- pMx1-mCherry at indicated time points. All cells carry the H2B-mTurquoise2 nuclear tag (blue) for quantifications. Scale bar, 100 µm. (B) Quantification of the number of rotavirus-infected cells and mCherry-positive cells from A. (C) Representative fluorescent images of NSP-1 deficient rotavirus infection of WT pMx1-mCherry cells and IFNLR-/- pMx1-mCherry at indicated time points. All cells carry the H2B-mTurquoise2 nuclear tag (blue) for quantifications. Scale bar, 100 µm. (D) Quantification of the

number of rotavirus-infected cells and mCherry-positive cells from C. Error bars indicate standard deviation. n = 3 biological replicates.

2.3 Characterization of rotavirus infection colonies

2.3.1 Rotavirus second rounds of infections take place as colonies

When T84 cells are infected with rotavirus at low MOIs and tracked over time, it is possible to observe that the second rounds of infection do not take place in a random manner, but rather as colony-looking infections. This process seems to follow a specific pattern, during which the first infected cell remains alive for a number of hours, followed by cell death and the formation of colony-looking second rounds of infection in the locations where the first infections took place (Figure 22A). Interestingly, not all cells infected during the first round of infection give rise to colonies, but no new infections take place in the vicinity of these cells either. To evaluate whether this phenomenon was cell type specific, the African green monkey kidney cell line MA104 was infected with rotavirus at a low MOI and the infection tracked over time. As observed in T84 cells, the formation of colonies was observed upon death of the first infected cells (Figure 22B). Interestingly, colonies observed in MA104 cells were considerably bigger than those of T84 cells, which is in line with the fact that the MA104 cell line is the gold standard cell line for amplification of rotavirus due to its lower level of immune response and control of infection. It is likely then that the first infected cells produce a large number of viral particles and thus form larger colonies, compared to T84 cells that can mount a strong immune response.

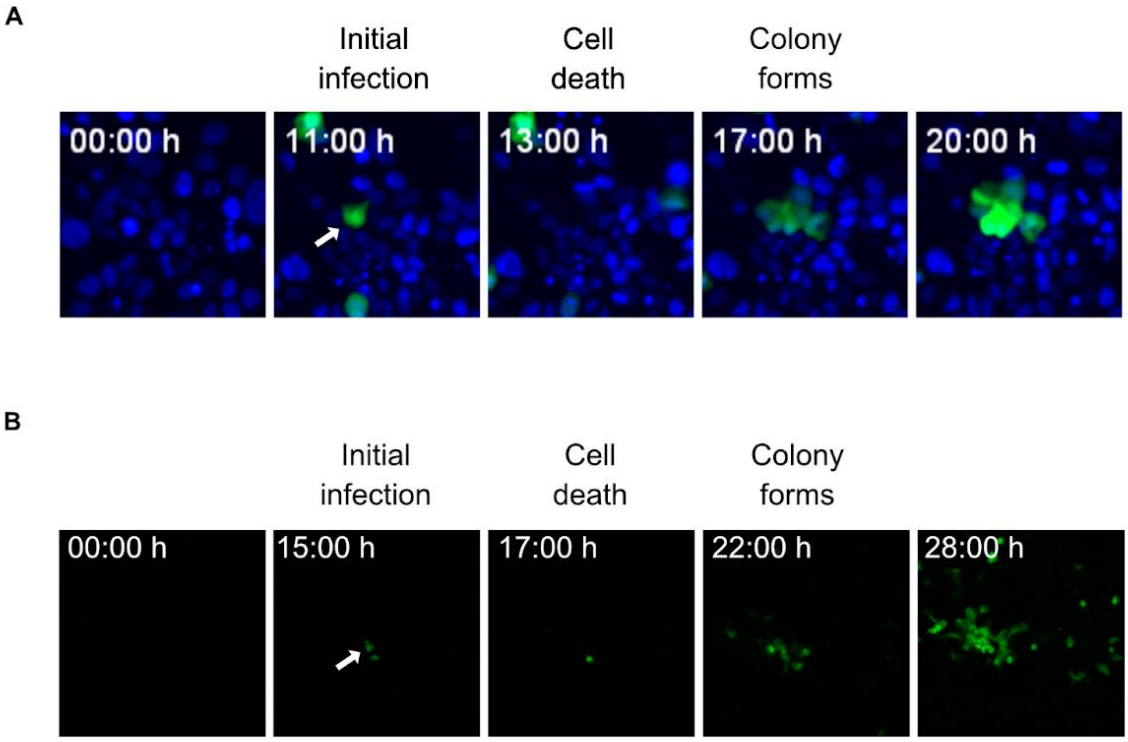

Figure 22. (A) T84 cells were infected with WT UnaG rotavirus and tracked over time. Initial infections can be visualized during the first 14 hours of infection. Cells undergo cell death and a second round of infections takes place shortly after in a colony-looking pattern. Cell nuclei are displayed in blue. A representative region of a full field of view is displayed. (B) As for T84 cells, MA104 cells infected with green rotavirus are tracked over time, observing also the initial infections giving rise to colonies upon cell death. A representative region of a full field of view is displayed.

2.3.2 Infection colonies are not delimited by interferon signaling

As described in section 2.2, type-III IFNs seem to play a key role in preventing the spread of rotavirus infection to neighboring cells. It is possible then that cells that are nearby the first infection do not have enough time to establish an IFN-mediated antiviral state, whereas those farther away are protected from infection in time. To elucidate if this is the case, I evaluated whether colonies could form in IFNLR KO cells and how they differ from those observed in WT cells. WT and IFNLR KO cells were infected at an MOI of 0.1 and the number of colonies formed throughout the 48-hour live experiment were quantified (Figure 23A). IFNLR KO cells allowed a significantly higher number of colonies than WT cells, which is likely due to cells being more permissive to infections due to a reduced antiviral state (Figure 23B). Interestingly, colonies observed in IFNLR KO cells exhibited a significantly increased area of infection,

meaning that a greater number of cells were infected during the second round of infection (Figure 23C). It is likely that IFNLR KO cells produce a higher amount of viral particles due to their inability to sense type-III IFNs, which translates into larger colonies. When quantifying the number of hours the first infected cells remain alive and the time for the colonies to form upon cell death, I could observe that these processes are conserved and there were no differences observed between WT and IFNLR KO cells (Figure 23D). Cells infected during the first round of infection remain alive for approximately 8 hours in both WT and IFNLR KO cells, and upon cell death, colonies form in approximately 3 hours after the death of the initial cell. These similarities observed in the two cell lines show that colonies are not due to IFN signaling, but rather to intrinsic characteristics of rotavirus infection.

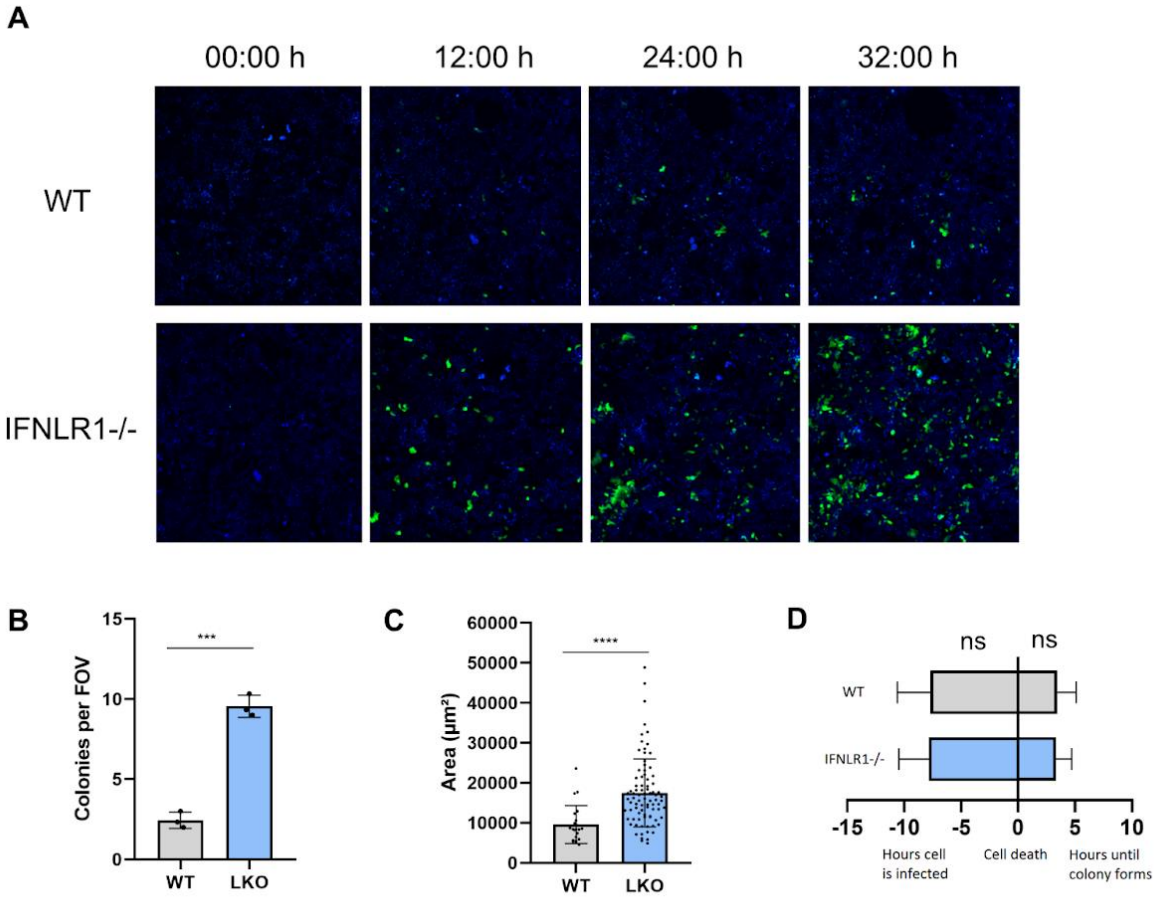

Figure 23. (A) WT and IFNLR1-/- T84 cells were infected at an MOI of 0.1 with UnaG rotavirus and tracked over time. A representative region of a full field of view is displayed. (B) All colonies formed throughout the 32-hour experiment were quantified and compared between WT and IFNLR-./- cell lines. (C) The area covered by all colonies observed in the experiment were measured and compared between WT and IFNLR-/- cell lines. (D) For each colony observed, the number of hours leading to the death of

the first infected cell and the time between cell death and the appearance of a new colony were quantified. Error bars indicate standard deviation. n = 3 biological replicates. ns=not significant; P<0.05 *, P<0.01 **, P<0.001 ***, P <0.0001 **** (Unpaired t test is used for comparison).

2.3.3 Rotavirus-infection induced calcium waves delimit the area of a second round of infection

A recent publication has shown that rotavirus infection generates intercellular calcium waves through ADP signaling [121], the shapes of which are similar to those of the infection colonies. This is caused by a release of Ca2+ from ER reservoirs through the viroporin action of NSP4, affecting cellular integrity and inducing the release of ADP (Figure 6). ADP can then bind to the purinergic receptor P2Y1 on neighboring cells, which causes the increase of cytoplasmic levels of Ca2+ and subsequent release of ADP, generating a calcium wave. In order to confirm that rotavirus also induces calcium waves in T84 colorectal cancer cells, I took advantage of the GcAMP5G reporter of calcium increase. GcAMP5G is composed of a circularly permuted GFP, calmodulin and the calmodulin-binding peptide M13, and cannot fluoresce in the absence of Ca2+. The pCMV-GCaMP5G plasmid was acquired from Addgene and introduced into the Gateway system using primers 44 and 45 to add AttB cloning sites to it. This fragment was used for generation of an entry vector through a BP Gateway reaction and a pWPI lentiviral vector through an LR Gateway reaction. T84 cells were transduced with the reporter and tested for their ability to report for an ADP-mediated increase in cytoplasmic Ca2+. To achieve this, GCaMP5G T84 cells were seeded in 48-well plates one day before the experiment, either mock treated or treated with 1 mM ADP (Sigma-Aldrich) and imaged using a CellDiscoverer 7 microscope. Since the activation of the GCaMP5G could be fast and transient, ADP treatment was carried out once cells were placed inside the microscope and the experiment setup was ready. Cells were imaged every 3 minutes for 60 minutes, and changes in GFP intensity were evaluated. Interestingly, ADP-treated cells exhibited a brief and unsynchronized increase in GFP that resembled “sparkles” (Figure 24). This increase in GFP signal started shortly after treatment and confirmed the relevance of GCaMP5G as a reporter of ADP-driven Ca2+ increase.

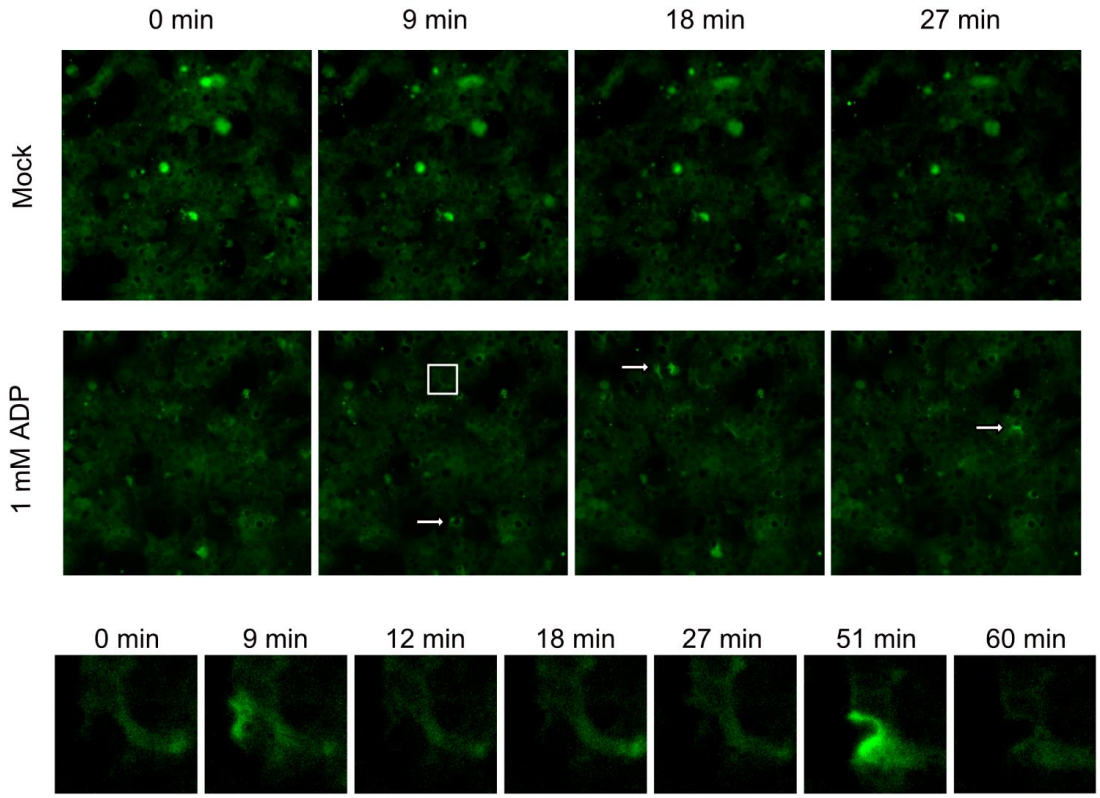

Figure 24. GaMP5G T84 cells were mock treated or treated with 1 mM ADP and imaged every 3 minutes for 60 minutes. Random and brief increases in eGFP signal could be observed in ADP treated cells (white arrows). A representative area of a full field of view is displayed. A magnification of an area in the field of view (white box) shows fluctuations in eGFP signal in one cell.

To evaluate whether rotavirus infection would also activate the GCaMP5G reporter, GCaMP5G T84 cells were infected with the red mKate rotavirus and monitored with a CellDiscoverer 7 microscope by imaging cells every 10 seconds for 3 minutes, after which a 1-hour pause was carried out and the imaging cycle restarted afterwards. This cycling imaging setup aimed to reduce large amounts of unwanted data and focused only on short lasting increases of calcium. I could observe an increase in cytoplasmic levels of Ca2+ in infected cells, which was detected as ‘sparkles’ of GFP signal, and this was followed by an increase in Ca2+ in neighboring uninfected cells, which lasted approximately 60 seconds (Figure 25A). This is in line with results found in the green African monkey cell line MA104 [121]. As mentioned above, the second round of infection took place in a cluster-looking manner, and it happened specifically in the region that was covered by the calcium wave (Figure 25B). These results highlight the possibility

that rotavirus-infection calcium waves help newly produced viruses infect cells by affecting the integrity of the monolayer.

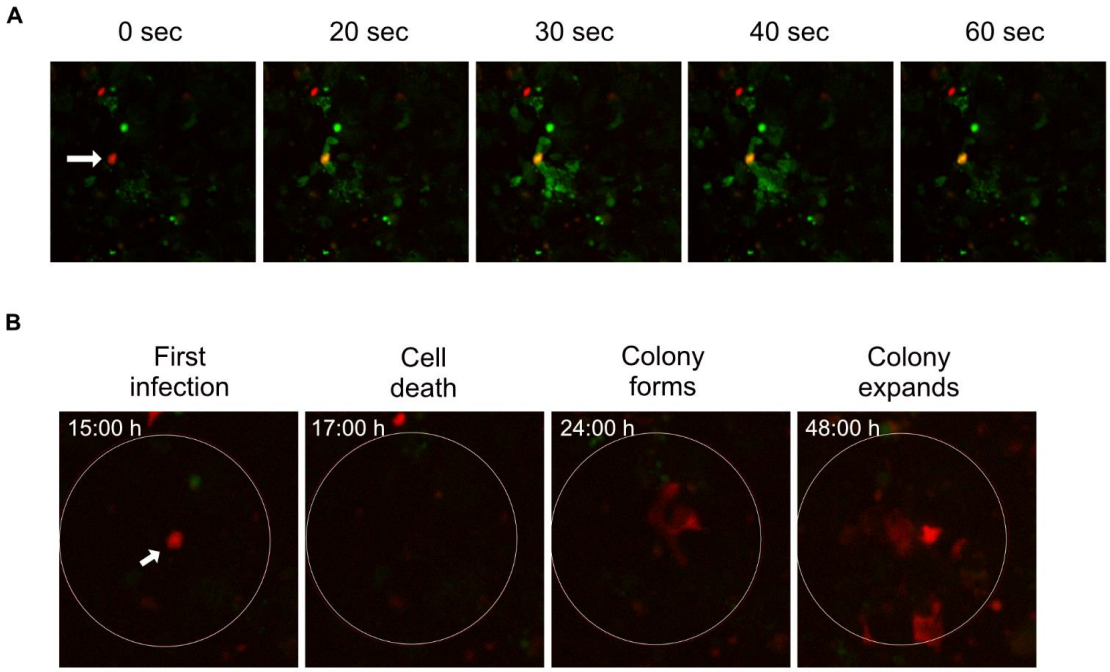

Figure 25. (A) T84 cells transduced with the GaMP5G Ca2+ reporter (green) were infected with mKate rotavirus (red) and tracked over time. Infected cells generated calcium waves around the infection which lasted approximately 60 seconds. A representative magnification of a field of view is displayed. (B) The area covered by the calcium wave (white circle) delimited the area in which a colony of infection could form.

2.3.4 Signaling through the P2Y1 purinergic receptor is key during rotavirus infection and spread

As mentioned above, Ca2+ release from ER reservoirs causes cell damage and ADP release, which binds to the P2Y1 purinergic receptor in neighboring cells and expands the signal along the tissue. To evaluate whether this ADP-driven calcium wave is essential during rotavirus infection, T84 cells were infected with UnaG rotavirus at an MOI of 1 and treated with either DMSO (control) or 10 μM BPTU (Tocris) at different timepoints. BPTU is an antagonist of the P2Y1 receptor, and thus prevents ADP binding and signaling. When BPTU was added at 0 and 3 hpi, it prevented the formation of colonies, although the first round of infection took place normally (Figure 26A-B). Interestingly, when BPTU was added at 6 hpi, there were no significant

differences in the number of colonies observed when compared to DMSO treated cells. These results show that ADP signaling takes place early during infection, approximately between 3-6 hpi, and that blocking it prevents second rounds of infection.

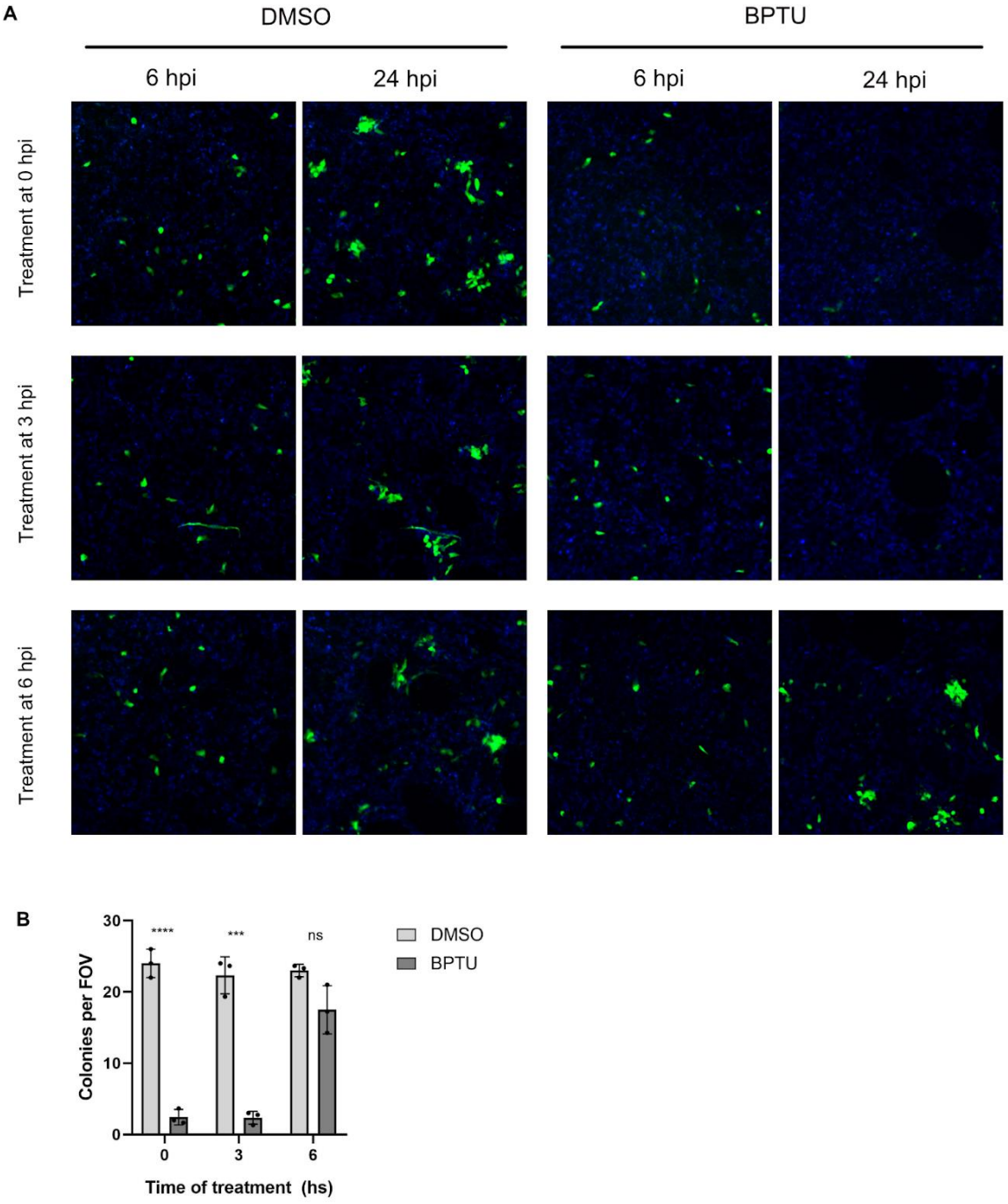

Figure 26. (A) T84 cells were infected with UnaG rotavirus at high MOI and treated with either DMSO or 10 μM BPTU at 0, 3 or 6 hpi. Infection was tracked for 48 hours. Representative fields of view observed at 6 and 24 hpi are displayed. Cell nuclei are shown in blue (H2B-mCherry). (B) Quantification of the total number of colonies observed throughout the entire experiment. Error bars indicate standard

deviation. n = 3 biological replicates. n.s.=not significant; P<0.05 *, P<0.01 **, P<0.001 ***, P <0.0001 **** (Unpaired t test is used for comparison).

To further characterize the importance of ADP and the P2Y1 receptor, a P2Y1 receptor KO T84 cell line was generated through CRISPR/Cas9 targeted deletion using the guide sequence 'CTACAGCATGTGCACGACCG', described before [121]. Oligos 46 and 47 were used for generation of a LentiCRISPRV2 vector carrying the guide sequence (See section 4.2.3.1). Single cloning of the knock-out cell pool and genome sequencing allowed identification of a fully knocked-out population. Infection of this clonal cell line resembled the results obtained through BPTU treatments, in which a first round of infection was visible, but no colonies could form (Figure 27A and 27C). Nevertheless, the number of infected cells was significantly less in the P2Y1 receptor KO cells, showing that ADP signaling is also needed during the initial infections and not only for second rounds of infection. Since it is likely that ADP-driven calcium waves are needed for tight junction damage, the differences in infection levels between WT and P2Y1 KO cells would only be observed at high densities. In the case of a sparser set up, epithelial cells do not form tight junctions efficiently and thus the phenotypes would be similar. Rotavirus infection of cells seeded at lower densities indeed showed an increase in number of infected cells in P2Y1 KO cells, and colonies could also take place in this setup (Figure 27B and 27D). A comparison of infected cells and number colonies observed in P2Y1 KO cells seeded at low and high densities showed a significant reduction of infectivity at high densities (Figure 27E). These results highlight the need of calcium wave-dependent mechanisms to allow infection of confluent cultures of intestinal epithelial cells, which represent a normal intestinal epithelium.

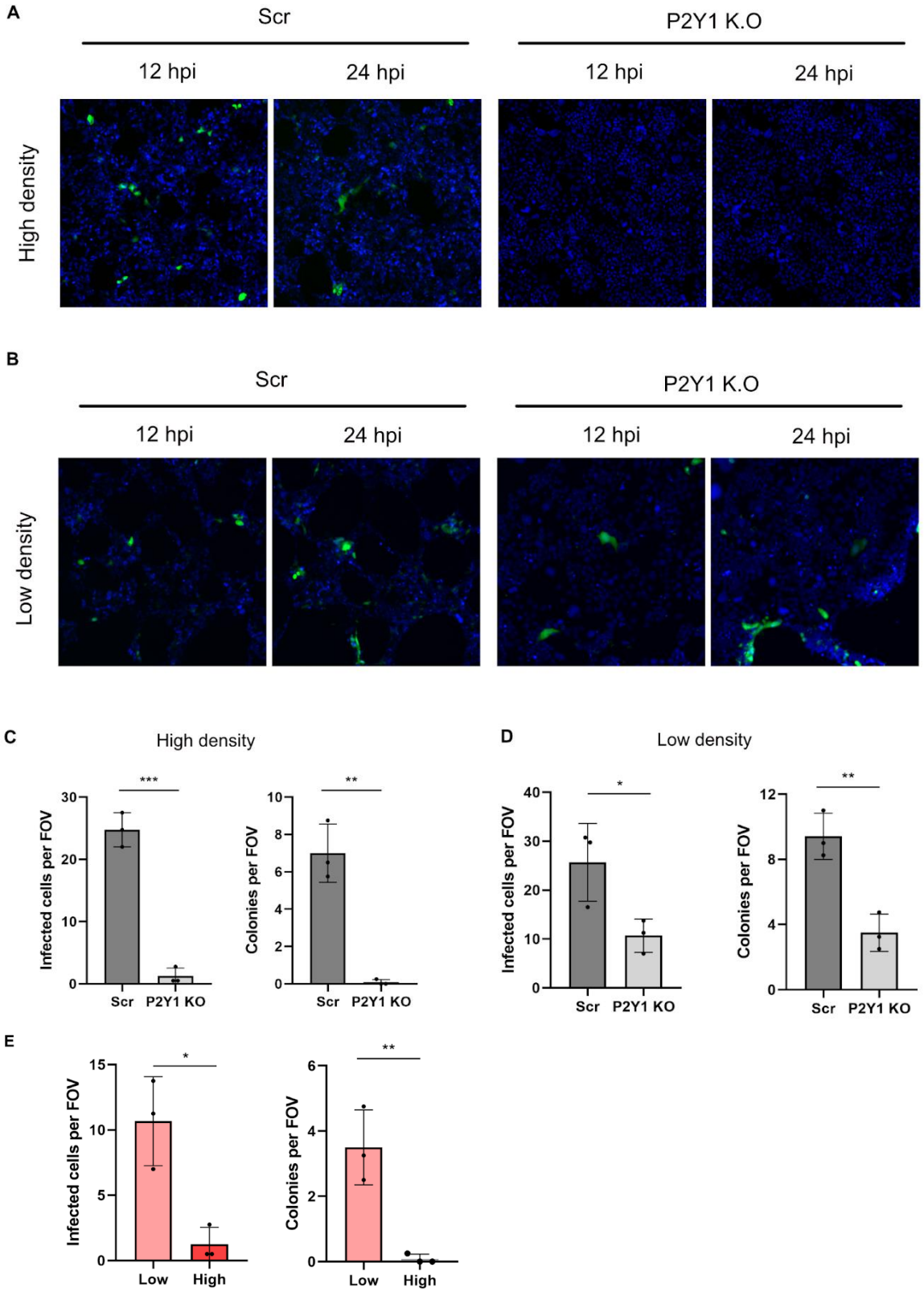

Figure 27. (A) Scr and P2Y1 KO T84 cells were seeded at full confluency and infected at an MOI of 0.1. Infection was tracked for 48 hours. Representative regions of fields of view observed at 12 and 24 hpi are displayed. Cell nuclei are shown in blue (H2B-mCherry). (B) Scr and P2Y1 K.O T84 cells were seeded at half confluency and infected at an MOI of 0.01. Infection was tracked for 48 hours. Representative regions of fields of view observed at 12 and 24 hpi are displayed. Cell nuclei are shown

in blue (H2B-mCherry). (C) Quantification of infected cells observed at 12 hpi and colonies formed at high density. (D) Quantification of infected cells observed at 12 hpi and colonies formed at low density. (E) Comparison of infected cells and colonies observed in P2Y1 cells seeded at low and high confluency. Error bars indicate standard deviation. n = 3 biological replicates. ns=not significant; P<0.05 *, P<0.01 **, P<0.001 ***, P <0.0001 **** (Unpaired t test is used for comparison).

2.3.5 A ZO-1 KO cell line emphasizes the importance of tight junction integrity during infection

To further evaluate the importance of tight junctions during rotavirus infection, the ZO-1 anchoring protein was knocked out from T84 cells through CRISPR KO (Figure 2). The guide sequence 'ATTCTGGTCGATCACACGAT', which targets exon 9, was cloned into the LentiCRISPRV2 vector using oligos 48 and 49 (See section 4.2.3.1). The integrity of ZO-1 was evaluated through immunofluorescence, showing a completely depleted population when compared to Scr cells (Figure 28A). It is expected that in ZO-1 KO cells second rounds of infection should take place in a sparser manner, since all cells already lack tight junctions and the infection area is not defined by calcium waves. Scr and ZO-1 KO T84 cells were seeded at full confluency, representing a healthy (Scr) and a damaged epithelium (ZO KO) respectively, and infected with UnaG rotavirus at an MOI of 0.1. Interestingly, a significantly higher number of infected cells and colonies was observed in ZO KO cells in comparison to Scr cells (Figure 28B-C). Furthermore, the area of infection covered by colonies was the same in WT and ZO-1 KO cells, showing that although infection is enhanced in the absence of tight junctions, other processes may help delimit the area where colonies form.

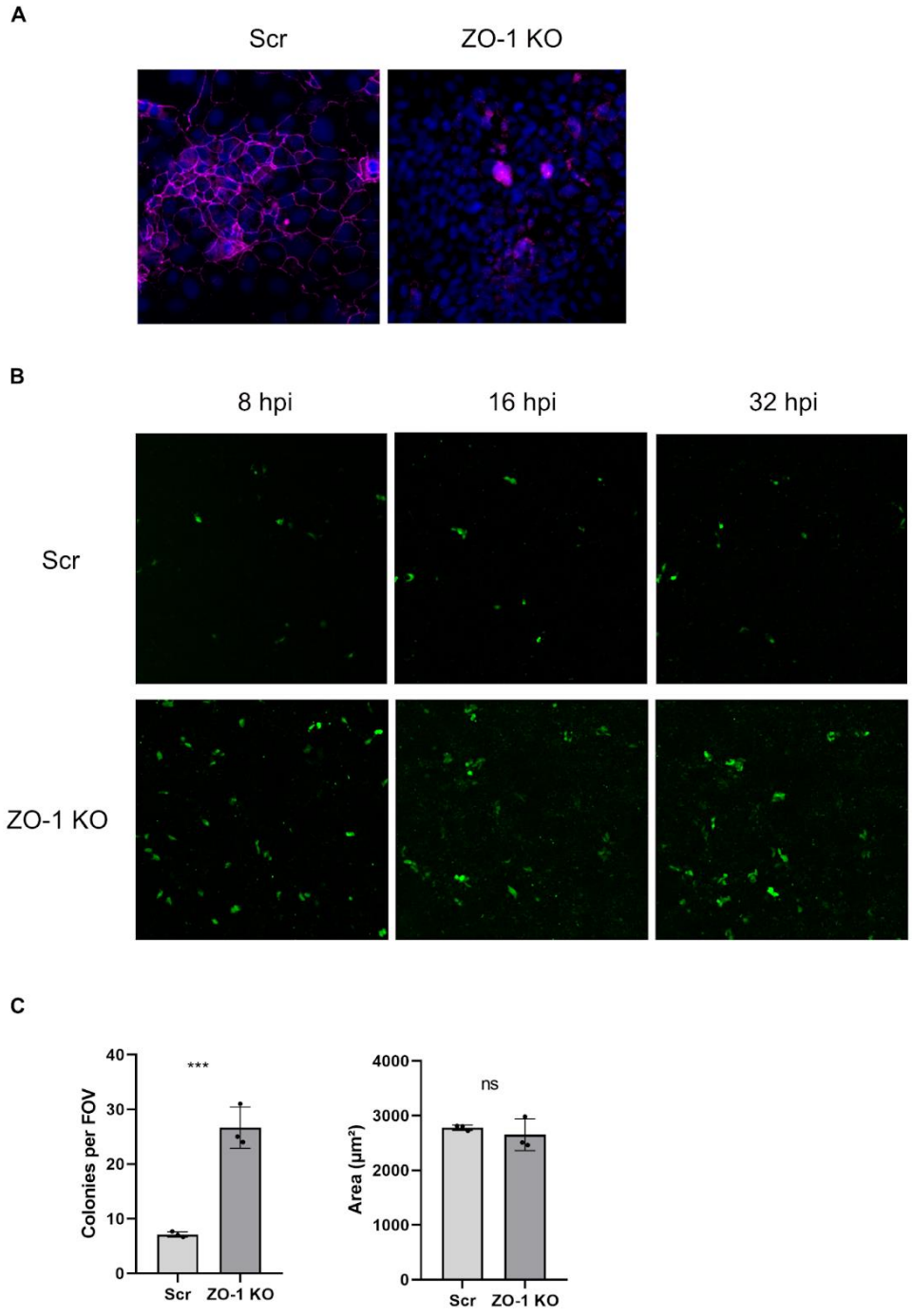

Figure 28. (A) Scr and ZO-1 KO T84 cells were seeded at full confluency 24 hours before fixation and immunofluorescence. Nuclei are stained with DAPI (blue) and ZO-1 is displayed in magenta. A representative region from a field of view is displayed. (B) Scr and ZO-1 KO cells were infected with UnaG rotavirus at an MOI of 0.1 and the infection was tracked for 48 hours. A representative region from a field of view is displayed. (C) The number of colonies observed in each field of view throughout the entire experiment, as well as the areas were quantified and compared between Scr and ZO-1 KO cells. Error bars indicate standard deviation. ns= not significant P<0.05 *, P<0.01 **, P<0.001 ***, P <0.0001 **** (Unpaired t test is used for comparison).

2.3.6 NSP4 silencing interferes with normal colony formation

Since the viral protein NSP4 drives calcium release and the subsequent ADP-driven calcium waves, I considered targeting this protein for shRNA-mediated silencing and evaluate its involvement in colony formation. T84 cells overexpressing an shRNA targeting NSP4 (NSP4 KD) or a non-targeting scramble shRNA (Scr) were generated through lentiviral transduction. These cell lines were seeded at high confluency, infected with UnaG rotavirus and the formation of colonies was tracked over time. Interestingly, I could observe the formation of colonies in both cell lines (Figure 29A), although those observed in the NSP4 KD cell line exhibited alterations in their development. Importantly, in Scr T84 cells cell death takes place as shown above (Figure 22), with infected cells simply detaching from the monolayer. On the contrary, infected NSP4 KD cells collapsed during infection (Figure 29A, bottom panel), and so did the colony they gave rise to. These differences in cell colony development had no impact on the number of colonies observed in both cell lines (Figure 29B). To evaluate whether the absence of the NSP4-induced increase in cytosolic Ca2+ has an impact on the time colonies take to form, the hours between cell death to colony formation were quantified. Interestingly, a significant decrease in colony formation time was observed between the two cell lines (Figure 29C), confirming that NSP4 plays a key role in preventing cell collapse during viral replication, and likely in supporting or accelerating the rotavirus replication cycle.

2.3.7 Rotavirus rapidly binds to intestinal epithelial cells

Since the formation of colonies could still be observed in P2Y1 KO cells seeded at low densities (Figure 27B), and also in cells expressing an shRNA targeting NSP4 (although abnormal) (Figure 29), it is possible that other mechanisms help drive colony formation. I hypothesized then that viruses produced by infected cells can rapidly and more easily bind to neighboring cells instead of those found farther away from the infection site. To study this, T84 cells were infected with UnaG rotavirus at an MOI of 0.1 for 0.1, 1, 5 and 60 minutes, cells were washed three times to remove unbound viral particles, and the formation of colonies was tracked for 48 hours. Interestingly, cells infected for 5 minutes showed the same number of colonies as those infected for

the full infection time (60 minutes) (Figure 30A-B). On the contrary, cells infected for 0.1 or 1 minute showed a significant decrease in colony number. These results stress the fast binding of rotavirus to cell receptors, which likely enhances infectivity in the area surrounding a first infection, in addition to the potential pro-viral processes activated by calcium waves.

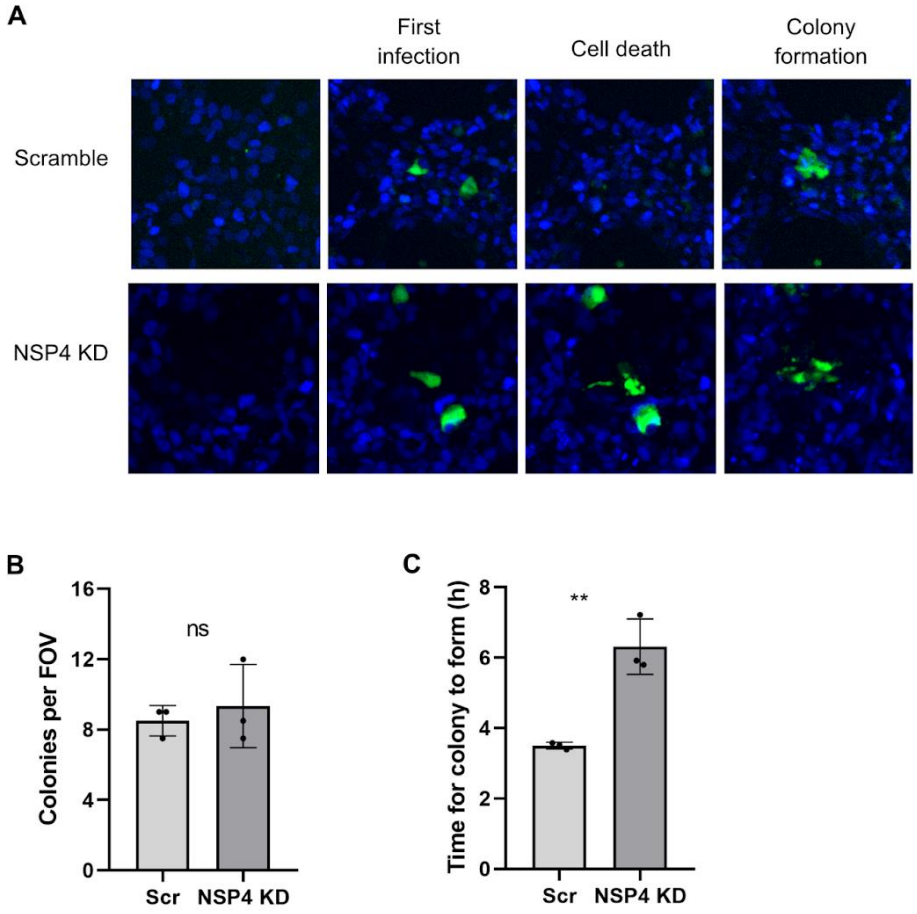

Figure 29. Scramble shRNA and NSP4 shRNA T84 cells were seeded at full confluency and infected with UnaG rotavirus (green) at an MOI of 0.1. Colony formation was tracked for 36 hours. (A) Representative images of scramble shRNA cells displaying formation of a normal colony, and NSP4 KD cells showing abnormal colony development. (B) Quantification of total number of colonies per field of view observed throughout the live experiment. (C) Quantification of hours between cell death and colony formation in Scr and NSP4 KD cells. Error bars indicate standard deviation. ns= not significant P<0.05 *, P<0.01 **, P<0.001 ***, P <0.0001 **** (Unpaired t test is used for comparison).

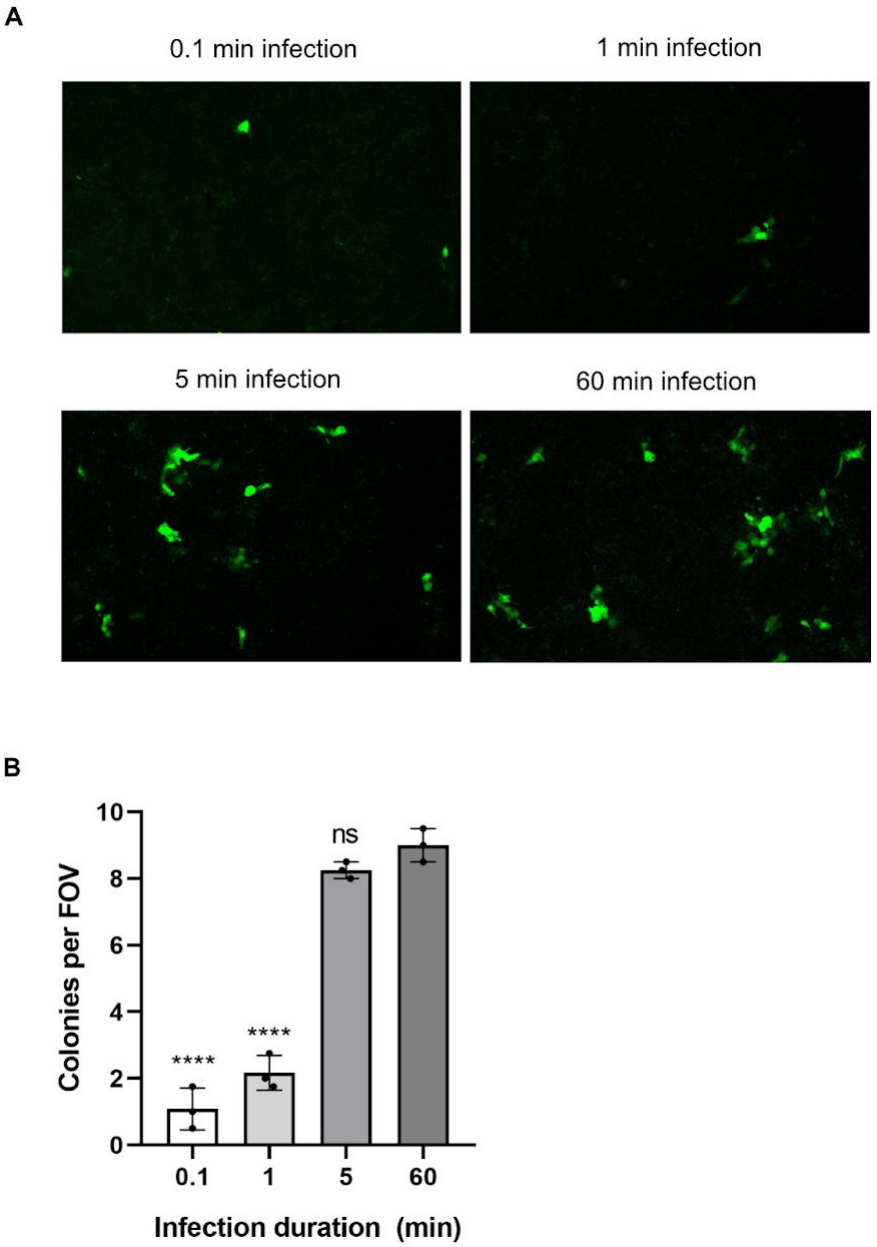

Figure 30. T84 cells were seeded at full confluency and infected with UnaG rotavirus (green) at an MOI of 0.1. Infection was carried out for 0.1, 1, 5 or 60 minutes and cells were washed to remove unbound viruses. Infection was tracked for 48 hours and the number of colonies per field of view was evaluated. (A) Representative regions of fields of view showing colony formation in each condition. (B) Quantification of colonies per field of view. Error bars indicate standard deviation. ns= not significant P<0.05 *, P<0.01 **, P<0.001 ***, P <0.0001 **** (Unpaired t test is used for comparison).

3 Discussion

3.1 Generation of fluorescent reporters for visualization of viral infection-induced innate immune response

Most studies aiming at describing the innate immune response elicited by enteric viruses focus on bulk results, in which entire populations of commercial cell lines are infected and studied together as one. Although these initial studies provide important information, it is likely that infected and uninfected cells behave differently throughout the course of the infection and also contribute differently to the overall innate response. Moreover, the timings and durations of each step of the cascade, as well as the differences in innate states established by different types of cytokines are not easily differentiated with these approaches. Because of this, the aim of my PhD project was to take advantage of fluorescent reporters that could allow the visualization and tracking of these different steps in single cells and obtain more thorough information of the innate cascade elicited by enteric viruses. In this work, I was able to generate and test a large amount of fluorescent tools through live fluorescence microscopy and to select the tools to address questions through the innate immune signaling pathway.

3.1.1 Fluorescently tagged IFN promoters efficiently report viral infection

Early during infection and detection of pathogens, the cytoplasmic IRF3 and IRF7 transcription factors can dimerize and translocate into the nucleus to activate the production of interferons. I have been able to show that fluorescently tagged versions of these proteins do not represent good reporters of infection, since their nuclear translocation seems impaired in confluent cultures. A relatively low number of translocation events is observed upon stimulation and they take place mostly in sparser cultures (Figure 7), which represents a drawback since intestinal epithelial cells are normally grown in confluency. It is evident that the polarized nature of intestinal epithelial cells alters their innate immune response, and that possibly different IRFs regulate IFN production depending on the polarized status of each cell, although this

has not been demonstrated. Moreover, in the case of viral infections, it is possible that cell receptors needed for binding viruses exhibit a polarized distribution, and their exclusive basolateral localization upon polarization makes them inaccessible [157]. This was shown to be the case for HCV, which uses the tight junction protein claudin-1 as a co-receptor and thus, infection is highly dependent on the polarized state of cells [158]. This was also found to be the case for Zika virus, which infects epithelial cells mainly by the apical membrane [159]. Similarly, Epstein-Barr virus infects polarized MDCK cells preferentially from their apical side [160]. Moreover, I have also focused on fluorescently tagging the promoter regions of type-I and type-III IFNs, the two main types of cytokines produced by intestinal cells to combat viral infections. Tagging of the IFNβ promoter with mCherry showed a relatively high basal level activity of the pathway in the T84 colorectal carcinoma cell, and thus an increased level of fluorescence in unstimulated cells (Figure 9). This is in accordance with studies showing basal expression of IFNβ in mouse embryonic fibroblasts [161], and primary cardiac myocyte cultures [162]. Similarly, the human lung epithelial cell line Calu-3 was shown to exhibit constitutive expression of IFNβ [163]. Moreover, in order to generate a fluorescent tool based on the activation of type-III IFNs, the IFNλ2,3 promoter was amplified from the genome of T84 cells and tagged with mCherry. In the case of this reporter, no basal mCherry fluorescence was visualized in unstimulated cells, and as observed with the IFNβ promoter-based reporter, a sustained and long lasting activation took place upon viral infection. Previous reports have shown that primary human trophoblasts produce IFNλ1 constitutively [164], as well as 3D models of syncytiotrophoblasts which produce IFNλ1 and IFNλ2 at basal levels [165]. This has not been studied thoroughly in the case of intestinal epithelial cells, but it is likely that IFNλ1 establishes a basal antiviral state, whereas IFNλ2,3 are only produced upon viral infection, as I have observed when studying the rotavirus-infection induced immune response in T84 cells (Figure 17). In this setup, the levels of IFNλ1 relative to those of a housekeeping gene are considerably high, and no basal IFNλ2,3 is observed. The generation of these type-I and type-III IFN promoters-based reporters is of great relevance when aiming at understanding the differences in timing and duration of the innate response established by each type of cytokine. The visualization of IFN activation provides information lost in bulk experiments regarding the number of cells able to mount the production of each cytokine and at what pace these events take place. Furthermore, this represents an advantage when focusing on the stochasticity of IFN production, showing whether a

fixed number of cells mount a type-I or type-III response. Additionally, these reporters mark infected cells in the culture, and in combination with fluorescent reporters of interferon sensing contribute to our understanding of how an antiviral state is elicited and controlled in the intestinal epithelium.

3.1.2 Viral infection reporters allow the visualization of norovirus and rotavirus infection

In addition to fluorescently tagged IFN promoters, other approaches were taken into account to detect what cells are infected in the culture. A fluorescent tool aimed at detecting HCV infection based on the cleavage of MAVS by the viral protease and the release of eGFP from the mitochondria was developed by another group in the past [150]. Continuing with this approach, I inserted cleavage sites found in the genome of norovirus in this reporter and expected that their cleavage by the viral protease would release eGFP from the mitochondria (or the ER) and show nuclear localization in infected cells. This reporter showed positive results, with clear eGFP signal in the nucleus of infected cells that were transfected with a plasmid encoding the norovirus protease (Figure 11C and 12C). In the case of the astrovirus infection reporters, no cleavage was observed upon infection (Figure 11B and 12B). It is likely that a structure more complex than that provided by short peptides is required for the correct positioning of the viral protease at the cleavage sites, or the structure of the reporter itself prevents the protease from reaching the cleavage sites. Moreover, fluorescent rotaviruses obtained from collaborators were of great importance in the project and showed advantages compared to other reporters. First, it is important to highlight that these viruses carry an extra gene encoding for a fluorescent protein in their genomes, and thus can only fluoresce during viral replication. This is beneficial since there is no increase in fluorescence due to viral particles in the media or attached to cells, but only from active viral protein translation. Moreover, the fluorescence generated during rotavirus infection was shown to be of high intensity, visualized early during infection and lasted until cell death (Figure 13). An important advantage of viral infection reporters when compared to fluorescently-tagged IFN promoters is that they can be visualized in any model regardless of the cytokine type produced. This is relevant for systems in which not all infected cells activate IFN production, generating false

negative results and an unrealistic starting point during the tracking of the innate immune response.

3.1.3 The activation of ISGs effectively reports sensing of IFNs

Once infected cells have been identified in the culture, it is of interest to detect which cells are able to sense secreted IFNs and are thus in an antiviral state. As a first approach to achieve this, I have focused and fluorescently tagging the three components of the ISGF3 complex: STAT1, STAT2 and IRF9. The canonical view is that the assembly of ISGF3 takes place in the cytoplasm, before it translocates into the nucleus for upregulation of ISGs [51]. Interestingly, it was not possible to generate an efficient fluorescent reporter based on the nuclear translocation of these proteins. In the case of IRF9, I have observed that the fusion protein eGFP-IRF9 localizes in the nucleus at a basal state and not in the cytoplasm (Figure 14A), which is in agreement with previous studies showing the nuclear localization of IRF9 in bone marrow-derived macrophages through immunofluorescence [166]. Moreover, overexpression of eGFP-IRF9 in the Atlantic salmon TO cells also showed nuclear localization of the fusion protein in unstimulated cells [167]. This highlights that the assembly of the full ISGF3 complex may take place in the nucleus, after the nuclear translocation of dimerized STAT1-STAT2 heterodimer. In the case of STAT1, it was not possible to generate a cell overexpressing the eGFP-STAT1 fusion protein, likely due to increased levels of STAT1 leading to cell death through an overactivation of a pathway. This is in agreement with a study carried out on human hepatocellular carcinoma cell line HepG2, in which overexpression of STAT1 induced cell cycle arrest and apoptosis [168]. Similar results were observed in cardiac myocytes transfected with a plasmid containing the sequence coding for STAT1 [169]. Interestingly, overexpression of the eGFP-STAT2 fusion protein did not induce cell death and exhibited an exclusive cytoplasmic localization. More importantly, it was possible to visualize the nuclear translocation of STAT2 upon IFN treatment, which lasted approximately 30 minutes (Figure 14B). A previous study has shown that after nuclear translocation, most STAT2 is exported back to the cytoplasm within one hour, which highlights the efficiency of the eGFP-STAT2 reporter in mimicking the behavior of endogenous STAT2 [170]. Because of the short duration and the low fluorescence intensity of the nuclear

translocation of eGFP-STAT2, this reporter would only be suitable for short-term experiments.

Upon nuclear translocation of the ISGF3 complex, its binding to the ISRE region of hundreds of ISGs establishes an antiviral state to prevent viral replication and spread. To be able to detect cells in an antiviral state, I took advantage of a previously generated mCherry tagged Mx1 construct. I have observed that upon type-I or type-III IFN treatment, cells overexpressing this construct exhibited an increase in mCherry signal over time, which lasted throughout the entire live fluorescence experiments (Figure 16). Importantly, this increase in mCherry signal matched an upregulation of transcript levels of endogenous Mx1 (Figure 20E), highlighting the efficacy of this fluorescent tool as a reporter of antiviral state. Moreover, upon treatment or viral infection the intensity of mCherry continued increasing for more than 24 hours, possibly due to mCherry being stable and not degraded. For the aims of this thesis, this represented an advantage, since it allowed the quantification of all cells that underwent an antiviral state during the entire experiment. If the intensity of mCherry were to decay, the quantification of positive cells would be hindered, as cells that turned mCherry positive earlier would be negative at later time points and not taken into account.

3.2 Intestinal epithelial cells rely exclusively on type-III IFNs to prevent rotavirus spread

3.2.1 WT and NSP1-deficient rotaviruses elicit different innate immune responses in T84 cells

Murine intestinal cells show upregulation of both type-I and type-III IFNs upon rotavirus infection, but the sensing of IFNs is limited to different cell types, with the lamina propria responding to type-I IFNs and epithelial cells to type-III IFNs [99,171]. In the case of human models, studies trying to elucidate the importance of type-I and type-III IFNs during rotavirus infection and spread have focused on the upregulation of IFN transcripts. The colorectal carcinoma cell line Caco2, for example, exhibits a strong upregulation of IFNλ1 upon infection, and small amounts of type-I IFNs [96]. Similarly, human intestinal organoids show induction of mainly IFNλ1 and IFNλ2 upon rotavirus infection and lower levels of type-I IFNs [98]. On the contrary, the human colon cancer cell line HT29 shows

a significant upregulation of IFNβ transcripts upon infection. In this thesis, I have observed that in the case of the T84 colorectal cancer cell line, WT SA11 rotavirus induces mainly the production of IFNλ2,3, and an upregulation of type-I IFNs could not be detected (Figure 17). The rotavirus protein NSP1 has been shown to efficiently block the production of both type-I and type-III IFNs, and thus it is likely that it plays a role in controlling the activation of type-I IFN production [105,172,173]. When comparing the innate immune response elicited in T84 cells by an NSP1-deficient rotavirus, I could observe a stronger upregulation of IFNλ2,3 than the one induced by WT virus, and significant amounts of IFNλ1 and IFNβ1 were also detected (Figure 17). These results highlight the possibility that type-III IFNs are regulated through a unique pathway that could have evolved to escape enteric viruses' halt of type-I IFN production. Moreover, it is also possible that small amounts of type-III IFNs are produced before the NSP1-mediated shutdown of the innate system takes place, and that this amount is enough to establish an antiviral response in the culture. Although IECs seem to favor type-III IFNs, type-I IFNs are of great importance to prevent dissemination of enteric viruses to other tissues. Mice lacking functional type-I IFN receptors have shown increased reovirus infection in their lamina propria, and this was also the case for norovirus [62,63]. It is not surprising then that rotavirus has evolved tools to efficiently block type-I IFNs, while IECs have evolved to favor type-III IFNs and combat viral replication in the epithelium. Importantly, previous studies could not detect the presence of IFNs in the supernatant of infected cells, although an upregulation of transcript was observed [96,98]. In this thesis, I took advantage of the HEK-Blue reporter cell lines developed by InvivoGen and knocked-out the IFNLR1 on them to generate a reliable assay to measure specifically the presence of either type-I or type-III IFNs (see section 4.2.10). These cell lines were used to successfully detect the presence of both types of IFNs in infected cells, which has not been possible in the past. This represents an important tool for elucidating the differences between type-I and type-III IFN-mediated antiviral responses, since viral shutdown can occur at the translation step or during IFN sensing, although upregulation of both transcripts is detected.

3.2.2 Type-III IFNs readily establish an antiviral state in IECs, whereas the type-I IFN mediated antiviral state is delayed and inefficient

Previous studies have shown that type-I and type-III IFNs can elicit similar antiviral states when added in trans, and thus protect cells from rotavirus infection to comparable levels [96,98]. In accordance with these studies, I have observed that pretreatment of T84 cells with either type-I or type-III IFNs are efficient in preventing infection (Figure 18), showing that cells are able to respond to these types IFNs at least when added in trans. Nevertheless, the timings and concentrations of IFNs required to prevent viral spread may differ in the context of an infection, and therefore cannot be evaluated with this setup. To better characterize the importance of type-I and type-III IFNs in preventing viral spread along the intestinal epithelium, I took advantage of previously generated T84 cells lacking functional IFN receptors [156]. These cell lines allow the reproduction of experiments carried out in IFNR KO mice and elucidate at what stage and to what extent one type of IFN is important to hinder viral replication/infection. Tracking the spread of WT and NSP1-deficient rotavirus in WT, IFNAR1-/-, IFNLR1-/- and double KO cells through live cell imaging showed that only cells able to respond to type-III IFNs can control viral spread (Figure 19). As observed through q-RT-PCR, WT rotavirus efficiently blocks the production of type-I IFNs, and thus it is likely that the small amounts of IFNλ2,3 produced are enough to prevent a second round of infection. Moreover, infection with the NSP1-deficient rotavirus showed almost no new infections after the first round of infection, likely due to the induction of higher amounts of IFNs (Figure 19C-D). Previous work has shown that type-I IFNs elicit a fast and acute immune response, whereas type-III IFNs do it in a delayed and sustained manner [68]. To evaluate whether this was the case in my setup, I took advantage of WT and IFNLR1-/- T84 cells transduced with the pMx1-mCherry fluorescent reporter. Interestingly, I observed a similar activation of the pMx1-mCherry fluorescent reporter during infection with either the WT or the NSP1-deficient rotavirus in WT cells, highlighting that indeed small amounts of IFNλ2,3 may be enough to prevent viral spread. Surprisingly, the NSP1-deficient rotavirus was able to activate the pMx1-mCherry reporter in IFNLR1-/- cells at late time points, showing a delayed activation of ISGs by type-I IFNs that cannot prevent viral spread. These results show opposite kinetics to those observed with IFNs added in trans [68], with type-III IFNs acting faster than type-I IFNs to establish an antiviral state during rotavirus infection. It is

possible then, that high amounts of type-I IFNs need to accumulate in order to elicit an antiviral response in IECs, since pretreatment of T84 cells with IFNβ before infection showed that these cells are indeed able to sense type-I IFNs efficiently and control viral replication (Figure 18).

3.2.3 Polarized intestinal epithelial cells exhibit preference for type-III IFNs

I have focused on using fully confluent T84 cultures to better mimic the intestinal epithelium, and thus cells exhibit an apical-basolateral polarized status. It is important then to highlight the possible implications that this setup may have on IFN sensing. The results observed in this work are in accordance with studies showing a possible set of ISGs that is exclusively activated by IFNλ2, as well as an upregulation of type-III IFN receptor levels as cells polarize [70]. Bhushal et al. (2017) have shown that murine intestinal epithelial cells respond differently to type-I and type-III IFNs depending on their polarity status [174]. In a non-polarized state, cells exhibit a strong response to type-I IFNs and a weak and delayed one to type-III IFNs. On the contrary, as cells polarize, their response to type-III IFNs increases and becomes comparable to that of type-I IFNs. This study has also shown a slight increase in type-III IFN receptor levels upon polarization. The polarized state of epithelial cells has an impact on the uneven distribution of proteins to the apical or basolateral membranes, and this has shown to be the case for interferon receptors. Human lung epithelial cells were shown to secrete IFNβ to both the apical and the basolateral side upon infection with influenza, but cells could only be stimulated from the latter [175]. This study showed that IFNAR is located mainly at the basolateral membrane, and thus limits the sensing of type-I IFNs from the apical side. This does not seem to be the case in T84 cells, since type-I IFNs can establish an antiviral state when added in trans. Nevertheless, during the course of infection with the NSP1-deficient rotavirus, type-I are secreted and detected in the supernatant, although they do not seem to be sensed efficiently by T84 cells. It is important to highlight then, that although both type-I and type-III IFNs are produced upon rotavirus infection, their sensing is influenced by the status of the culture, with a polarized state favoring type-III IFN-mediated immune response. Altogether, I propose that low amounts of type-III IFNs are enough to establish an antiviral state in a large number of cells, efficiently preventing the spread of a WT or NSP1-deficient rotavirus.

On the contrary, the concentrations of type-I IFNs needed to establish an antiviral response seem to be high, in addition to the possible implications that the polarized nature of T84 cells could have on IFN sensing.

3.3 Rotavirus-induced ADP-mediated calcium waves promote infection

3.3.1 Second rounds of infection take place as colonies and these are not delimited by IFN signaling

When tracking the spread of rotavirus over time, it was possible to observe that the pattern of infection does not seem to be random, but rather takes place in a conserved manner. This highlights the importance of the approach taken in this thesis, in which the use of fluorescent reporters and live cell microscopy contributed in ways that regular methods cannot, for example immunofluorescence of fixed samples or q-RT-PCR. During rotavirus infection, it is possible to visualize how the first round of infection takes place, and upon death of these cells, a second round of infection takes place in the same area where the first infections took place. Taking into account the efficiency of the paracrine action of type-III IFNs in establishing an antiviral state in a large number of cells, it is possible that new viruses can only infect cells nearby the first infection, which did not yet mount an antiviral response. In this scenario, colonies would form due to new viruses being able to infect nearby cells and not those farther away, which are able to undergo an antiviral state. Nevertheless, the formation of colonies is also observed in cells unable to sense type-III IFNs, highlighting that rotaviruses evolved IFN-independent tools to enhance and promote infection in the intestinal epithelium.

3.3.2 Calcium waves are necessary to allow second rounds of infection

Since the shape of infection colonies resemble the shape of rotavirus infection-induced calcium waves recently described by Chang-Graham et al. (2020) [121], a relationship between the two phenomena is likely. It has been shown in different publications that

the viral protein NSP4 is key in the induction of diarrhea, which is caused by a release of Ca2+ from ER reservoirs through the viroporin action of NSP4 [118,176,177]. An increase in cytoplasmic levels of Ca2+ induces the release of ADP, which acts as a signaling molecule and binds to the purinergic receptor P2Y1 on neighboring cells, inducing a release of Ca2+ from ER reservoirs, expanding the signal. The impact that calcium waves have on viral replication and spread of newly produced viruses has not been an important focus of previous studies. In this thesis, I evaluated the impact of the NSP4 protein and subsequent ADP release has on promoting infection of intestinal epithelial cells. I have observed that silencing NSP4 through overexpression of a targeted shRNA interferes with normal infection and the subsequent formation of infection colonies (Figure 29). Absence of NSP4 induces cell collapse during the first round of infection, and thus it is likely that a significantly low number of new viral particles is produced, reflected in the formation of abnormal colonies (Figure 29). The proviral properties of cytoplasmic Ca2+ have been demonstrated in a great variety of viruses. It has been shown that cytoplasmic Ca2+ levels play a role in the replication of HIV [178], and in the expression of the HCV core protein [179]. Moreover, the 2B protein of enteroviruses was shown to generate pores in the ER membranes [180], generating an influx of Ca2+ from the ER that allows viral replication [181]. Importantly, it has been shown that early during poliovirus, interplay with the viral genome activates cell death programs, but these are aborted as viruses replicate [182,183]. Coxsackieviruses mutant for the 2B protein, and thus unable to generate an increase in cytoplasmic Ca2+, failed to stop these apoptosis programs [180]. This is in agreement with the results obtained when silencing the rotavirus NSP4 protein, in which failure in increasing cytoplasmic Ca2+ caused a cells collapse in T84 cells and a delay in colony formation (Figure 29). Although NSP4 prevents cell death, it has been shown to induce diarrhea in mice when purified protein was added exogenously, likely due to the damage induced on tight junctions upon Ca2+ increase and subsequent leakage through the epithelium [184]. These mechanisms increase diarrhea and vomiting responses presumably to increase viral spread and dissemination along the intestines [121,185].

Interestingly, blocking ADP signaling through the purinergic receptor P2Y1 by adding the agonist molecule BPTU during infection did not allow colonies to form (Figure 26). Furthermore, the first round of infection was able to take place, showing that the binding of ADP to the P2Y1 receptor may be more relevant for the second round of infection to take place. The same phenotype was observed in T84 cells knocked out

for the P2Y1 receptor (Figure 27), although the number of infected cells during the first round of infection was also significantly reduced, confirming the importance of the pathway in promoting infection. These results are in accordance with those carried out by Chang-Graham et al. (2020) [121] in MA104 cells, which showed a significant decrease in viral yield in either BPTU treated or P2Y1 knock-out cells compared to WT. Since the results of this study were obtained through plaque assays, it is not possible to identify that this reduction in viral particles originates from an absence of new rounds of infection. Previous studies have shown similar scenarios for ATP, in which its release during viral infection promotes viral entry or replication. This was shown to be the case early during HIV infection, in which ATP released by the infected cells facilitates infection, and blocking of the pathway inhibits it [186]. Interestingly, Mariët et al. (2007) showed that infection of endothelial cells by Human cytomegalovirus (CMV) increased the expression levels of P2Y1 and P2Y2, highlighting the importance of purinergic signaling during infection [187]. Similarly, blocking of the purinergic receptor P2X7 in human hepatocytes was shown to prevent infection by human hepatitis B virus [188].

3.3.3 Tight junction integrity determines rotavirus infectivity level in intestinal epithelial cells

Intestinal epithelial cells lacking a functional P2Y1 receptor were shown to have a higher immunity towards rotavirus infection, although this was the case only when cells were grown at full confluency (Figure 27A). On the contrary, when cells were seeded in a sparsper manner, infectivity increased significantly (Figure 27B). These results highlighted an intrinsic difference between polarized and non-polarized cells, which determines the ability of rotavirus to enter or replicate in these cells. As described in section 1.1.2, as epithelial cells come in contact with each other they undergo polarization, characterized by the formation of tight junctions between adjacent cells. Previous studies have shown how during rotavirus infection, epithelial cells suffer rearrangements of their cytoskeleton and damage of some components of their tight junctions. Binding of rotavirus to cell receptors induce the formation of stress fibers through the activation of RhoA GTPases and the displacement of microtubules to the cellular periphery [114]. Activation of the RhoA/ROCK/MLC signaling pathway early

during infection was shown to alter the distribution of TJ proteins in MDCK cells, and also disrupt TJ integrity through contractions of the actomyosin ring [189]. Importantly, Realpe et al. (2010) have shown that rotavirus infects epithelial cells preferentially from their basolateral side, which was reflected on higher infectivity at the edges of cell colonies, where there is easier access to their basal side. Moreover, they could observe higher infectivity in cultures that were subjected to tight junction damage either chemically or physically. Furthermore, an early study has described that integrins are key during rotavirus infections, and these molecules have a polarized nature, localizing at the basolateral membrane [190]. All these studies are in accordance with the results obtained in this thesis, since it is likely that rotavirus induces tight junction damage early during infection through ADP-mediated calcium waves. Disruption of cell-to-cell contacts in the area where first infections took place would allow newly produced viruses to more easily reach co-receptors located in the basolateral side of these cells. Moreover, this explains why rotavirus can only infect P2Y1 KO cells when they are not seeded at full confluency, since their basolateral side does not need to be exposed by calcium wave-mediated TJ damage.

3.4 Conclusions and perspectives

The ability of type-I and type-III interferons to prevent the replication and spread of enteric viruses along the intestinal epithelium have been investigated in the past. These studies have focused on the use of murine models lacking specific interferon receptors, or analyzing the immune response mounted by bulk populations of commercial cell lines upon infection. Here, I utilized fluorescent reporters and live cell fluorescence microscopy to obtain a visual understanding of the timings and extent that these types of interferon elicit on intestinal epithelial cells during rotavirus infection and spread. I could observe that type-III IFNs establish an antiviral state in a large number of cells very efficiently, even in the presence of IFN antagonist viral protein NSP1. On the contrary, type-I IFNs could only be produced in the absence of NSP1, and the antiviral state established by these cytokines were delayed and not sufficient to prevent rotavirus spread. Taking advantage of fluorescent reporters, I could track how even when a low number of cells is infected, most of the cells in the culture can rapidly go into an antiviral state, highlighting the importance of the paracrine function of type-III IFNs in preventing rotavirus spread. It is possible to conclude that the intestinal epithelium favors type-III IFNs over type-I IFNs, since their production cannot be completely shut down by viruses and small quantities seem to be needed to upregulate ISGs. Besides antagonizing the innate immune response, I could observe that rotaviruses have evolved other tools to facilitate infection by newly produced viral particles. This is shown by the need of calcium wave-mediated mechanisms that define the area in which rotavirus can infect cells more easily. Overall I have shown that both the IFN antagonizing through NSP1 and the NSP4-mediated calcium waves play a key role in maximizing rotavirus infection and spread in intestinal epithelial cells. It is likely that rotavirus has evolved these tools to simultaneously increase viral titer whilst also destabilizing the cell-to-cell contacts that make the intestinal epithelium a barrier. This not only maximizes viral replication in a defined damaged area of the tissue, but also generates a ‘leaky epithelium’ that helps the propagation of rotavirus along the gastrointestinal tract.

4 Materials and methods

4.1 Materials

4.1.1 General chemicals, media, enzymes and reagents

Reagents and chemicals not listed below are described in the methods section in which they were used.

Table 4: List of chemicals, media, enzymes and reagents

Name	Manufacturer
ADP	Sigma-Aldrich
Agarose Standard	Carl Roth
Ampicillin (100 mg/mL)	Carl Roth
Bovine Serum Albumin	New England BioLabs
BPTU	Tocris
BsmBI	New England BioLabs
Collagen (from rat tail)	Sigma-Aldrich
CutSmart Buffer	New England BioLabs
DAPI	Sigma-Aldrich
dNTP set (100 mM)	Thermo Fisher Scientific
Dulbecco's Modified Eagle Medium (DMEM)	Gibco/Invitrogen
Dulbecco's Modified Eagle Medium: Nutrient Mixture F-12 (DMEM/F-12) (1:1) (1X)	Gibco/Invitrogen
DMSO (Dimethyl Sulfoxide), anhydrous	Life Technologies
EMEM 2X withouth Phenol Red and L-Glutamine	Sigma-Aldrich
Ethanol	Thermo Fisher Scientific
Ethidium bromide solution (10 mg/mL)	Carl Roth

Fetal Bovine Serum (FBS) Superior	Biochrom AG
Gateway BP-Clonase Enzyme Mix II	Thermo Fisher Scientific
Gateway LR-Clonase Enzyme Mix II	Thermo Fisher Scientific
Gel Loading Dye, purple, 6X	New England Biolabs
HEPES	Invitrogen
Human recombinant IFN-beta1a (IFNβ)	Biomol
Human recombinant IFNλ2 (IL28A)	Peprotech
Human recombinant IFNλ3 (IL-28B)	Cell signaling
Iscove's Modified Dulbecco's Medium (IMDM)	Gibco/Invitrogen
Isopropanol	Carl Roth
Kanamycin (50 mg/mL)	Carl Roth
LB agar and medium powder	Carl Roth
Minimum Essential Medium (MEM)	Gibco/Invitrogen
NdeI	New England BioLabs
NEB Buffer 2	New England BioLabs
NEB Buffer 3.1	New England BioLabs
NEBuilder HiFi DNA Assembly Master Mix	New England BioLabs
NucleoSpin Gel and PCR clean-up kit	MACHEREY-NAGEL
PenStrep (Penicillin Streptomycin)	Gibco/Invitrogen
Phosphate buffered saline (PBS)	Sigma-Aldrich
Phusion HF buffer (5x)	Thermo Fisher Scientific
Phusion hot start II DNA polymerase	Thermo Fisher Scientific
Poly I:C	InvivoGen
Proteinase K	Thermo Fisher Scientific
Puromycin (10 mg/ml)	Sigma-Aldrich
Quick-Load 1 kb DNA ladder	New England Biolabs

SOC Outgrowth medium	New England Biolabs
Sodium dodecyl sulfate (SDS)	Carl Roth
SsoAdvanced Universal SYBR Green	Bio-Rad
TritonX-100	Sigma-Aldrich
Trypsin – EDTA 0,25% and 0,05%	Gibco by Life Technologies and PAN biotech
Trypsin from bovine pancreas, TPCK treated	Sigma-Aldrich
T4 DNA Ligase	New England Biolabs
β-mercapoethanol	Sigma-Aldrich

4.1.2 Media and buffers

Table 5: List of media and buffers

Name	Composition
Culture medium for cells	DMEM / DMEM-F12 / IMDM / MEM 5 % FBS 1 % PenStrep
LB agar (pH 7.0)	10 g LB agar powder 150 mL H2O
LB medium (pH 7.0)	12,5 g LB medium powder 500 mL H2O
Phosphate buffered saline (PBS) 10x	137 mM NaCl 2.7 mM KCl 10 mM Na2HPO4 2 mM KH2PO4
SOC medium	2.66% (w/v) SOB-medium powder 20 mM D-(+)-Glucose

TE Buffer	10 mM Tris-HCl, 1 mM EDTA, pH 8.0
TNC Buffer pH 8	10 ml 1M Tris-HCl, pH 8.0 (20 mM Tris-HCl) 10 ml of 5M NaCl (100 mM NaCl) 0.5 ml of 1M CaCl2 (1 mM CaCl2) 479.5 ml distilled, deionized water
Tris-borate EDTA (TBE) running buffer 5x (agarose gel electrophoresis)	60,5 g Tris base 31 g H3BO3 3,7 g EDTA in H2O

4.1.3 Antibodies

Table 6: List of primary antibodies

Antibody	Source	Species	Application
Astrovirus	Santa Cruz (#sc-53559)	Monoclonal mouse	IF: 1:1,000
Cytochrome C	BD Biosciences (#556432)	Monoclonal mouse	IF: 1:1,000
Norovirus NSP6 (protease)	Generated in cooperation with the antibody unit of the Genomics and Proteomics Core Facility of DKFZ	Polyclonal guinea pig	IF: 1:5,000
Protein disulfide isomerase (PDI)	Cell Signaling (#2446)	Polyclonal rabbit	IF: 1:200
ZO-1	Thermo Fisher Scientific (#40-2300)	Polyclonal rabbit	IF: 1:1,000

Table 7: List of secondary antibodies

Antibody	Source	Species	Application
anti-mouse IgG Alexa Fluor 647	Invitrogen (A-21236)	Polyclonal goat	IF: 1:1,000
anti-guinea pig IgG Alexa Fluor 568	Invitrogen (A-11075)	Polyclonal goat	IF: 1:1,000
anti-rabbit IgG Alexa Fluor 647	Invitrogen (A-27040)	Polyclonal goat	IF: 1:1,000

4.1.4 Plasmids

Table 8: List of plasmids used in this thesis

Name	Resistance	Source
pWPI Puro eGFP-IRF3	Ampicillin / Puromycin	Dr. Binder (DKFZ)
pENTR221 IRF7	Kanamycin	Dr. Binder (DKFZ)
pWPI puro DEST	Ampicillin / Puromycin	Dr. Binder (DKFZ)
pENTR221 eGFP-IRF7	Kanamycin	This thesis
pWPI Puro eGFP-IRF7	Ampicillin / Puromycin	This thesis
pENTR221 IRF7-eGFP	Kanamycin	This thesis
pWPI Puro IRF7-eGFP	Ampicillin / Puromycin	This thesis
pLV pIFNB-mCherry	Ampicillin / Puromycin	Dr. Dijkman (University of Bern)
pENTR221 pIFNλ2,3-mCherry	Kanamycin	This thesis
pLentiX1 Puro pIFNλ2,3-mCherry	Ampicillin / Puromycin	This thesis
pWPI eGFP-NLS-MAVS	Ampicillin / Puromycin	Prof. Volker Lohman
pWPI eGFP-NLS-NdeI-MAVS	Ampicillin / Puromycin	This thesis

pWPI eGFP-NLS-Astro cleavage 1-MAVS	Ampicillin / Puromycin	This thesis
pWPI eGFP-NLS-Astro cleavage 2-MAVS	Ampicillin / Puromycin	This thesis
pWPI eGFP-NLS-Noro cleavage 1-MAVS	Ampicillin / Puromycin	This thesis
pWPI eGFP-NLS-Noro cleavage 2-MAVS	Ampicillin / Puromycin	This thesis
pTM_HA_Age_NS6	Ampicilin	Prof. Dr. Lohmann (Universitätsklinikum Heidelberg)
pENTR221 eGFP-NLS-NdeI-MAVS	Kanamycin	This thesis
pENTR221 eGFP-NLS-NdeI-SEC61B	Kanamycin	This thesis
pWPI eGFP-NLS-Astro cleavage 1-SEC61B	Ampicillin / Puromycin	This thesis
pWPI eGFP-NLS-Astro cleavage 2-SEC61B	Ampicillin / Puromycin	This thesis
pWPI eGFP-NLS-Noro cleavage 1-SEC61B	Ampicillin / Puromycin	This thesis
pWPI eGFP-NLS-Noro cleavage 2-SEC61B	Ampicillin / Puromycin	This thesis
pLV WT-STAT1	Ampicillin / Puromycin	Addgene (Plasmid #71454)
pLV STAT2	Ampicillin / Puromycin	Addgene (Plasmid #71451)
pLV IRF9	Ampicillin / Puromycin	Addgene (Plasmid #71452)
pENTR221 eGFP-STAT1	Kanamycin	This thesis
pWPI Puro eGFP-STAT1	Ampicillin / Puromycin	This thesis
pENTR221 STAT1-eGFP	Kanamycin	This thesis
pWPI Puro STAT1-eGFP	Ampicillin / Puromycin	This thesis
pENTR221 eGFP-STAT2	Kanamycin	This thesis
pWPI Puro eGFP-STAT2	Ampicillin / Puromycin	This thesis

pENTR221 STAT2-eGFP	Kanamycin	This thesis
pWPI Puro STAT2-eGFP	Ampicillin / Puromycin	This thesis
pENTR221 eGFP-IRF9	Kanamycin	This thesis
pWPI Puro eGFP-IRF9	Ampicillin / Puromycin	This thesis
pENTR221 IRF9-eGFP	Kanamycin	This thesis
pWPI Puro IRF9-eGFP	Ampicillin / Puromycin	This thesis
pLV pMx1-mCherry	Ampicillin / Puromycin	Dr. Dijkman (University of Bern)
pLV pISG56-mCherry	Ampicillin / Puromycin	Dr. Dijkman (University of Bern)
pLV pISG54-mCherry	Ampicillin / Puromycin	Dr. Dijkman (University of Bern)
pENTR221 pMx1-mCherry	Kanamycin	This thesis
pLenti X1 Zeo DEST	Zeocin	Addgene (Plasmid #17299)
pLenti X1 Zeo pMx1-mCherry	Zeocin	This thesis
LentiCRISPRv2 blast	Ampicillin / Blasticidin	Addgene (Plasmid #98293)
pCMV-GCaMP5G	Kanamycin	Addgene (Plasmid #31788)
pENTR221 GCaMP5G	Kanamycin	This thesis
pWPI puro GCaMP5G	Ampicillin / Puromycin	This thesis
LentiCRISPRv2 blast ZO-1	Ampicillin / Blasticidin	This thesis
LentiCRISPRv2 blast P2Y1	Ampicillin / Blasticidin	This thesis

4.1.5 Oligonucleotides and primers

Table 9: List of primers and oligonucleotides used for cloning and sequencing

Number	Sequence (5'-3')	Ta (°C)	Target
1	TCCTCCTGATCCTCCCTTGTACAGCTCGTCCATGCC	55-62	pENTR221 backbone with eGFP at the N' terminus
2	GACCCAGCTTTCTTGTACAAAG	65	
3	GGTGGCAGCCTGCTTTTTTG	55-62	pENTR221 backbone with eGFP at the C' terminus
4	ATGGTGAGCAAGGGCGAG	58-65	
5	CAAAAAAGCAGGCTGCCACCATGGCCTTGGCTCCTGAGAGG	58-70	IRF7 to be fused at the N' terminus of pENTR221
6	TCCTCGCCCTTGCTCACCATGGCGGGCTGCTCCAGCTC	58-70	
7	CAAGGGAGGATCAGGAGGAATGGCCTTGGCTCCTGAG	58-70	IRF7 to be fused at the C' terminus of pENTR221
8	GTACAAGAAAGCTGGGTCTTAGGCGGGCTGCTCCAGCTC	58-70	
9	GTACAAAAAAGCAGGCTTCGCAACGCGTCATATTCCTGAGTCCTTCCTTGC	65	pIFNλ2,3
10	CTCGCCCTTGCTCACCATCCCGGTACCGTCTGTGTCACAGAGAGAAAGGGAG	65	
11	GAAGCCTGCTTTTTTGTACAAA	58-65	pENTR221 backbone with mCherry at the C' terminus
12	**TATG**AAATATGGTCGGGTGTTAGCAGTCCATCAAACAAACACTGGGTACACTGG AGGTGCTGTC**CA**	-	Astrovirus restriction site 1 (Gln567-Thr568)
13	**TATG**GACAGCACCTCCAGTGTACCCAGTGTTTGTTTGATGGACTGCTAACACCC GACCATATTT**CA**	-	
14	**TATG**GAACGTGAGATGAAGGTGCTGCGTGATGAAATCAATGGAATACTTGCACC ATTCCTACAA**CA**	-	Astrovirus restriction site 2 (Glu654-Ile655)
15	**TATG**TTGTAGGAATGGTGCAAGTATTCCATTGATTTCATCACGCAGCACCTTCAT CTCACGTTC**CA**	-	
16	**TATG**CTTGGTGACTACGAGCTACAAGGACCTGAGGATCTTGCGGTG**CA**	-	Norovirus restriction site 1 (NS1.2-NS3)
17	**TATG**CACCGCAAGATCCTCAGGTCCTTGTAGCTCGTAGTCACCAAG**CA**	-	
18	**TATG**TTAGATGAATTTGAACTACAGGGCCCAGCTCTCACCACCTTC**CA**	-	Norovirus restriction site 2 (NS3-NS4)
19	**TATG**GAAGGTGGTGAGAGCTGGGCCCTGTAGTTCAAATTCATCTAA**CA**	-	
20	GGGGACAAGTTTGTACAAAAAAGCAGGCTTCGCCACCATGGTGAGCAAGGGCG AG	65	AttB sites are added to viral cleavage reporters
21	GGGGACCACTTTGTACAAGAAAGCTGGGTCCTAGTGCAGACGCCGCCG	65	
22	AGCACCAGCACCAGCACCCATATG	59-62	pENTR221 backbone with cleavage reporters and no MAVS

23	CATATGGGTGCTGGTGCTGGTGCTATGCCTGGTCCGACCCC	63	Sec61B
24	GTACAAGAAAGCTGGGTCCTACGAACGAGTGTACTTGCCCC	63	
25	ACTGAGACATAGATCTGAGTCCGGACTTGTAC	61	eGFP
26	TGTACAAAAAAGCAGGCTTCGCCACCATGGTGAGCAAG	61	
27	TACAAGAAAGCTGGGTCTTATACTGTGTTCATCATACTGTCG	60	STAT1
28	ACTCAGATCTATGTCTCAGTGGTACGAACTTC	60	
29	TTCTGACTTCTAAGACCCAGCTTTCTTG	63	pENTR221 for STAT2
30	ACTGCGCCATAGATCTGAGTCCGGACTTG	63	
31	GTCCCTGGTGTAAGACCCAGCTTTCTTG	64	pENTR221 for IRF9
32	CTGATGCCATAGATCTGAGTCCGGACTTG	64	
33	ACTCAGATCTATGGCGCAGTGGGAAATG	65	STAT2
34	CTGGGTCTTAGAAGTCAGAAGGCATCAAGGG	65	
35	ACTCAGATCTATGGCATCAGGCAGGGCA	68	IRF9
36	CTGGGTCTTACACCAGGGACAGAATGGCTG	68	
37	GGAGGATCAGGAGGAATGGTGAGCAAGGGCGAG	62	pENTR221 backbone with linker and eGFP at the C terminus
38	GCAGGCTGCCACCATGTCTCAGTGGTACGAAC	62	STAT1 for fusing to a C terminal eGFP
39	CCATGTCCTCCTGATCCTCCTACTGTGTTCATCATACTGTCG	62	
40	GCAGGCTGCCACCATGGCGCAGTGGGAAATG	62	STAT2 for fusing to a C terminal eGFP
41	CCATGTCCTCCTGATCCTCCGAAGTCAGAAGGCATCAAGGG	62	
42	GCAGGCTGCCACCATGGCATCAGGCAGGGCA	62	IRF9 for fusing to a C terminal eGFP
43	CCATGTCCTCCTGATCCTCCCACCAGGGACAGAATGGCTG	62	
44	GGGGACAAGTTTGTACAAAAAAGCAGGCTTCGCCACCATGGGTTCTCATCATCATC	65	GcAMP5G
45	GGGGACCACTTTGTACAAGAAAGCTGGGTCTCACTTCGCTGTCATCATTTG	65	
46	**CACC**CTACAGCATGTGCACGACCG	-	P2Y1 KO
47	**AAAC**CGGTCGTGCACATGCTGTAG	-	
48	**CACC**ATTCTGGTCGATCACACGAT	-	ZO-1 KO
49	**AAAC**ATCGTGTGATCGACCAGAAT	-	

Table 10: List of primers used for qRT-PCR

Name	Sequence (5'-3')
IFNβ1	Fw: GCCGCATTGACCATCTAT Rev: GTCTCATTCCAGCCAGTG
IFNλ1	Fw: GCAGGTTCAAATCTCTGTCACC Rev: AAGACAGGAGAGCTGCAACTC
IFNλ2,3	Fw: GCCACATAGCCCAGTTCAAG Rev: TGGGAGAGGATATGGTGCAG
Mx1	Fw: GAGCTGTTCTCCTGCACCTC Rev: CTCCCACTCCCTGAAATCTG
TBP	Fw: CCACTCACAGACTCTCACAAC Rev: CTGCGGTACAATCCGAGAACT

4.2 Methods

4.2.1 Culture of cells

I maintained T84 human colon carcinoma cells (ATCC CCL-248) in a 50:50 mixture of Dulbecco's Modified Eagle's Medium (DMEM) (Gibco) and F12 (Gibco) supplemented with 10% fetal bovine serum (FBS) and 1% penicillin/streptomycin (P/S) (Gibco). Caco-2 human colon adenocarcinoma cells (ATCC HTB 37) were grown in DMEM with 10% FBS and 1% (P/S). T84 and Caco-2 cells were maintained in T25 flasks coated with rat tail collagen and split 1:2 with 0.25% Trypsin/EDTA every 3-4 days.

I cultured HEK293T human embryonic kidney cells (ATCC CRL-3216) in Iscove's modified Dulbecco's medium (IMDM) supplemented with 10% FBS and 1% penicillin/streptomycin. MA104 cells were maintained in Minimum Essential Medium (MEM) (Gibco) supplemented with 10% FBS, 1% P/S and 2 mM L-Glutamine (Gibco). Lunet cells were cultured in DMEM with 5 µg/mL Zeocin (for selection of cells overexpressing a T7 polymerase), 10% FBS and 1% (P/S). These three cell lines were kept in T75 flasks and split 1:10 at 90% confluency using 0.05% Trypsin/EDTA.

All cells were kept at 37°C with a constant humid atmosphere containing 5% CO_2 and 21% O_2.

4.2.2 Viruses and viral infections

WT and NSP1-deficient rotaviruses expressing fluorescent markers were a kind gift from John Patton (Indiana University). I amplified, purified and tittered these viruses in MA104 cells as previously reported [191]. Briefly, I cultured MA104 cells in T150 flasks until confluency was reached. Cells were washed twice with serum-free MEM medium and 3 mL of serum-free MEM containing 2 µg/mL trypsin (Sigma) and 10 µL of rotavirus stock were added. I rocked the flasks every 10 minutes for one hour, and added 20 mL of serum-free MEM containing 0.5 µg/mL trypsin. Most flasks showed 5-10% infection, and viruses were left to replicate for 4-5 days until monolayers were completely detached. I freeze-thawed the flasks three times by placing them with their caps loose at -80°C until freezing completely, and then in an incubator at 37°C until thawing completely. I collected the media into 50 mL Falcon tubes, spun them down for 5 minutes at 2,000 rpm and semi-purified it with a sucrose gradient (35% sucrose in TNC Buffer). To achieve this, 35 mL of supernatants are aliquoted into 25×89 mm ultracentrifuge tubes (Beckman), and 2 mL of 35% sucrose are added carefully at the bottom using a 2-mL pipette. More supernatant was then added to fill the tube and centrifuged in a SW32Ti rotor for 2 hours at 27,000 rpm and 4°C. Supernatants were then discarded by inverting the tubes and each pellet was resuspended in 1 mL of TNC buffer. All resuspended pellets can be combined into 15 mL Falcon tubes and sonicated carefully on ice with a microtip probe to homogenize the suspensions. Semi-purified stocks were maintained at 4°C without loss in titer.

I tittered the semi-purified stocks by carrying out a plaque assay on MA104 cells and quantifying the plaque-forming units. 300,000 MA104 cells were seeded per well of 6-well plates and incubated until confluence was reached. 400 µL of semi-purified stock were incubated at 37°C for 1 hour in the presence of 10 µg/mL of trypsin. For ten-fold serial dilutions, eight Falcon tubes were prepared and 2.7 mL of serum-free MEM added to each. 300 µL of activated virus were added to the first tube, vortexed, and 300 µL taken into the second tube, until reaching a 10^-7 dilution. MA104 cells were washed twice using serum-free media, and 1 mL of each dilution added to cells in

duplicates. Infection was carried out for 1 hour, rocking the plates every 10 minutes for even distribution of viruses. After infection, cells were washed once with serum-free media, the media was aspirated and cells were covered with agarose as follows. 1.2% agarose was melted by microwaving, 10 mL were aliquoted into Falcon tubes (one per 6-well plate) and kept at 55°C in a water bath to avoid solidification. One at a time, Falcon tubes were taken to RT for 10 seconds, 10 mL of serum-free 2X EMEM containing 0.5 µg/mL trypsin were added, and 3 mL of the mix were gently added to each well. After the agarose solidified, 6-well plates were taken to the incubator and kept upside down at 37°C for 4 days. For visualization of plaques, 2 mL of a 1:1 mixture of 1.2% agarose and serum-free 2X EMEM containing 50 µg/mL neutral red were added on top of the first agarose layer and incubated for 16 hours at 37°C. One or two dilutions are selected for quantification of plaques, and the PFU/mL are calculated as follows:

$$30 \times 1/(\text{dilution factor}) \times 1/(1\ \text{mL} = \text{volume of infection media}) = \text{PFU/mL}$$

All rotavirus infections were carried out following the same procedure. First, I activated the rotavirus stock by adding the virus to serum-free media containing 2 µg/mL trypsin and incubated it at 37°C for 30 minutes in the absence of cells. Then, I washed cells twice with serum free media and added a volume of infection media depending on the well size used: 30 µL for 96 well plates, 100 µL for 48 well plates and 900 µL for 6 well plates. Unless stated otherwise, I rocked the plates every 10 minutes for 30 minutes. Following the 30 min infection, I aspirated the infection media and re-added serum-free media containing 1 µg/mL trypsin. All MOIs mentioned in the results section were calculated in MA104 cells.

I amplified human astrovirus in Caco-2 cells by growing cells to full confluency in T75 flasks, adding 100 µL from previous stocks and waiting for cells to show cytopathic effects. When cells started to detach, I freeze-thawed flasks three times from 37°C to 80°C, spun down the media and aliquoted the supernatant for future use. Mammalian orthoreovirus (MRV) was amplified and purified through a CsCl gradient previously in the group [192]. I carried out infections with astrovirus and MRV by adding the viruses at the indicated MOIs in media and adding it to the cells.

4.2.3 Cloning

4.2.3.1 Restriction cloning

Restriction cloning was carried out following manufacturer's instructions. In the case of NdeI restriction for generation of viral cleavage reporters, 1 µg of plasmids were incubated at 37°C for 1 hour in CutSmart Buffer before annealing. For generation of CRISPR/Cas9 KO vectors, 2 µg of the LentiCRISPRv2 blast vector were incubated in 2.5 µL of 10X NEB Buffer 3.1, 1 µL of BsmBI in NEB Buffer 3.1 and nuclease-free water to 25 µL of final volume. The reaction was carried out for 1 hour at 55°C. This generates an empty backbone of 12,983 bp and a smaller fragment of 1,890bp, which can be separated and purified from a 1% agarose gel through electrophoresis and gel purification.

For annealing of oligonucleotides to empty backbones, the following overhangs are added at the 5' end of guide sequences:

Forward oligo: CACC + guide sequence

Reverse oligo: AAAC + complementary sequence of guide sequence

2.5 µg of forward oligos and 2.5 µg of reverse oligos were first incubated in 5 µL of NEB Buffer 2 and 40 µL of nuclease-free water for 5 minutes at 95°C. The mix was cooled down at room temperature before proceeding. 2 µL of oligos mix were incubated with 150 ng of digested vectors, 2 µL of T4 Ligase buffer, 1 µL of T4 Ligase and nuclease-free water for a final volume of 20 µL. The reaction took place for 2 hours at room temperature and the entire volume was used for bacterial transformation (see section 4.2.4).

4.2.3.2 HiFi DNA Assembly

DNA fusion was carried out through HiFi DNA Assembly (New England BioLabs) as per manufacturer's instructions. I first amplified the sequences of interest through PCR using primers shown in section 4.1.5 at the indicated annealing temperatures. Reactions were carried out in a volume of 50 µL, using a Phusion High-Fidelity DNA

Polymerase (New England BioLabs). The time of extension was 30 seconds per kb of target sequence. I then ran the entire reaction in a 1% agarose gel and purified the DNA using a NucleoSpin Gel and PCR clean-up kit (MACHEREY-NAGEL). The amount of DNA was determined using a NanoDrop Lite spectrophotometer (Thermo Scientific). The pmols/µL found in each reaction were then calculated using Promega Biomath Calculators. When fusing two fragments, 0.05 pmols of the vector was combined with 0.1 pmols of the insert. When three fragments were fused, 0.03 pmols of the vector was combined with 0.06 pmols of each insert. When fusing four fragments, 0.05 pmols of each sequence was combined. Nuclease-free water was used to reach a final volume of 10 µL and 10 µL of NEBuilder HiFi DNA Assembly Master Mix was added for 1 hour at 50°C. 1 µL of DpnI was then added and incubated for 1 hour at 37°C to eliminate template DNA from the mix. Bacteria were then transformed with the entire reaction (see section 4.2.4).

4.2.3.3 Gateway cloning

Generation of entry and lentiviral vectors was carried out through Gateway cloning (Thermo Fisher Scientific) as per manufacturer's instructions. For generation of an entry vector (pENTR221), I either built it directly through HiFi DNA assembly, or the fragment of interest was first amplified with flanking AttB sites through PCR. To achieve this, the following sequences were added as overhangs at the 5' end of primers:

Forward AttB sequence: GGGGACAAGTTTGTACAAAAAAGCAGGCTTC**GCCACC (kozak sequence in bold, optional)**

Reverse AttB sequence: GGGGACCACTTTGTACAAGAAAGCTGGGTC

150 ng of this fragment were then mixed with 150 ng of a pDONR221 vector, TE Buffer pH 8 was added to a final volume of 8 µL and then 2 µL BP Clonase II enzyme mix were added. The reaction was incubated for 1 hour at 25°C and stopped with 1 µL of Proteinase K at 37°C for 10 minutes. For generation of a lentiviral vector, 150 ng of the entry vector pENTR221 containing the sequence of interest were incubated with 150 ng of the destination lentiviral vector. TE Buffer pH 8 was added to a final volume of 8

µL and then 2 µL LR Clonase II enzyme was added and the mixture was incubated for 1 hour at 25°C. The reaction was stopped by adding 1 µL of Proteinase K to the mix for 10 minutes at 37°C. The entire BP or LR reaction are used for transformation of bacteria (see section 4.2.4).

All plasmids were evaluated using SnapGene to verify the correct design of primers and reading frame of fusion proteins.

4.2.4 Bacteria transformation

For amplification of vectors generated through DNA cloning, Subcloning Efficiency DH5α bacteria (Thermo Fisher Scientific) were used. I first aliquoted the bacteria stock on ice into 50 µL aliquots and used one for each transformation. Bacteria were mixed carefully with the plasmid of interest and left on ice for 30 minutes, then they were heat-shocked at 42°C for 25 seconds and taken back to ice for 2 minutes. I added 250 µL of SOC medium to each tube close to a flame and left the bacteria to grow for 1 hour at 37°C in a tube shaker. The entire reaction was plated afterwards on LB agar plates containing antibiotics and left to grow at 37°C overnight. Individual colonies were picked from the plates, grown in 5 mL of LB medium for 14 hours and plasmid extraction was carried out using a NucleoSpin plasmid kit (MACHEREY-NAGEL). In the event that larger amounts of a plasmid were needed, 50 µL from the previously cultivated bacteria were added to 100 mL of LB medium in an Erlenmeyer flask and grown overnight at 37°C. In this case, plasmid purification was carried out using a NucleoBond Midi kit. The plasmids of interest were then sent for sequencing to confirm their identity and bacteria were frozen at -80°C in a 1:1 mix with 60% glycerol for long-term storage.

4.2.5 Transfection, transduction and lentivirus production

Transfection of plasmids and poly I:C was carried out on cells seeded at half confluency in 24-well plates. First, 2 µL of Lipofectamine 2000 were incubated with 48

µL of Opti-MEM in an eppendorf tube for 5 minutes. In another tube, 800 ng of plasmid were added to 50 µL of Opti-MEM and the contents of the two tubes were mixed carefully and incubated for 20 minutes. In the case of poly I:C, a mixture of 500 ng of high molecular weight poly I:C and 500 ng of low molecular weight poly:IC are used. 500 µL of fresh media were added to cells, and the transfection mix was added dropwise. Cell media was changed after 8 hours and cells were imaged 24 hours post transfection.

For production of lentiviruses, HEK293T cells were seeded in cell culture treated 10 cm dish two days before transfection. Upon reaching 50-60% confluency, 48 µL of polyethylenimine (PEI) were incubated with 202 µL of Opti-MEM for 5 minutes. In parallel, 4 µg of each helper plasmid pMD2.G and psPAX2 were combined with 8 µg of lentiviral vector in 250 µL of Opti-MEM. The contents of the tubes were then combined carefully and incubated for 20 min. 10 mL of fresh media were added to the cells, and the transfection mixture added dropwise. 8 hours after transfection the media was replaced. 3 days post transfection, the supernatants were collected and centrifuged at 4,000 g for 5 minutes to remove cells. Supernatants were then filtered through 0.45 µm filters (Millex-HA, 0.45µm, Millipore, SLHA033SS), moved to 14x95 mm Ultra-clear centrifuge tubes (Beckman Coulter), and concentrated by ultracentrifugation at 27,000 rpm for 2 hours in a SW40 Ti rotor (Beckman Coulter). Supernatants were discarded by inverting the tubes, 100 µL of Opti-MEM were added and centrifuge tubes were left in ice at 4°C overnight. 20 µL aliquots were prepared and stored at -80°C.

Lentiviral transduction was carried out in cells seeded at low confluency, using 300,000 cells per well of 6-well plates. One aliquot of lentiviruses was added to 2 mL of media containing 10 µg/mL polybrene and cell media was replaced with transduction media. Three days post transduction, cell media was replaced with antibiotic-containing media for selection. The concentrations of antibiotics used for T84 cells were: 10 µg/mL puromycin, 10 µg/mL blasticidin, 500 µg/mL neomycin (G418), 100 µg/mL zeocin. For CaCo2 cells 10 µg/mL puromycin were used, and 1 µg/mL puromycin for Lunet cells.

4.2.6 Site-directed mutagenesis

The pWPI eGFP-NLS-MAVS lentiviral vector was modified by inserting a restriction site for the NdeI restriction enzyme in between NLS and MAVS. I designed primers containing the restriction site CATATG in between the target sequence:

Forward primer (5'-3'): caaagtgaagcttcgaattctcCATATGggtgctggtgctggtgctgg

Reverse primer (5'-3'): ccagcaccagcaccagcaccCATATGgagaattcgaagcttcactttg

These primers were ordered with a phosphorylation at the 5' terminus for ligation of the nick generated after amplification. PCR was carried out with a Phusion hot start II DNA polymerase using an annealing temperature of 65°C. Due to the large size of the target vector (approximately 12 kb), successful generation of the mutated plasmid is very low. Several PCR reactions were carried out simultaneously and the entire reactions used for bacteria transformation until a colony was obtained.

4.2.7 Indirect Immunofluorescence (IF) assay

Following experimental set-up, cells were fixed with 2% PFA for 20 minutes at room temperature. Cells were washed three times with PBS, and permeabilized using 0.5% Triton X-100 for 10 minutes. Blocking was carried out using 3% BSA/PBS for 30 minutes at room temperature, and incubated with primary antibodies in 1% BSA/PBS. Cells were washed three times with PBS and incubated with secondary antibodies and DAPI in 1% BSA/PBS for 20 minutes in the dark. Cells were washed and PBS was added to prevent drying. A PerkinElmer spinning disk confocal microscope was used for imaging fixed samples.

4.2.8 RNA-FISH

RNA-FISH probes tagged with the fluorescent dye Quasar 670 were synthesized by Stellaris, and were designed manually to target the entire genome of SA11 rotavirus. Four probes were designed per gene, except for NSP4 which has three and NSP5 that

has five (Table 11). RNA-FISH probes were dissolved in 400 µL of TE Buffer to obtain a 12.5 µM stock. Rotavirus-infected cells were fixed with 2% PFA for 20 minutes at room temperature, washed twice with 1X PBS and permeabilized in 70% ethanol for 1 hour at 4°C. 70% ethanol was discarded and 100 µL of complete wash buffer A (Stellaris) prepared as follows was added to cells at RT for 5 minutes: 2 mL Stellaris RNA FISH Wash Buffer A (#SMF-WA1-60), 7 mL nuclease-free water and 1 mL deionized formamide (Thermo Fisher Scientific). Complete wash buffer A was aspirated and replaced with 100 µL of 10% (vol./vol.) deionized formamide in hybridization buffer (Stellaris #SMF-HB1-10) containing a 1:100 dilution of RNA-FISH probes for 4 hours at 37°C. To prevent evaporation, 48-well plates were sealed with parafilm and covered on wet tissue paper during hybridization. Hybridization buffer was then aspirated and 100 µL of complete wash buffer A was added to each well for 30 minutes at 37°C in the dark. To stain the nuclei, buffer was aspirated and 5 ng/mL DAPI in wash buffer A is added for 30 minutes at 37°C in the dark and aspirated. 100 µL of wash buffer B (Stellaris, #SMF-WB1-20) was added per well at RT for 5 minutes and aspirated. A drop of VECTASHIELD Mounting Medium (Vector laboratories, #H-1000-10) was added to preserve fluorescence.

Table 11: List of RNA-FISH probes targeting the SA11 rotavirus genome

Gene	Probe sequence
VP1	CTTTCGCATACTTCACCAAT ATCTGTACTTTGCGTTATGC GCATAGTTATCATCTCCATC GTTTCTCTTACATCGTTCGA
VP2	TAGGCAATTGTTTCGGTTCA CTCCATCAGGAAGAGTATCT CGTAGCATTTCCAATTAGCA ACATTTGGTCATCTGGTACT
VP3	AAGCGTCGTTCAATCTGTTC ATGTTAATTTCCATCCAGGT AGAGTCCTAAACAACCGTCG GTAGCAGATTCCGAAAACCT
VP4	ACCTTCAACAATTACGCCAG AATAATGTGCTGTCCTAGCG AGTCATCATTTGATGGCACT CTCCTAACTGCCTTTCTAAA
VP6	CAATTTTGTCTCTAGCGTCT CCATGCATACATTGTCTACA CATGTTTGGTGGTCTCATTA

	AAGACTGGTCCAACTGGTAT
VP7	GAGCCTGTGATTGGAAGATT AATATACGGATCCAGTTGGC TTGTGACATCCAGCTTATGA CAGTTAATTCGCATCATCCG
NSP1	AGGAAGCATCTTCTGTTCTG CCTACATTCTCTTTGCTTTA CTGGATATCGGAAGCATTGC CAACTGACACTGGCGACATG
NSP2	ACTTATCCATGTCCTTTTTG TCCTGTGGATTTTCTTTACG AAATGCATACCAGTTTTGCC AAGCCATCATCATCCTCAAA
NSP3	ATCTTGAGCATCAACCACTG ATTCCCATATTCTCAAGAGC CTGCTCTAGAAGTATCAGCA GTTTGTTTACATCCTCATCT
NSP4	TTGAGGTCGGTAAGCTTTTC GAAAATACGCCATTCCTGGA TGTCCATTTGCTTTTCTATC
NSP5	ACTGTAGCGCTTTAAAAGCC AGGAAGACTCGTCACGTCAA GTTCACTCCTACCAATAGAT AGCAGAATCAGATGGTCCAA AACTGGTGAGTGGATCGTTT

4.2.9 RNA extraction, cDNA and qRT-PCR

T84 cells were lysed using a NucleoSpin RNA extraction kit (MACHERY-NAGEL) following manufacturer's instructions and the amount of total RNA was measured using a NanoDrop Lite spectrophotometer (Thermo Scientific). 100 ng of RNA were used to synthesize cDNA using an iScript cDNA Synthesis kit (Bio-Rad Laboratories) following manufacturer's instructions: 100 ng of RNA in 15 µL of nuclease-free water, 4 µL of iScript reaction buffer and 1 µL of reverse transcriptase. The reaction was carried out in a thermal cycler (Biorad), using the following program: Priming for 5 min at 25°C, reverse transcription for 30 minutes at 42°C and reverse transcription termination/inactivation for 5 min at 85°C.

The reverse transcribed cDNA was diluted 1:1 in nuclease-free water, and q-RT-PCR was carried out SsoAdvanced Universal SYBR green Supermix (Bio-Rad), using the following scheme: 7.5 µL of SsoAdvanced Universal SYBR Green Supermix, 1.9 µL of

forward primer (2 µM), 1.9 µL of reverse primer (2 µM), 1.7 µL of nuclease-free water and 2 µL of cDNA. The reaction was carried out for 40 cycles using the following program: activation for 30 sec at 95°C, melting for 5 sec at 95°C, primer annealing and elongation for 30 sec at 60°C and plate read. The expression levels of genes of interest were analyzed using the Bio-Rad CFX Manager 3.0 and normalized to the levels of the housekeeping gene TBP.

4.2.10 HEK-Blue assay

For detection of interferons in supernatants, I have made use of the HEK-Blue reporter cell lines developed by InvivoGen, HEK-Blue IFN-α/β for type-I IFNs and HEK-Blue IFN-λ for type-III. Cells were maintained in culture as described in section 4.2.1, avoiding full confluency and high passage numbers (above passage 20). Since HEK-Blue IFN-α/β cells are able to respond to type-III IFNs, I first generated a modified cell line by knocking-out the IFN Lambda receptor I (IFNLR1) with our previously generated lentiviral vector (sgRNA #2 from [156]). I seeded HEK-Blue IFN-α/β cells in 6-well plates at low confluency (approximately 10-20%) and transfected them with the lentiviral vector. For each well, 34 µL of Opti-MEM are incubated with 8 µL of PEI for 5 minutes in an Eppendorf tube; in a second tube, 1 µg of plasmid is added to 34 uL of OptiMEM and the tubes are combined carefully and incubated for 20 minutes. Media is then aspirated from the wells and slowly replaced with 1 mL of fresh media, to which the transfection mixed is added dropwise while rocking the plate. 8 hours after transfection, I changed the media and gave the cells 2 days to express resistance to hygromycin. Cells were then split and moved to T25 flasks at different densities, giving them 1 day to recover and attach. A flask with cells at approximately 25% confluency was selected and treated with 200 µg/mL hygromycin, replacing the media every 2 days and avoiding confluency by splitting cells into larger flasks. I avoided adding hygromycin on cells after splitting them and waited for them to attach, since I have observed that they are sensitive to the antibiotic before proper attachment to the flask. Cell death occurred after 3-4 days of treatment, and the selected cell line showed no response to type-III IFNs, being named HEK-Blue IFN-α/β IFNLR1-/-. This cell line was then maintained in cultured in the presence of 10 µg/mL blasticidin, 1 µg/mL puromycin and 200 µg/mL hygromycin. HEK-Blue IFN-λ cells were cultured in the presence of 10 µg/mL blasticidin, 1 µg/mL puromycin and 100 µg/mL zeocin.

To carry out HEK-Blue assays, the supernatants of interest and the one used to culture HEK-Blue cells need to match and contain heat inactivated serum. I prepared DMEM/F12 medium containing 1% P/S and 10% FBS previously inactivated in a water bath at 56°C for 30 minutes, and used it to culture both T84 and HEK-Blue cells. One day before the assay, 25,000 HEK-Blue cells were seeded per well of a 96-well plate, with extra 12 wells for the standard curve were seeded in duplicates. If the supernatants are frozen, the standard curve needs to be prepared in the same conditions and frozen before thawing all samples for the assay. 50 µL of sample are added carefully to each well for 24 hours. For the type-I IFNs standard curve, I treated HEK-Blue cells with five 1:1 serial dilutions of IFNβ1 starting at 10,000 IU/mL and leaving the last dilution without IFNs. For the type-III IFNs standard curve, I used five 1:3 dilutions of 1:1 mixture of IFNλ2 and IFNλ3 starting at 100 ng/mL total, leaving the last wells empty as controls. For the colorimetric assay, QUANTI-Blue (InvivoGen) was used to determine the amount of Secreted embryonic alkaline phosphatase (SEAP). First, the supernatant from each well was pipetted up and down several times and 30 µL were transferred to a new 96-well plate. I added 120 µL of QUANTI-Blue media to each well with a multi pipette, covered the plates with aluminum foil and kept them at 37°C to accelerate the reaction. Plates were checked every 5 minutes until the standard curve started changing from pink to blue, and plates were scanned at 620 nm with a Biorad iMark microplate reader. The amount of IFNs was determined by comparison to the standard curve. The presence of rotavirus in supernatants did not alter the assay, since infected HEK-Blue cells do not seem to produce detectable levels of IFNs.

4.2.11 Live cell fluorescence microscopy and image analysis

T84 cells were seeded in 48-well plates at full confluency 24 hours before experiments. Cells were infected as previously described, and the spread of viruses and activation of fluorescent reporters were imaged over time using a Celldiscoverer 7 (Zeiss). Cells were kept at 37°C and 5% CO2 during all experiments. For rotavirus infection and spread, UnaG was imaged with a 470 nm LED lamp at 30% laser power and 300 ms exposure time. H2B-mCherry was imaged with a 590 nm LED lamp at 50% laser power and 300 ms exposure time. For visualization of activation of the pMx1-mCherry reporter, H2B-mTurquoise was imaged using a 420 nm LED lamp at 50% laser power

and 300 ms, UnaG using a 511 nm LED lamp at 50% and 300 ms, and pMx1-mCherry with a 590 nm LED lamp at 60% laser power and 500 ms. Quantifications of infection and quantification of Mx1-mCherry positive cells were carried out using ilastik (https://www.ilastik.org) to generate object masks using the H2B-tagged nuclei as reference. The basal fluorescence of the reporters was subtracted from infected or treated samples in Fiji (https://fiji.sc) based on the levels found in mock treated samples. To determine the values used to separate positive from negative cells, the mean intensity of fluorescence found in nuclei was measured in mock treated and treated samples. CellProfiler (https://cellprofiler.org) was then used to measure the mean intensity of fluorescence in all objects found in the masks (nuclei) in all conditions, and positive cells were quantified using the threshold values obtained from Fiji.

5 References

1. Pott, J. & Hornef, M. Innate immune signalling at the intestinal epithelium in homeostasis and disease. *Nat. Publ. Gr.* **13**, (2012).
2. Sato, T. *et al.* Paneth cells constitute the niche for Lgr5 stem cells in intestinal crypts. *Nat. 2010 4697330* **469**, 415–418 (2010).
3. Miron, N. & Cristea, V. Enterocytes: active cells in tolerance to food and microbial antigens in the gut. *Clin. Exp. Immunol.* **167**, 405 (2012).
4. Kim, Y. S. & Ho, S. B. Intestinal goblet cells and mucins in health and disease: recent insights and progress. *Curr. Gastroenterol. Rep.* **12**, 319–330 (2010).
5. Johansson, M. E. V., Holmén Larsson, J. M. & Hansson, G. C. The two mucus layers of colon are organized by the MUC2 mucin, whereas the outer layer is a legislator of host-microbial interactions. *Proc. Natl. Acad. Sci. U. S. A.* **108 Suppl 1**, 4659–4665 (2011).
6. Schonhoff, S. E., Giel-Moloney, M. & Leiter, A. B. Minireview: Development and differentiation of gut endocrine cells. *Endocrinology* **145**, 2639–2644 (2004).
7. Ting, H.-A. & von Moltke, J. The Immune Function of Tuft Cells at Gut Mucosal Surfaces and Beyond. *J. Immunol.* **202**, 1321–1329 (2019).
8. Jang, M. H. *et al.* Intestinal villous M cells: an antigen entry site in the mucosal epithelium. *Proc. Natl. Acad. Sci. U. S. A.* **101**, 6110–6115 (2004).
9. Hartsock, A. & Nelson, W. J. Adherens and Tight Junctions: Structure, Function and Connections to the Actin Cytoskeleton. *Biochim. Biophys. Acta* **1778**, 660 (2008).
10. Perez-Moreno, M., Jamora, C. & Fuchs, E. Sticky Business: Orchestrating Cellular Signals at Adherens Junctions. *Cell* **112**, 535–548 (2003).
11. Itoh, M. *et al.* Junctional adhesion molecule (JAM) binds to PAR-3: a possible mechanism for the recruitment of PAR-3 to tight junctions. *J. Cell Biol.* **154**, 491–497 (2001).
12. Cummins, P. M. Occludin: One Protein, Many Forms. *Mol. Cell. Biol.* **32**, 242 (2012).
13. Milatz, S. & Breiderhoff, T. One gene, two paracellular ion channels-claudin-10 in the kidney. *Pflugers Arch.* **469**, 115–121 (2017).
14. Furuse, M. *et al.* Claudin-based tight junctions are crucial for the mammalian epidermal barrier: a lesson from claudin-1-deficient mice. *J. Cell Biol.* **156**, 1099–1111 (2002).
15. Agarwal, R., D'Souza, T. & Morin, P. J. Claudin-3 and claudin-4 expression in ovarian epithelial cells enhances invasion and is associated with increased matrix metalloproteinase-2 activity. *Cancer Res.* **65**, 7378–7385 (2005).
16. Bazzoni, G. The JAM family of junctional adhesion molecules. *Curr. Opin. Cell Biol.* **15**, 525–530 (2003).

17. Liu, X.-F., Ishida, H., Raziuddin, R. & Miki, T. Nucleotide Exchange Factor ECT2 Interacts with the Polarity Protein Complex Par6/Par3/Protein Kinase Cζ (PKCζ) and Regulates PKCζ Activity. *Mol. Cell. Biol.* **24**, 6665 (2004).

18. Zihni, C. *et al.* Dbl3 drives Cdc42 signaling at the apical margin to regulate junction position and apical differentiation. *J. Cell Biol.* **204**, 111 (2014).

19. Wells, C. D. *et al.* A Rich1/Amot complex regulates the Cdc42 GTPase and apical-polarity proteins in epithelial cells. *Cell* **125**, 535–548 (2006).

20. Artis, D. Epithelial-cell recognition of commensal bacteria and maintenance of immune homeostasis in the gut. *Nat. Rev. Immunol. 2008 86* **8**, 411–420 (2008).

21. Macpherson, A. J. & Harris, N. L. Interactions between commensal intestinal bacteria and the immune system. *Nat. Rev. Immunol.* **4**, 478–485 (2004).

22. Bishop, R. F. & Kirkwood, C. D. Enteric Viruses. *Encycl. Virol.* 116 (2008) doi:10.1016/B978-012374410-4.00386-1.

23. El Sayed Zaki, M. & Abo El Kheir, N. Molecular study of astrovirus, adenovirus and norovirus in community acquired diarrhea in children: One Egyptian center study. *Asian Pac. J. Trop. Biomed.* **7**, 987–990 (2017).

24. Hoffmann, H. H., Schneider, W. M. & Rice, C. M. Interferons and viruses: an evolutionary arms race of molecular interactions. *Trends Immunol.* **36**, 124–138 (2015).

25. Odendall, C. *et al.* Diverse intracellular pathogens activate type III interferon expression from peroxisomes. *Nat. Immunol.* **15**, 717–726 (2014).

26. Kato, H. *et al.* Length-dependent recognition of double-stranded ribonucleic acids by retinoic acid-inducible gene-I and melanoma differentiation-associated gene 5. *J. Exp. Med.* **205**, 1601–1610 (2008).

27. Gao, D. *et al.* Cyclic GMP-AMP synthase is an innate immune sensor of HIV and other retroviruses. *Science* **341**, 903–906 (2013).

28. Fukata, M. & Arditi, M. The role of pattern recognition receptors in intestinal inflammation. *Mucosal Immunol.* **6**, 451 (2013).

29. Nan, Y., Nan, G. & Zhang, Y. J. Interferon Induction by RNA Viruses and Antagonism by Viral Pathogens. *Viruses* **6**, 4999 (2014).

30. Kawai, T. & Akira, S. The role of pattern-recognition receptors in innate immunity: update on Toll-like receptors. *Nat. Immunol. 2010 115* **11**, 373–384 (2010).

31. Moynagh, P. N. TLR signalling and activation of IRFs: revisiting old friends from the NF-kappaB pathway. *Trends Immunol.* **26**, 469–476 (2005).

32. Sharma, S. *et al.* Triggering the interferon antiviral response through an IKK-related pathway. *Science* **300**, 1148–1151 (2003).

33. Takahasi, K. *et al.* Nonself RNA-sensing mechanism of RIG-I helicase and activation of antiviral immune responses. *Mol. Cell* **29**, 428–440 (2008).

34. Hou, F. *et al.* MAVS forms functional prion-like aggregates to activate and propagate antiviral innate immune response. *Cell* **146**, 448–461 (2011).

35. A, I. & J, L. Virus interference. I. The interferon. *Proc. R. Soc. London. Ser. B, Biol. Sci.* **147**, 258–267 (1957).

36. Levy, D. E., Marié, I. J. & Durbin, J. E. Induction and Function of Type I and III Interferon in Response to Viral Infection. *Curr. Opin. Virol.* **1**, 476 (2011).

37. Swiecki, M. & Colonna, M. Type I interferons: diversity of sources, production pathways and effects on immune responses. *Curr. Opin. Virol.* **1**, 463–475 (2011).

38. Durbin, R. K., Kotenko, S. V. & Durbin, J. E. Interferon Induction and Function at the Mucosal Surface. *Immunol. Rev.* **255**, 25 (2013).

39. Gibbert, K., Schlaak, J. F., Yang, D. & Dittmer, U. IFN-α subtypes: distinct biological activities in anti-viral therapy. *Br. J. Pharmacol.* **168**, 1048–1058 (2013).

40. Schroder, K., Hertzog, P. J., Ravasi, T. & Hume, D. A. Interferon-gamma: an overview of signals, mechanisms and functions. *J. Leukoc. Biol.* **75**, 163–189 (2004).

41. Pestka, S. *et al.* The interferon gamma (IFN-gamma) receptor: a paradigm for the multichain cytokine receptor. *Cytokine Growth Factor Rev.* **8**, 189–206 (1997).

42. Kotenko, S. V. & Durbin, J. E. Contribution of type III interferons to antiviral immunity: location, location, location. *J. Biol. Chem.* **292**, 7295–7303 (2017).

43. Hemann, E. A., Gale, M. & Savan, R. Interferon Lambda Genetics and Biology in Regulation of Viral Control. *Front. Immunol.* **8**, 1707 (2017).

44. Gad, H. H. *et al.* Interferon-λ Is Functionally an Interferon but Structurally Related to the Interleukin-10 Family. *J. Biol. Chem.* **284**, 20869 (2009).

45. Ank, N. *et al.* An Important Role for Type III Interferon (IFN-λ/IL-28) in TLR-Induced Antiviral Activity. *J. Immunol.* **180**, 2474–2485 (2008).

46. Sommereyns, C., Paul, S., Staeheli, P. & Michiels, T. IFN-Lambda (IFN-λ) Is Expressed in a Tissue-Dependent Fashion and Primarily Acts on Epithelial Cells In Vivo. *PLOS Pathog.* **4**, e1000017 (2008).

47. Jewell, N. A. *et al.* Lambda Interferon Is the Predominant Interferon Induced by Influenza A Virus Infection In Vivo . *J. Virol.* **84**, 11515–11522 (2010).

48. Baños-Lara, M. D. R. *et al.* Impact and regulation of lambda interferon response in human metapneumovirus infection. *J. Virol.* **89**, 730–742 (2015).

49. Galani, I. E. *et al.* Interferon-λ Mediates Non-redundant Front-Line Antiviral Protection against Influenza Virus Infection without Compromising Host Fitness. *Immunity* **46**, 875-890.e6 (2017).

50. van Boxel-Dezaire, A. H. H., Rani, M. R. S. & Stark, G. R. Complex modulation of cell type-specific signaling in response to type I interferons. *Immunity* **25**, 361–372 (2006).

51. Fu, X. Y., Kessler, D. S., Veals, S. A., Levy, D. E. & Darnell, J. E. ISGF3, the transcriptional activator induced by interferon alpha, consists of multiple interacting polypeptide chains. *Proc. Natl. Acad. Sci. U. S. A.* **87**, 8555 (1990).

52. Darnell, J. E., Kerr, I. M. & Stark, G. R. Jak-STAT pathways and transcriptional activation in response to IFNs and other extracellular signaling proteins. *Science* **264**, 1415–1421 (1994).

53. Iwasaki, A. A virological view of innate immune recognition. *Annu. Rev. Microbiol.* **66**, 177–196 (2012).

54. Gao, S. *et al.* Structural basis of oligomerization in the stalk region of dynamin-like MxA. *Nature* **465**, 502–506 (2010).

55. Goujon, C. *et al.* Human MX2 is an interferon-induced post-entry inhibitor of HIV-1 infection. *Nature* **502**, 559–562 (2013).

56. Villarroya-Beltri, C., Guerra, S. & Sánchez-Madrid, F. ISGylation - a key to lock the cell gates for preventing the spread of threats. *J. Cell Sci.* **130**, 2961–2969 (2017).

57. Zhao, C. *et al.* Influenza B virus non-structural protein 1 counteracts ISG15 antiviral activity by sequestering ISGylated viral proteins. *Nat. Commun. 2016 71* **7**, 1–12 (2016).

58. Wang, X., Hinson, E. R. & Cresswell, P. The Interferon-Inducible Protein Viperin Inhibits Influenza Virus Release by Perturbing Lipid Rafts. *Cell Host Microbe* **2**, 96–105 (2007).

59. Nasr, N. *et al.* HIV-1 infection of human macrophages directly induces viperin which inhibits viral production. *Blood* **120**, 778–788 (2012).

60. Odendall, C. & Kagan, J. C. The unique regulation and functions of type III interferons in antiviral immunity. *Curr. Opin. Virol.* **12**, 47–52 (2015).

61. Mordstein, M. *et al.* Lambda interferon renders epithelial cells of the respiratory and gastrointestinal tracts resistant to viral infections. *J. Virol.* **84**, 5670–5677 (2010).

62. Mahlakõiv, T., Hernandez, P., Gronke, K., Diefenbach, A. & Staeheli, P. Leukocyte-Derived IFN-α/β and Epithelial IFN-λ Constitute a Compartmentalized Mucosal Defense System that Restricts Enteric Virus Infections. *PLOS Pathog.* **11**, e1004782 (2015).

63. Nice, T. J. *et al.* Interferon-λ cures persistent murine norovirus infection in the absence of adaptive immunity. *Science (80-.).* **347**, 269–273 (2015).

64. Nice, T. J. *et al.* Type I Interferon Receptor Deficiency in Dendritic Cells Facilitates Systemic Murine Norovirus Persistence Despite Enhanced Adaptive Immunity. *PLOS Pathog.* **12**, e1005684 (2016).

65. Lin, J. Da *et al.* Distinct Roles of Type I and Type III Interferons in Intestinal Immunity to Homologous and Heterologous Rotavirus Infections. *PLOS Pathog.* **12**, e1005600 (2016).

66. Kohli, A. *et al.* Distinct and overlapping genomic profiles and antiviral effects of Interferon-λ and -α on HCV-infected and noninfected hepatoma cells. *J. Viral Hepat.* **19**, 843–853 (2012).

67. Voigt, E. A. & Yin, J. Kinetic Differences and Synergistic Antiviral Effects Between Type I and Type III Interferon Signaling Indicate Pathway

Independence. *J. Interferon Cytokine Res.* **35**, 734–747 (2015).

68. Pervolaraki, K. *et al.* Differential induction of interferon stimulated genes between type I and type III interferons is independent of interferon receptor abundance. *PLoS Pathog.* **14**, (2018).

69. Pervolaraki, K. *et al.* Type I and type III interferons display different dependency on mitogen-activated protein kinases to mount an antiviral state in the human gut. *Front. Immunol.* **8**, 459 (2017).

70. Selvakumar, T. A. *et al.* Identification of a predominantly interferon-λ-induced transcriptional profile in murine intestinal epithelial cells. *Front. Immunol.* **8**, 1302 (2017).

71. Prevention of rotavirus gastroenteritis among infants and children: recommendations of the Advisory Committee on Immunization Practices (ACIP) - PubMed. https://pubmed.ncbi.nlm.nih.gov/19194371/.

72. Parashar, U. D., Nelson, E. A. S. & Kang, G. Diagnosis, management, and prevention of rotavirus gastroenteritis in children. *BMJ (Online)* vol. 347 (2013).

73. Carvalho, M. F. & Gill, D. Rotavirus vaccine efficacy: current status and areas for improvement. *Hum. Vaccin. Immunother.* **15**, 1237 (2019).

74. Desselberger, U. Rotaviruses. *Virus Res.* **190**, 75–96 (2014).

75. Crawford, S. E. *et al.* Trypsin cleavage stabilizes the rotavirus VP4 spike. *J. Virol.* **75**, 6052–6061 (2001).

76. López, S. & Arias, C. F. Multistep entry of rotavirus into cells: a Versaillesque dance. *Trends Microbiol.* **12**, 271–278 (2004).

77. Silva-Ayala, D. *et al.* Genome-wide RNAi screen reveals a role for the ESCRT complex in rotavirus cell entry. *Proc. Natl. Acad. Sci. U. S. A.* **110**, 10270–10275 (2013).

78. Díaz-Salinas, M. A., Silva-Ayala, D., López, S. & Arias, C. F. Rotaviruses reach late endosomes and require the cation-dependent mannose-6-phosphate receptor and the activity of cathepsin proteases to enter the cell. *J. Virol.* **88**, 4389–4402 (2014).

79. Ludert, J. E., Michelangeli, F., Liprandi, F. & Esparza, J. Penetration and Uncoating of Rotaviruses in Cultured Cells. *Intervirology* **27**, 95–101 (1987).

80. Settembre, E. C., Chen, J. Z., Dormitzer, P. R., Grigorieff, N. & Harrison, S. C. Atomic model of an infectious rotavirus particle. *EMBO J.* **30**, 408–416 (2011).

81. Jayaram, H., Estes, M. K. & Prasad, B. V. V. Emerging themes in rotavirus cell entry, genome organization, transcription and replication. *Virus Res.* **101**, 67–81 (2004).

82. Silvestri, L. S., Taraporewala, Z. F. & Patton, J. T. Rotavirus replication: plus-sense templates for double-stranded RNA synthesis are made in viroplasms. *J. Virol.* **78**, 7763–7774 (2004).

83. Fabbretti, E., Afrikanova, I., Vascotto, F. & Burrone, O. R. Two non-structural rotavirus proteins, NSP2 and NSP5, form viroplasm-like structures in vivo. *J. Gen. Virol.* **80 (Pt 2)**, 333–339 (1999).

84. Taylor, J. A., O'Brien, J. A. & Yeager, M. The cytoplasmic tail of NSP4, the endoplasmic reticulum-localized non-structural glycoprotein of rotavirus, contains distinct virus binding and coiled coil domains. *EMBO J.* **15**, 4469 (1996).

85. Hyser, J. M., Collinson-Pautz, M. R., Utama, B. & Estes, M. K. Rotavirus disrupts calcium homeostasis by NSP4 viroporin activity. *MBio* **1**, (2010).

86. Hyser, J. M., Utama, B., Crawford, S. E., Broughman, J. R. & Estes, M. K. Activation of the endoplasmic reticulum calcium sensor STIM1 and store-operated calcium entry by rotavirus requires NSP4 viroporin activity. *J. Virol.* **87**, 13579–13588 (2013).

87. Piron, M., Vende, P., Cohen, J. & Poncet, D. Rotavirus RNA-binding protein NSP3 interacts with eIF4GI and evicts the poly(A) binding protein from eIF4F. *EMBO J.* **17**, 5811–5821 (1998).

88. Groft, C. M. & Burley, S. K. Recognition of eIF4G by rotavirus NSP3 reveals a basis for mRNA circularization. *Mol. Cell* **9**, 1273–1283 (2002).

89. Graff, J. W., Ewen, J., Ettayebi, K. & Hardy, M. E. Zinc-binding domain of rotavirus NSP1 is required for proteasome-dependent degradation of IRF3 and autoregulatory NSP1 stability. *J. Gen. Virol.* **88**, 613–620 (2007).

90. Nandi, S. *et al.* MAVS protein is attenuated by rotavirus nonstructural protein 1. *PLoS One* **9**, (2014).

91. Trask, S. D., McDonald, S. M. & Patton, J. T. Structural insights into the coupling of virion assembly and rotavirus replication. *Nat. Rev. Microbiol.* **10**, 165–177 (2012).

92. Taylor, J. A., O'Brien, J. A. & Yeager, M. The cytoplasmic tail of NSP4, the endoplasmic reticulum-localized non-structural glycoprotein of rotavirus, contains distinct virus binding and coiled coil domains. *EMBO J.* **15**, 4469 (1996).

93. Greenberg, H. B. & Estes, M. K. Rotaviruses: from pathogenesis to vaccination. *Gastroenterology* **136**, 1939–1951 (2009).

94. McNulty, M. S., Curran, W. L. & McFerran, J. B. The morphogenesis of a cytopathic bovine rotavirus in Madin-Darby bovine kidney cells. *J. Gen. Virol.* **33**, 503–508 (1976).

95. Gardet, A., Breton, M., Fontanges, P., Trugnan, G. & Chwetzoff, S. Rotavirus spike protein VP4 binds to and remodels actin bundles of the epithelial brush border into actin bodies. *J. Virol.* **80**, 3947–3956 (2006).

96. Hakim, M. S. *et al.* Basal interferon signaling and therapeutic use of interferons in controlling rotavirus infection in human intestinal cells and organoids. *Sci. Rep.* **8**, (2018).

97. Pott, J. *et al.* IFN-λ determines the intestinal epithelial antiviral host defense. *Proc. Natl. Acad. Sci.* **108**, 7944–7949 (2011).

98. Saxena, K. *et al.* A paradox of transcriptional and functional innate interferon responses of human intestinal enteroids to enteric virus infection. *Proc. Natl. Acad. Sci. U. S. A.* **114**, E570–E579 (2017).

99. Pott, J. *et al.* IFN-lambda determines the intestinal epithelial antiviral host

defense. *Proc. Natl. Acad. Sci. U. S. A.* **108**, 7944–7949 (2011).

100. Frias, A. H. *et al.* Intestinal epithelia activate anti-viral signaling via intracellular sensing of rotavirus structural components. *Mucosal Immunol.* **3**, 622–632 (2010).

101. Broquet, A. H., Hirata, Y., McAllister, C. S. & Kagnoff, M. F. RIG-I/MDA5/MAVS Are Required To Signal a Protective IFN Response in Rotavirus-Infected Intestinal Epithelium. *J. Immunol.* **186**, 1618–1626 (2011).

102. Sachdev, H. P. S., Chadha, V., Malhotra, V., Verghese, A. & Puri, R. K. Rotavirus induces alpha-interferon release in children with gastroenteritis. *J. Pediatr. Gastroenterol. Nutr.* **16**, 33–38 (1993).

103. McKimm-Breschkin, J. L. & Holmes, I. H. Conditions required for induction of interferon by rotaviruses and for their sensitivity to its action. *Infect. Immun.* **36**, 857–863 (1982).

104. K, T., K, K. & S, U. Nondefective rotavirus mutants with an NSP1 gene which has a deletion of 500 nucleotides, including a cysteine-rich zinc finger motif-encoding region (nucleotides 156 to 248), or which has a nonsense codon at nucleotides 153-155. *J. Virol.* **70**, 4125–4130 (1996).

105. Barro, M. & Patton, J. T. Rotavirus nonstructural protein 1 subverts innate immune response by inducing degradation of IFN regulatory factor 3. *Proc. Natl. Acad. Sci.* **102**, 4114–4119 (2005).

106. Barro, M. & Patton, J. T. Rotavirus NSP1 inhibits expression of type I interferon by antagonizing the function of interferon regulatory factors IRF3, IRF5, and IRF7. *J. Virol.* **81**, 4473–4481 (2007).

107. Arnold, M. M., Barro, M. & Patton, J. T. Rotavirus NSP1 mediates degradation of interferon regulatory factors through targeting of the dimerization domain. *J. Virol.* **87**, 9813–9821 (2013).

108. Graff, J. W., Ettayebi, K. & Hardy, M. E. Rotavirus NSP1 inhibits NFkappaB activation by inducing proteasome-dependent degradation of beta-TrCP: a novel mechanism of IFN antagonism. *PLoS Pathog.* **5**, (2009).

109. Sen, A., Rott, L., Phan, N., Mukherjee, G. & Greenberg, H. B. Rotavirus NSP1 protein inhibits interferon-mediated STAT1 activation. *J. Virol.* **88**, 41–53 (2014).

110. Graff, J. W., Mitzel, D. N., Weisend, C. M., Flenniken, M. L. & Hardy, M. E. Interferon regulatory factor 3 is a cellular partner of rotavirus NSP1. *J. Virol.* **76**, 9545–9550 (2002).

111. Ball, J. M., Tian, P., Zeng, C. Q. Y., Morris, A. P. & Estes, M. K. Age-Dependent Diarrhea Induced by a Rotaviral Nonstructural Glycoprotein. *Science (80-.).* **272**, 101–104 (1996).

112. Morris, A. P. *et al.* NSP4 elicits age-dependent diarrhea and Ca(2+)mediated I(-) influx into intestinal crypts of CF mice. *Am. J. Physiol.* **277**, (1999).

113. Pham, T., Perry, J. L., Dosey, T. L., Delcour, A. H. & Hyser, J. M. The Rotavirus NSP4 Viroporin Domain is a Calcium-conducting Ion Channel. *Sci. Rep.* **7**, (2017).

114. Zambrano, J. L. *et al.* Rotavirus infection of cells in culture induces activation of RhoA and changes in the actin and tubulin cytoskeleton. *PLoS One* **7**, (2012).

115. Beau, I., Cotte-Laffitte, J., Amsellem, R. & Servin, A. L. A Protein Kinase A-Dependent Mechanism by Which Rotavirus Affects the Distribution and mRNA Level of the Functional Tight Junction-Associated Protein, Occludin, in Human Differentiated Intestinal Caco-2 Cells. *J. Virol.* **81**, 8579 (2007).

116. Dickman, K. G. *et al.* Rotavirus alters paracellular permeability and energy metabolism in Caco-2 cells. *https://doi.org/10.1152/ajpgi.2000.279.4.G757* (2000) doi:10.1152/AJPGI.2000.279.4.G757.

117. Tafazoli, F., Zeng, C. Q., Estes, M. K., Magnusson, K.-E. & Svensson, L. NSP4 enterotoxin of rotavirus induces paracellular leakage in polarized epithelial cells. *J. Virol.* **75**, 1540–1546 (2001).

118. Ousingsawat, J. *et al.* Rotavirus toxin NSP4 induces diarrhea by activation of TMEM16A and inhibition of Na+ absorption. *Pflugers Arch.* **461**, 579–589 (2011).

119. Seo, N. S. *et al.* Integrins α1β1 and α2β1 are receptors for the rotavirus enterotoxin. *Proc. Natl. Acad. Sci.* **105**, 8811–8818 (2008).

120. Hagbom, M. *et al.* Rotavirus stimulates release of serotonin (5-HT) from human enterochromaffin cells and activates brain structures involved in nausea and vomiting. *PLoS Pathog.* **7**, (2011).

121. Chang-Graham, A. L. *et al.* Rotavirus induces intercellular calcium waves through ADP signaling. *Science (80-.).* **370**, eabc3621 (2020).

122. Berchtold, M. W., Brinkmeier, H. & Müntener, M. Calcium ion in skeletal muscle: its crucial role for muscle function, plasticity, and disease. *Physiol. Rev.* **80**, 1215–1265 (2000).

123. Kaeser, P. S. & Regehr, W. G. Molecular mechanisms for synchronous, asynchronous, and spontaneous neurotransmitter release. *Annu. Rev. Physiol.* **76**, 333–363 (2014).

124. Machaca, K. Ca(2+) signaling, genes and the cell cycle. *Cell Calcium* **48**, 243–250 (2010).

125. Bhosale, G., Sharpe, J. A., Sundier, S. Y. & Duchen, M. R. Calcium signaling as a mediator of cell energy demand and a trigger to cell death. *Ann. N. Y. Acad. Sci.* **1350**, 107–116 (2015).

126. Dolmetsch, R. E., Lewis, R. S., Goodnow, C. C. & Healy, J. I. Differential activation of transcription factors induced by Ca2+ response amplitude and duration. *Nature* **386**, 855–858 (1997).

127. Rottingen, J. A. & Iversen, J. G. Ruled by waves? Intracellular and intercellular calcium signalling. *Acta Physiol. Scand.* **169**, 203–219 (2000).

128. Berridge, M. J., Bootman, M. D. & Roderick, H. L. Calcium signalling: dynamics, homeostasis and remodelling. *Nat. Rev. Mol. Cell Biol. 2003 47* **4**, 517–529 (2003).

129. Brini, M., Calì, T., Ottolini, D. & Carafoli, E. The plasma membrane calcium pump in health and disease. *FEBS J.* **280**, 5385–5397 (2013).

130. Toyoshima, C. How Ca2+-ATPase pumps ions across the sarcoplasmic reticulum membrane. *Biochim. Biophys. Acta* **1793**, 941–946 (2009).

131. Berridge, M. J. Inositol trisphosphate and calcium signalling mechanisms. *Biochim. Biophys. Acta* **1793**, 933–940 (2009).

132. Dupont, G., Combettes, L., Bird, G. S. & Putney, J. W. Calcium oscillations. *Cold Spring Harb. Perspect. Biol.* **3**, 1–18 (2011).

133. Sanderson, M. J., Charles, A. C., Boitano, S. & Dirksen, E. R. Mechanisms and function of intercellular calcium signaling. *Mol. Cell. Endocrinol.* **98**, 173–187 (1994).

134. Sanderson, M. J., Charles, A. C. & Dirksen, E. R. Mechanical stimulation and intercellular communication increases intracellular Ca2+ in epithelial cells. *Cell Regul.* **1**, 585–596 (1990).

135. Frame, M. K. & De Feijter, A. W. Propagation of mechanically induced intercellular calcium waves via gap junctions and ATP receptors in rat liver epithelial cells. *Exp. Cell Res.* **230**, 197–207 (1997).

136. Domenighetti, A. A., Bény, J. L., Chabaud, F. & Frieden, M. An intercellular regenerative calcium wave in porcine coronary artery endothelial cells in primary culture. *J. Physiol.* **513**, 103 (1998).

137. Cao, D., Lin, G., Westphale, E. M., Beyer, E. C. & Steinberg, T. H. Mechanisms for the coordination of intercellular calcium signaling in insulin-secreting cells. *J. Cell Sci.* **110 (Pt 4)**, 497–504 (1997).

138. Cornell-Bell, A. H., Finkbeiner, S. M., Cooper, M. S. & Smith, S. J. Glutamate induces calcium waves in cultured astrocytes: long-range glial signaling. *Science* **247**, 470–473 (1990).

139. Hassinger, T. D., Guthrie, P. B., Atkinson, P. B., Bennett, M. V. L. & Kater, S. B. An extracellular signaling component in propagation of astrocytic calcium waves. *Proc. Natl. Acad. Sci.* **93**, 13268–13273 (1996).

140. Charles, A. C. *et al.* Intercellular calcium signaling via gap junctions in glioma cells. *J. Cell Biol.* **118**, 195–201 (1992).

141. Sneyd, J., Wetton, B. T. R., Charles, A. C. & Sanderson, M. J. Intercellular calcium waves mediated by diffusion of inositol trisphosphate: a two-dimensional model. *https://doi.org/10.1152/ajpcell.1995.268.6.C1537* **268**, (1995).

142. Osipchuk, Y. & Cahalan, M. Cell-to-cell spread of calcium signals mediated by ATP receptors in mast cells. *Nature* **359**, 241–244 (1992).

143. Nigam, S. K., Rodriguez-Boulan, E. & Silver, R. B. Changes in intracellular calcium during the development of epithelial polarity and junctions. *Proc. Natl. Acad. Sci. U. S. A.* **89**, 6162–6166 (1992).

144. Ye, J., Tsukamoto, T., Sun, A. & Nigam, S. K. A role for intracellular calcium in tight junction reassembly after ATP depletion-repletion. *Am. J. Physiol. - Ren. Physiol.* **277**, (1999).

145. Stuart, R. O., Sun, A., Bush, K. T. & Nigam, S. K. Dependence of Epithelial Intercellular Junction Biogenesis on Thapsigargin-sensitive Intracellular Calcium

Stores*. *J. Biol. Chem.* **271**, 13636–13641 (1996).

146. Balda, M. S., Gonzalez-Mariscal, L., Matter, K., Cereijido, M. & Anderson, J. M. Assembly of the tight junction: the role of diacylglycerol. *J. Cell Biol.* **123**, 293–302 (1993).

147. Seo, S. H., Kim, S. E. & Lee, S. E. ER stress induced by ER calcium depletion and UVB irradiation regulates tight junction barrier integrity in human keratinocytes. *J. Dermatol. Sci.* **98**, 41–49 (2020).

148. Stanifer, M. L., Kischnick, C., Rippert, A., Albrecht, D. & Boulant, S. Reovirus inhibits interferon production by sequestering IRF3 into viral factories. *Sci. Rep.* **7**, (2017).

149. Kaukinen, P. *et al.* Hepatitis C virus NS2 and NS3/4A proteins are potent inhibitors of host cell cytokine/chemokine gene expression. *Virol. J.* **3**, (2006).

150. Jones, C. T. *et al.* Real-time imaging of hepatitis C virus infection using a fluorescent cell-based reporter system. *Nat. Biotechnol.* **28**, 167 (2010).

151. Kiang, D. & Matsui, S. M. Proteolytic processing of a human astrovirus nonstructural protein. *J. Gen. Virol.* **83**, 25–34 (2002).

152. Geigenmüller, U., Chew, T., Ginzton, N. & Matsui, S. M. Processing of Nonstructural Protein 1a of Human Astrovirus. *J. Virol.* **76**, 2003–2008 (2002).

153. Sosnovtsev, S. V. *et al.* Cleavage Map and Proteolytic Processing of the Murine Norovirus Nonstructural Polyprotein in Infected Cells. *J. Virol.* **80**, 7816 (2006).

154. Philip, A. A. *et al.* Generation of Recombinant Rotavirus Expressing NSP3-UnaG Fusion Protein by a Simplified Reverse Genetics System. *J. Virol.* **93**, (2019).

155. Arnold, M. M. & Patton, J. T. Diversity of Interferon Antagonist Activities Mediated by NSP1 Proteins of Different Rotavirus Strains. *J. Virol.* **85**, 1970–1979 (2011).

156. Pervolaraki, K. *et al.* Type I and type III interferons display different dependency on mitogen-activated protein kinases to mount an antiviral state in the human gut. *Front. Immunol.* **8**, 459 (2017).

157. Blau, D. M. & Compans, R. W. Polarization of viral entry and release in epithelial cells. *Semin. Virol.* **7**, 245–253 (1996).

158. Mee, C. J. *et al.* Effect of Cell Polarization on Hepatitis C Virus Entry. *J. Virol.* **82**, 461 (2008).

159. Tamhankar, M. & Patterson, J. L. Directional entry and release of Zika virus from polarized epithelial cells. *Virol. J.* **16**, 1–8 (2019).

160. Chodosh, J., Gan, Y.-J., Holder, V. P. & Sixbey, J. W. Patterned Entry and Egress by Epstein-Barr Virus in Polarized CR2-Positive Epithelial Cells. (2000) doi:10.1006/viro.1999.0082.

161. Takaoka, A. *et al.* Cross talk between interferon-γ and -α/β signaling components in caveolar membrane domains. *Science (80-.).* **288**, 2357–2360 (2000).

162. Stewart, M. J., Smoak, K., Blum, M. A. & Sherry, B. Basal and Reovirus-Induced Beta Interferon (IFN-β) and IFN-β-Stimulated Gene Expression Are Cell Type Specific in the Cardiac Protective Response. *J. Virol.* **79**, 2979–2987 (2005).

163. Hsu, A. C. Y. *et al.* Critical Role of Constitutive Type I Interferon Response in Bronchial Epithelial Cell to Influenza Infection. *PLoS One* **7**, e32947 (2012).

164. Bayer, A. *et al.* Type III Interferons Produced by Human Placental Trophoblasts Confer Protection against Zika Virus Infection. *Cell Host Microbe* **19**, 705–712 (2016).

165. Corry, J., Arora, N., Good, C. A., Sadovsky, Y. & Coyne, C. B. Organotypic models of type III interferon-mediated protection from Zika virus infections at the maternal–fetal interface. *Proc. Natl. Acad. Sci. U. S. A.* **114**, 9433–9438 (2017).

166. Platanitis, E. *et al.* A molecular switch from STAT2-IRF9 to ISGF3 underlies interferon-induced gene transcription. *Nat. Commun. 2019 101* **10**, 1–17 (2019).

167. Sobhkhez, M. *et al.* Structural and functional characterization of salmon STAT1, STAT2 and IRF9 homologs sheds light on interferon signaling in teleosts. *FEBS Open Bio* **4**, 858–871 (2014).

168. Chen, J., Wang, H., Wang, J., Huang, S. & Zhang, W. STAT1 inhibits human hepatocellular carcinoma cell growth through induction of p53 and Fbxw7. *Cancer Cell Int.* **15**, 1–10 (2015).

169. Stephanou, A. *et al.* Ischemia-induced STAT-1 expression and activation play a critical role in cardiomyocyte apoptosis. *J. Biol. Chem.* **275**, 10002–10008 (2000).

170. Banningeri, G. & Reich, N. C. STAT2 nuclear trafficking. *J. Biol. Chem.* **279**, 39199–39206 (2004).

171. Winkle, J. A. Van, Constant, D. A., Li, L. & Nice, T. J. Selective Interferon Responses of Intestinal Epithelial Cells Minimize Tumor Necrosis Factor Alpha Cytotoxicity. *J. Virol.* **94**, (2020).

172. Arnold, M. M., Barro, M. & Patton, J. T. Rotavirus NSP1 Mediates Degradation of Interferon Regulatory Factors through Targeting of the Dimerization Domain. *J. Virol.* **87**, 9813–9821 (2013).

173. G, I. *et al.* Rotavirus NSP1 Inhibits Type I and Type III Interferon Induction. *Viruses* **13**, (2021).

174. Bhushal, S. *et al.* Cell Polarization and Epigenetic Status Shape the Heterogeneous Response to Type III Interferons in Intestinal Epithelial Cells. *Front. Immunol.* **0**, 671 (2017).

175. Jaspers, I., Ciencewicki, J. M. & Brighton, L. E. Localization of Type I Interferon Receptor Limits Interferon-Induced TLR3 in Epithelial Cells. *J. Interf. Cytokine Res.* **29**, 289 (2009).

176. Hou, Z. *et al.* Anti-NSP4 antibody can block rotavirus-induced diarrhea in mice. *J. Pediatr. Gastroenterol. Nutr.* **46**, 376–385 (2008).

177. Sasaki, S., Horie, Y., Nakagomi, T., Oseto, M. & Nakagomi, O. Group C rotavirus NSP4 induces diarrhea in neonatal mice. *Arch. Virol.* **146**, 801–806 (2001).

178. Papp, B. & Byrn, R. A. Stimulation of HIV expression by intracellular calcium pump inhibition. *J. Biol. Chem.* **270**, 10278–10283 (1995).

179. Bergqvist, A., Sundström, S., Dimberg, L. Y., Gylfe, E. & Masucci, M. G. The

hepatitis C virus core protein modulates T cell responses by inducing spontaneous and altering T-cell receptor-triggered Ca2+ oscillations. *J. Biol. Chem.* **278**, 18877–18883 (2003).

180. Campanella, M. *et al.* The coxsackievirus 2B protein suppresses apoptotic host cell responses by manipulating intracellular Ca2+ homeostasis. *J. Biol. Chem.* **279**, 18440–18450 (2004).

181. Van Kuppeveld, F. J. M. *et al.* Coxsackievirus protein 2B modifies endoplasmic reticulum membrane and plasma membrane permeability and facilitates virus release. *EMBO J.* **16**, 3519–3532 (1997).

182. Chami, M., Oulès, B. & Paterlini-Bréchot, P. Cytobiological consequences of calcium-signaling alterations induced by human viral proteins. *Biochim. Biophys. Acta - Mol. Cell Res.* **1763**, 1344–1362 (2006).

183. Agol, V. I. *et al.* Competing Death Programs in Poliovirus-Infected Cells: Commitment Switch in the Middle of the Infectious Cycle. *J. Virol.* **74**, 5534 (2000).

184. Ball, J. M., Tian, P., Zeng, C. Q. Y., Morris, A. P. & Estes, M. K. Age-dependent diarrhea induced by a rotaviral nonstructural glycoprotein. *Science* **272**, 101–104 (1996).

185. Lorrot, M. & Vasseur, M. Virology Journal How do the rotavirus NSP4 and bacterial enterotoxins lead differently to diarrhea? (2007) doi:10.1186/1743-422X-4-31.

186. Séror, C. *et al.* Extracellular ATP acts on P2Y2 purinergic receptors to facilitate HIV-1 infection. *J. Exp. Med.* **208**, 1823–1834 (2011).

187. Zandberg, M., Van Son, W. J., Harmsen, M. C. & Bakker, W. W. Infection of human endothelium in vitro by cytomegalovirus causes enhanced expression of purinergic receptors: A potential virus escape mechanism? *Transplantation* **84**, 1343–1347 (2007).

188. Taylor, J. M. & Han, Z. Purinergic Receptor Functionality Is Necessary for Infection of Human Hepatocytes by Hepatitis Delta Virus and Hepatitis B Virus. *PLoS One* **5**, e15784 (2010).

189. Soliman, M. *et al.* Rotavirus-Induced Early Activation of the RhoA/ROCK/MLC Signaling Pathway Mediates the Disruption of Tight Junctions in Polarized MDCK Cells. *Sci. Rep.* **8**, (2018).

190. Coulson, B. S., Londrigan, S. L. & Lee, D. J. Rotavirus contains integrin ligand sequences and a disintegrin-like domain that are implicated in virus entry into cells. **94**, 5389–5394 (1997).

191. Arnold, M., Patton, J. T. & McDonald, S. M. Culturing, storage, and quantification of rotaviruses. *Current Protocols in Microbiology* vol. CHAPTER Unit (2009).

192. Stanifer, M. L. *et al.* Reovirus intermediate subviral particles constitute a strategy to infect intestinal epithelial cells by exploiting TGF-β dependent pro-survival signaling. *Cell. Microbiol.* **18**, 1831–1845 (2016).

6 List of abbreviations

AJ	Adherens junctions
CARD	Caspase activation and recruitment domain
cGAMP	Cyclic GMP-AMP
cGAS	Cyclic GMP-AMP synthase
DLP	Double-layered particle (rotavirus)
ER	Endoplasmic reticulum
GTPase	Guanosine triphosphatase
HCV	Hepatitis C virus
IEC	Intestinal epithelial cell
IFN	Interferon
IFNAR1	Interferon-α receptor 1
IFNAR2	Interferon-α receptor 2
IFNGR1	Interferon-γ receptor 1
IFNGR2	Interferon-γ receptor 2
IFNLR1	Interferon-λ receptor 1
IP3	Inositol-1,4,5-trisphosplate
IRF	Interferon regulatory factor
ISG	Interferon stimulated genes
ISGF3	IFN-stimulated gene factor 3
ISRE	IFN-stimulated regulatory elements
JAK	Janus kinases
LGP2	Laboratory of Genetics and Physiology 2
MDA-5	Melanoma differentiation-associated protein 5
NF-kB	Nuclear factor kB
NLS	Nuclear localization sequence
PABP	PolyA binding protein
PAMP	Pathogen associated molecular pattern

Poly I:C	Poly-inosinic:cytidylic acid
PRR	Pattern-recognition receptor
RIG-I	Retinoic acid-inducible gene I
RLR	RIG-I-like family of receptors
SERCA	Sarco/endoplasmic reticulum calcium pump
STAT	Signal transducer and activator of transcription
TBP	TATA-binding protein
TJ	Tight junction
TLP	Triple-layered particles (rotavirus)
TLR	Toll-like receptor
VSV	Vesicular stomatitis virus
ZO	Zonula occludens